Linear and Nonlinear Convective Instabilities in Porous Media

Bidin, Biliana

Award date:
2019

Awarding institution:
University of Bath

Linear and Nonlinear Convective Instabilities in Porous Media

Biliana Binti Bidin

A thesis submitted for the degree of Doctor of Philosophy

University of Bath

Department of Mechanical Engineering

October 2018

COPYRIGHT

Table of Contents

Acknowledgments

First and foremost I would like to thank the Ministry of Higher Education Malaysia (MOHE), particularly the University Malaysia Perlis (UniMAP), for the opportunity and trust given to hold the scholarship which enabled me to further my study at the University of Bath, UK.

Secondly, my highest gratitude goes to my supervisor, D.A.S Rees, who has been patient and has given his guidance and support endlessly in every aspect throughout my studies. I cannot thank him enough for all the help he gave as well as the extra effort that he has put in to improve this thesis. Apart from that, thank you so much to Dr. Nigel Johnston who has involved indirectly towards the end of my study years for his support and advice.

Thirdly, I give all my respect and gratitude to my lovely husband and kids for being with me in my ups and downs. I am also indebted to my close family members especially my mother, father and sister for their prayers and encouragements. Lastly, I express my sincere regards to and great pride of my mother in-law who is a cancer fighter for being strong and she has taught me the meaning of hope when I almost gave up in my fight.

Summary

After the first studies on the onset of convection in porous medium by Horton & Rogers [7] and Lapwood [8], the Horton-Rogers-Lapwood problem, also well-known as Darcy-Bénard problem, this problem has attracted much attention from researchers to study the onset of convection in porous medium due to its industrial and environmental applications in fields such as thermal insulation engineering, the growth of crystalline materials, patterned ground formation under water and application to oceanic and planetary mantle. By being derived from these early studies of the Darcy-Bénard problem, this thesis extends those studies in different directions and it consists of three main studies on convection in a porous medium. Thus, it is important in this chapter (from section 1.1 to 1.5) to introduce, explain and define all the terms and conditions used in studies of Darcy-Bénard problems to provide better understanding in the subsequent chapters.

The first study on the onset of convection in porous medium is presented in Chapter 2. The given title is "the onset of convection in the unsteady thermal boundary layer above a sinusoidally heated surface embedded in a porous medium." This study investigates the instability of the unsteady thermal boundary layer which is induced by varying the temperature of the horizontal boundary sinusoidally in time about the ambient temperature of the porous medium. This study has application in the diurnal heating and cooling from above in subsurface groundwater. The investigation of the occurrence of the instability is undertaken by finding the critical Darcy-Rayleigh number that marks the onset of convection. In order to do that, a linear stability analysis is applied by perturbing the basic state using a disturbance with a small amplitude. An unsteady solver is used together with Newton-Raphson iteration to find marginal instability. One finding is that the disturbance has a period which is twice that of the underlying basic state. Cells which rotate clockwise at first tend to rise upwards from the surface and weaken, but they induce an anticlockwise

cell near the surface at the end of one forcing period which is otherwise identical to the corresponding clockwise cell found at the start of that forcing period.

The second study is presented in chapter 3 entitled the linear stability of the unsteady thermal boundary layer in a semi-infinite layered porous medium. The general aim of this study is to examine the stability criteria of two dimensional unsteady thermal boundary layer that is bounded from below by an impermeable surface which is induced by suddenly raising the temperature of the lower horizontal boundary of the two layers semi-infinite porous domain. Due to the sudden temperature increase, it is suspected that an evolving thermal boundary layer formed is potentially unstable. A full linear stability analysis is performed using the small-amplitude disturbance to perturb the basic state of the temperature profile and the parabolic equations are solved using the Keller box method to mark the onset of convection. The growth or decay of the disturbances is monitored by the computation of the thermal energy of the disturbance. This study results in the finding of the locus in parameter space where two modes with different critical wavenumbers have simultaneous onset, and also find cases where the two minima in the neutral curve and the intermediate maximum merge to form a quartic minimum.

Still concerning about the layering effect, the third subsequent study is presented in "The effect of layering on unsteady conduction: an analytical solution method" which is in chapter 4. We considered a semi-infinite solid domain which exhibits layering and the thermal conductivity and diffusivity of each layer is different, therefore the non-dimensional parameters are conductivity ratios and diffusivity ratios. The boundary of that domain is suddenly raised to a new temperature and detailed study is performed to the 2-layer and 3-layer system over a wide range of variation of the governing non-dimensional parameters. The analytical solution of the governing equation is obtained by employing the Laplace transform. It is concluded that the thermal diffusivity ratio and the thermal conductivity ratio are the coefficients that play the important role in determining the manner in which

conduction occurs. In particular, the thermal diffusivity ratio affects how quickly the temperature field evolves in time.

The first three studies in this thesis considers the case of local thermal equilibrium (LTE), therefore we are keen to study the effect of local thermal nonequilibrium (LTNE) to the onset of Darcy-Bénard convection in porous medium which is presented in the last chapter; chapter 5. This work is the extension of work by Banu and Rees [1] into the weakly nonlinear regime. The aim of this chapter is achieved by employing a weakly nonlinear analysis to determine whether the convection pattern immediately post-onset is two dimensional (rolls) or three dimensional (square cells) which will be decided based on the coupling coefficients value set at 1. On those occasions where the coupling coefficient of the amplitude equation is above 1 then roll solutions are stable i.e two dimensional. Alternatively, if the coupling coefficient is below 1, then the roll solutions are unstable and three-dimensional square cells form the stable pattern. It is found in this study that the roll solutions are stable.

Chapter 1

Introduction

1.1 Nomenclature

A	cross-sectional area
c	specific heat
e	height of the porous layer
f	reduced streamfunction
g	reduced temperature
$\hat{g}$	gravity
h	inter-phase heat transfer coefficient
K	permeability
l	length scale
n	mode number
p	pressure
Q	volumetric flow rate
Ra, Ra_c	Darcy-Rayleigh number, critical Darcy-Rayleigh number
t	time

T	temperature (dimensional)
u	velocity in the x-direction
x	horizontal coordinate
z	vertical coordinate

Greek letters

α	thermal diffusivity
β	thermal expansion coefficient
ΔT	dimensional temperature difference
θ	temperature (nondimensional)
Θ	temperature disturbance
λ	exponential growth rate
μ	dynamic viscosity
ν	kinematic viscosity
ρ	reference density
σ	heat capacity ratio
ψ	streamfunction
Ψ	streamfunction disturbance
ϕ	porosity

Subscripts

-	dimensional

f	fluid phase
s	solid phase
r	reference

1.2 Definitions

1.2.1 Porous media

By definition, a porous medium is a solid which has containing pores or voids between some particulate phase, contained within a vessel, or some control volume. The skeletal portion of the material is called the matrix. Typically, the voids or pores are filled with fluid (liquid or gas or both). Examples of man-made materials are such as sponges; metallic foams which are widely used in the automotive industry, orthopedics, energy absorption devices, architectural composition such as the brick work, timber and concrete; filter beds to cleanse water; concrete blocks and porous ceramics (see figure 1.1). Examples of natural materials include beach sands, sandstone, limestone, rye bread, wood and the human lung (see Figure 1.2).

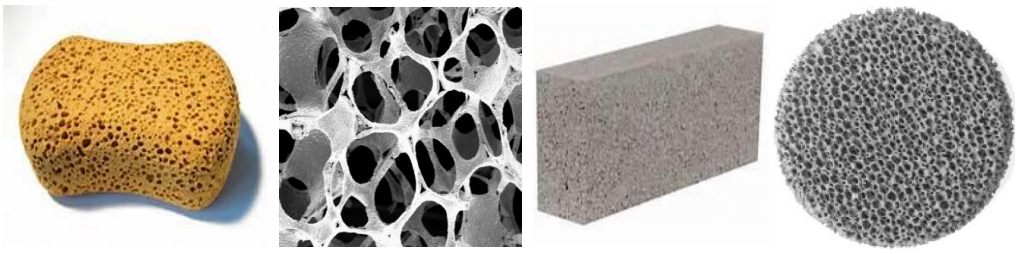

Figure 1.1: (a) Sponges; (b) Metallic foams; (c) Concrete blocks; (d) Porous ceramics

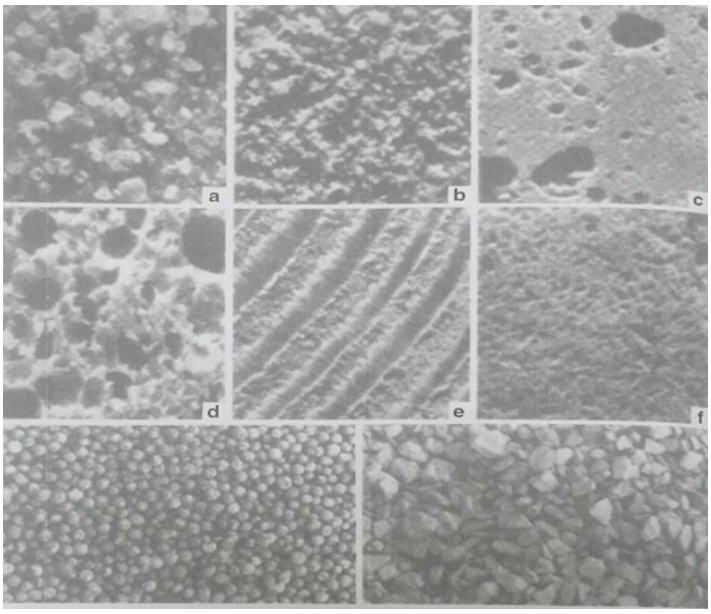

Figure 1.2: Examples of porous materials: (A) beach sand, (B) sandstone, (C) limestone, (D) rye bread, (E) wood and (F) human lung. Bottom row: (left) Granular porous materials used in the construction industry, 0.5 cm diameter Liapor® spheres, (right) 1 cm sized crushed limestone (taken from Nield and Bejan, 2013).

1.2.2 Porosity

According to Nield and Bejan [1], the porosity of a porous medium is the fraction of the total volume of the medium that is occupied by void space. One type of porous medium consists of a solid matrix with interconnecting pores. These interconnecting pores allow fluid to flow throughout the material. A second type is particulate, such as sand, where the fluid moves around the particles. A situation where the void space is saturated only by single fluid is called "single-phase flow". When the voids are saturated by a liquid and a gas this is called "two-phase flow" or multiphase flow.

Porous media may be isotropic or anisotropic. An artificial example of the former is a solid with an array of particles equally spaced in the three coordinate

directions. An example of the latter is wood where fluid seeps more easily along the grain than perpendicular to it.

For an isotropic medium, the surface porosity is defined as the fraction of the void area to the total area of a typical cross section, and this will normally be equal to ϕ, the volumetric porosity. If ϕ represents the fraction of the volume that is occupied by void space, then $1-\phi$ is the fraction that is occupied by solid material. If some of the void space is disconnected from the remainder, then the effective porosity is a more useful concept and it is defined as the ratio of the volume of the connected void space to the total volume. The porosity, ϕ, for natural materials normally does not exceed 0.6, however some natural material such as hair on mammals can take the value $\phi > 0.9$ (see table 1.1). On the other hand synthetic porous materials such as aerogel have porosities as large as 0.998**.**

Material	Porosity, ϕ	Permeability, K (cm^2)	Surface per unit volume (cm^{-1})
Agar-agar		2×10^{-10} to 4.4×10^{-9}	
Black slate powder	0.57-0.66	4.9×10^{-10} to 1.2×10^{-9}	7×10^{3} to 8.9×10^{3}
Brick	0.12-0.34	4.8×10^{-11} to 2.2×10^{-9}	
Catalyst (Fisher-Tropsch granules only)	0.45		5.6×10^{5}
Cigarrate		4.8×10^{-5}	
Cigaratte filter	0.17-0.49		
Coal	0.02-0.12		
Concrete (ordinary mixes)			
Concrete (bituminius)		1×10^{-9} to 2.3×10^{-7}	
Copper powder (hot compacted)	0.09-0.34	3.3×10^{-6} to 1.5×10^{-5}	
Cork board		2.4×10^{-7} to 5.1×10^{-7}	
Fiberglass	0.88-0.93		560-770
Granular crushed rock	0.45		
Hair (on mammals)	0.95-0.99		
Hair felt		8.3×10^{-6} to 1.2×10^{-5}	
Leather	0.56-0.59	9.5×10^{-10} to 1.2×10^{-9}	1.2×10^{4} to 1.6×10^{4}
Limestone (dolomite)	0.04-0.10	2×10^{-11} to 4.5×10^{-10}	
Sand	0.37-0.50	2×10^{-7} to 1.8×10^{-6}	150-220
Sandstone ("oil sand")	0.08-0.38	5×10^{-12} to 3×10^{-8}	
Silica grains	0.65		
Silica powder	0.37-0.49	1.3×10^{-10} to 5.1×10^{-10}	6.8×10^{3} to 8.9×10^{3}
Soil	0.43-0.54	2.9×10^{-9} to 1.4×10^{-7}	
Spherical packings (well shaken)	0.36-0.43		
Wire crimps	0.68-0.76	3.8×10^{-5} to 1×10^{-4}	29-40

Table 1.1: Properties of common porous materials (Nield and Bejan, 2013)

1.2.3 Permeability

The permeability of a material is commonly symbolized as K (and occasionally as k) and is defined as a measure of the ability of a porous material to allow fluids to pass through it. The SI unit for permeability is m^2. Permeability is part of proportionality constant in Darcy's law which relates the flow rate to the applied pressure gradient. Therefore

$$u = -\frac{K}{\mu}\frac{\partial p}{\partial x}, \tag{1.1}$$

for unidirectional flow where u is the superficial velocity (i.e. the average of the detached microscopic velocity over applied pressure gradient), also called the Darcy velocity, μ is the dynamic viscosity and $\frac{\partial p}{\partial x}$ is the applied pressure gradient in the direction of the fluid flow, *x*.

1.2.4 Heat transfer: Convection

According to the law of conservation of energy, energy cannot be destroyed, but it may be transformed from one form to another. Whenever two systems with different temperatures interact or contact one each other, a process of exchanging thermal energy will happen and it is known as heat transfer. This process continues until it reaches a condition called thermal equilibrium, in which the two systems have reached the same temperature. There are three mechanisms of heat transfer which are radiation, conduction and convection.

Radiation is a surface phenomenon. It does not need a transmitting medium for it to occur. It can happen within or without a perfect vacuum. Whenever heat energy hits a surface of an object, some of the heat will be reflected back, some will be absorbed and some will pass through and leave the object. Thus the study of thermal radiation involves a surface's physical condition directly. In order to ease the analysis of thermal radiation, the object is assumed to be ideal. For an ideal object, the amount of energy-in is equal to energy-out. An object that has this type of behavior is called a black body. An example of thermal radiation is infrared radiation which comes from household radiators, electric heaters and the human body. Radiation also can be a volumetric effect such as for a radioactive fluid.

Heat transfer by conduction is the process of exchanging thermal energy by molecular motion, supplemented in some cases by the flow of free electrons within and through a medium e.g. solid, liquid or gases due to the temperature gradient.

Conduction can only take place within an object or material, or between two objects that are in direct contact with each other.

Lastly, we consider heat transfer by convection which is one of the main interests in this study. Convection occurs due to the temperature differences between a fluid and the bounding surfaces and is also due to temperature gradients within the fluid. The density of the fluid usually decreases during the heating process. Fluid that is less dense will tend to move upwards and will be replaced by a more dense, usually cooler, fluid. This cycle continues until both the liquid and surface reach a state of thermal equilibrium or else the system is thermoconvectively unstable and a new pattern of fluid motion will arise. Generally, there are two types of convection: natural convection and forced convection (Pop and Ingham [2]). Natural (or free) convection is caused by differences in density resulting from the temperature differences and does not involve any external force, such as a background flow or an applied pressure gradient, while forced convection is produced by motion from an external agency such as a fan heater. The combination of natural and forced convection is called mixed convection.

1.3 Theories

1.3.1 Darcy's law

In 1856, Darcy conducted an experiment in an unnamed hospital in Dijon, France to determine the relationship between the volumetric flow rate of water through the sand beds and the hydraulic head loss (Brown [3]). In his experiment, he was considering flow through such conduits to remove the particles within the water to make it clear. At that time, the primary methods that were used to clean the water were precipitation and filtration. Darcy has claimed that these methods, particularly the precipitation method, were inefficient due to the greater time required. Besides,

long exposure times also encouraged bacterial growth in the water and additionally, they needed very large sized tanks to provide sufficient water supply to entire city.

Darcy then introduced a simple filtration technique where the water could be filtered by passing it through passageways small enough to retain any foreign particles that might be entrained. An example is the passing of water through layer of decreasing porosity, such as small stones, gravel and fine sand. Darcy has used various experimental data from across England and France to support his idea but unfortunately, due to the different origin of the sand, he obtained various filtering properties, along with the water's contamination level before filtration process and therefore failed to obtain the governing equation of motion. Thus, he decided to set up a standardised experiment. He then set up a vertical cylinder separated into three compartments. The initial compartment at the top of the cylinder was a reservoir for the incoming water, which was supplied directly from the hospital house line. The second compartment, which was below the first compartment, was divided into numerous separating grids to support a section of sand. The final compartment was the collecting reservoir where the filtered water went and was tapped off. The pressures in the first and third compartments were monitored using manometers during each experiment where different volumes of water were added to vary the pressure and therefore the flow rate. Through these experiments, Darcy successfully determined the flow rate for certain pressure differences between the upper and lower compartments. He proposed an empirical equation for estimating the volumetric flow rate (Q) given by (Lage [4]):

$$Q = \frac{kA}{e}\left[\left(P + H\right) + e - \left(P + H_0\right)\right], \tag{1.2}$$

where $\left(P + H\right)$ is the pressure above the sand layer (atmospheric pressure, P augmented by the pressure head, H, i.e hydrostatic pressure due to the fluid) and $\left(P + H_0\right)$ is pressure under the sand layer. Equation (1.2) then reduces to:

$$Q = \frac{kA}{e}\left[H + e - H_0\right], \tag{1.3}$$

where *k*, *A* and *e* are hydraulic conductivity related to the porous medium, the cross-sectional area and the height of the sand layer, respectively. Darcy then concluded with equation (1.4) derived from equation (1.3) which is:

$$u = k\frac{\Delta p}{e}, \tag{1.4}$$

where $u = \frac{Q}{A}$ is what we now call the Darcy velocity and the total pressure difference is $\Delta p = \rho g\left[H + e - H_0\right]$. However, equation (1.4) is limited to incompressible flow of very slow speed, where the fluid is Newtonian and through a relatively long, uniform and isotropic porous medium of low hydraulic conductivity (Lage [4]).

1.3.2 The Hazen-Darcy equation

The empirical hydraulic equation for flow through porous medium proposed by Darcy as in equation (1.4) does not display viscous effects directly. This is because Darcy just considered one fluid, which is water and additionally it was impossible for him to investigate fluid viscosity effects with his experimental apparatus. Hazen was the first to notice the viscosity effect in the connection to the original flow equation proposed by Darcy (Lage [4]). With this consideration, equation (1.4) becomes:

$$u = -\frac{K}{\mu}\frac{\Delta p}{e}, \tag{1.5}$$

where K is permeability, μ is dynamic viscosity and $\frac{\Delta p}{e}$ is the pressure gradient. Equation (1.5) may also be written in the form given in equation (1.6), which is considered to be the refined form of those efforts by Darcy and Hagen (Lage, 1998):

$$u = -\frac{K}{\mu}\frac{dp}{dx}. \tag{1.6}$$

1.4 Parameter: Rayleigh number

In fluid mechanics the Rayleigh number is a dimensionless number associated with buoyancy-driven flow (natural convection or forced convection). It is named after Lord Rayleigh who was first to solve the problem of the onset of thermal convection in a plane horizontal fluid layer heated from below (Getling [5]). Rayleigh found that certain temperature differences across the upper and lower boundary of the layer lead to the onset of convection, where the buoyancy forces due to the density changes overcome the viscosity forces in the fluid. The Rayleigh number at this point is called the critical Rayleigh number where the convection starts to form and grow. In fact, Rayleigh number is important as indication of the presence and strength of convection within a fluid.

Mathematically, the Rayleigh number can be described as a product of the Grashof number and the Prandtl number. The Grashof number and the Prandtl number are defined as the relationship between buoyancy and viscosity and the relationship between momentum diffusivity and thermal diffusivity, respectively. Thus, the Rayleigh number itself can be defined as the ratio of buoyancy and viscosity forces times the ratio of momentum and thermal diffusivities. Below are the definitions of the Grashof number, Prandtl number and Rayleigh number:

$$Gr = \frac{\hat{g}\beta\Delta T l^3}{\nu^2}, \tag{1.7}$$

$$\Pr = \frac{\nu}{\alpha}; \quad \nu = \frac{\mu}{\rho}, \tag{1.8}$$

$$Ra = \frac{\rho\hat{g}\beta\Delta T l^3}{\mu\alpha}, \tag{1.9}$$

where $\beta, \hat{g}, \rho, \alpha, \mu, \nu, l$ and ΔT are the thermal expansion coefficient, acceleration due to gravity, fluid density, thermal diffusivity, dynamic viscosity, kinematic viscosity, length scale and reference temperature drop, respectively.

Since in this study, we were looking at the onset of convection in porous media, it is more relevant to use the porous Rayleigh number also known as the Darcy-Rayleigh number. It is the product of the Rayleigh number in equation (1.9) and the Darcy number:

$$\text{Darcy number} = \frac{K}{l^2}, \tag{1.10}$$

which produces the following

$$\text{Darcy-Rayleigh number} = \frac{\rho\hat{g}\beta\Delta T K l}{\mu\alpha}. \tag{1.11}$$

This number plays the same role as the clear fluid Rayleigh number as it represents the balance of viscous and buoyancy forces. Note that when *Ra* is used in this thesis it is the Darcy-Rayleigh number which is being referred to. We also use Ra_c to denote the critical Darcy-Rayleigh number.

1.5 Approximations and assumptions

1.5.1 Oberbeck-Boussinesq approximation

The Oberbeck-Boussinesq approximation is commonly included within the formulation of the momentum equation to consider the effect of buoyancy. By employing this approximation, all the properties of the porous medium are assumed to be constant except for the density. However, the changes in density are then also neglected except in the buoyancy term. In modern notation the flow in a porous medium was defined by Darcy as:

$$u = -\frac{K}{\mu}\frac{\partial p}{\partial x}, \tag{1.12}$$

and this applied when the fluid is isothermal, but when considering natural or mixed convection, it is necessary to add a gravitational term to the right hand side of the Darcy's equation because equation (1.12) is valid for a horizontal direction, whereas in the vertical direction (*z*), the pressure varies naturally with height. This can be related to Darcy's law through the hydrostatic $\rho_f \hat{g} z$ term as follows:

$$p = p^* + \rho_f \hat{g} z. \tag{1.13}$$

In order for convection to occur, the density of the fluid must be dependent on the temperature. Thus the equation for fluid density is equal to:

$$\rho_f = \rho_r \left[1 - \beta\left(T - T_r\right)\right], \tag{1.14}$$

where ρ_f, ρ_r, β, T, T_r, p, p^*, $\hat{g}$ and z are fluid density, fluid density at reference temperature, coefficient of thermal expansion, temperature, reference temperature, fluid pressure, atmospheric pressure, acceleration due to gravity and vertical distance, respectively. We consider only the vertical or *z*-direction at this point, for which the velocity is *w*. Thus, we have

$$w = -\frac{K}{\mu}\left[\frac{\partial p^*}{\partial z} + \rho_f \hat{g}\right], \tag{1.15}$$

and the substitution of equation (1.14) into equation (1.15) followed by the factorizing of the first two terms in the resulting equation to define a reference for some reference density and temperature, equation (1.14) becomes:

$$w = -\frac{K}{\mu}\frac{\partial p}{\partial z} + \frac{\rho_r \hat{g}\beta K}{\mu}\left(T - T_r\right), \tag{1.16}$$

where $\frac{\partial p}{\partial z} = \frac{\partial p^*}{\partial z} + \rho_r \hat{g}$. The horizontal counterpart is dimensionalised version required for conclusion with the continuity equations becomes:

$$u = -\frac{K}{\mu}\frac{\partial p}{\partial x}. \tag{1.17}$$

According to Tritton [6], the Boussinesq approximation relies on a few assumptions. These include (i) the neglecting of the viscous heating; (ii) the ignoring of the temperature variation of the viscosity; (iii) the density differences produced from the imposed temperature differences are small and (iv) the heights over which various parameters change by appreciable fraction are much larger than the size of the physical domain being considered.

1.5.2 Local thermal equilibrium

The condition where a single temperature is used to describe a heat transfer process in a multiple phase system is referred as local thermal equilibrium (LTE). Note that this doesn't need to be considered and doesn’t exist as a concept for a pure fluid flow, but the temperature at a point in a porous medium is formally an averaged quantity over a small region surrounding that point over both the fluid and the solid

phases. The first law of thermodynamics in porous medium is applied when the porous medium is assumed to be isotropic and the viscous dissipation , radiation, and work done by pressure changes are negligible. Thus, the governing equations are then given by (see Nield and Bejan [1]):

$$\phi(\rho c)_f \frac{\partial T_f}{\partial t} + (\rho c)_f \left(u.\nabla T_f\right) = \phi k_f \nabla^2 T_f + \phi q_f''', \tag{1.18}$$

$$(1-\phi)(\rho c)_s \frac{\partial T_s}{\partial t} = (1-\phi) k_s \nabla^2 T_s + (1-\phi) q_s'''. \tag{1.19}$$

The subscripts s and f are refer to solid and fluid phases respectively. *c* is the specific heat, *k* is the thermal conductivity and q''' is the heat production per unit volume respectively. We could neglect the q''' terms in the solid and fluid since there is no heat generation involved in either the solid or fluid phases. Therefore, equation (1.18) and (1.19) become:

$$\phi(\rho c)_f \frac{\partial T_f}{\partial t} + (\rho c)_f \left(u.\nabla T_f\right) = \phi k_f \nabla^2 T_f, \tag{1.20}$$

$$(1-\phi)(\rho c)_s \frac{\partial T_s}{\partial t} = (1-\phi) k_s \nabla^2 T_s. \tag{1.21}$$

In most of the chapters of this thesis, it is assumed that the system in porous medium is in the state of LTE that is the temperature and the rate of heat flux at the interface between fluid and solid are in equilibrium such that $T_s = T_f = T$. Adding equation (1.20) and (1.21) therefore resulted to:

$$(\rho c)_m \frac{\partial T}{\partial t} + (\rho c)_f \left(u.\nabla T\right) = k_m \nabla^2 T, \tag{1.22}$$

which

$$(\rho c)_m = \phi(\rho c)_f + (1-\phi)(\rho c)_s, \tag{1.23}$$

$$k_m = \phi k_f + (1-\phi) k_s. \tag{1.24}$$

Dividing equation (1.22) with $(\rho c)_f$ yields the governing heat transport equation used in this thesis.

$$\sigma \frac{\partial T}{\partial t} + (u.\nabla T) = \alpha \nabla^2 T, \tag{1.25}$$

which

$$\sigma = \frac{(\rho c)_m}{(\rho c)_f}, \text{ and } \alpha = \frac{k_m}{(\rho c)_f}. \tag{1.26}$$

1.5.3 Local thermal nonequilibrium

It is possible to create a situation where a temperature which has been averaged over the fluid phase will be different from that which is averaged over the solid phase. An example is the sudden flushing of a cold saturated porous medium by a hot fluid. In the study of fluid flow and heat transfer, it is commonly assumed that the system is in LTE in which the temperature at the boundary between the fluid and solid are at equal. However, there are situations such as highly transient problems and several steady state problems where the assumptions break down, these cases are referred to as local thermal nonequilibrium (LTNE) cases. In one of the chapters of this thesis, it is assumed that the system in porous medium is in the state of LTNE and the governing equations are then given by (see Nield and Bejan [1]):

$$\phi(\rho c)_f \frac{\partial T_f}{\partial t} + (\rho c)_f (u.\nabla T_f) = \phi k_f \nabla^2 T_f + h(T_s - T_f), \tag{1.27}$$

$$(1-\phi)(\rho c)_s \frac{\partial T_s}{\partial t} = (1-\phi) k_s \nabla^2 T_s - h(T_s - T_f). \quad (1.28)$$

The subscripts *f* and *s* refer to the fluid and solid phase respectively, while other fluid and medium properties are as follow: ϕ is the porosity, ρ is the reference density, c is the specific heat, T is the temperature and k is the thermal conductivity. Finally h is the inter-phase heat transfer coefficient and this term acts as a source/sink to model the microscopic transfer of heat between the phases whenever they are locally different in the macroscopic or averaged sense. There are very many correlations in the literature relating the value of *h* to the conductivities of the phases and the geometry of the porous medium.

1.6 Stability of Darcy-Bénard problem

The theoretical study of convection in a porous medium heated uniformly from the lower boundary dates back to the stability analyses of Horton & Rogers [7] and Lapwood [8] which is the well-known Horton-Rogers-Lapwood, porous Bénard or Darcy-Bénard problem. These three authors have pointed out the possibility of free convection in a porous medium heated uniformly from the lower boundary and is similar to Bénard convection. Since then, the stability of the system becomes the main concern when the fluid is heated from below because it might cause instability which cannot arise when the heating is initiated from above. The effect of the heating process from below change the temperature of the system and this initiate the convection process, thus changes the stability of the system. The occurrences of stability to instability convection are determined by the critical value of Darcy-Rayleigh number, Ra_c. When the temperature difference is great enough, which is the effect from the heating process that changes the temperature of the fluid, the stabilising effects of thermal conductivity and viscosity are overcome by the destabilising buoyancy forces. This phenomenon is called *the onset of convection.* At

this point the value of the Darcy-Rayleigh number is now called the critical Darcy-Rayleigh number, Ra_c which is the lowest point of the neutral or marginal stability curve. Practically, Ra_c can be found by perturbing the basic state of the system analytically or numerically and by using linear stability analysis**.** In linear stability analysis, the initial idea is to perturb the basic state with a small magnitude disturbance whose amplitude is proportional to exp[λt] and by solving the resulting eigenvalue problem to find the exponential growth rate, λ by setting:

$$\psi = \Psi \text{ and } \theta = 1 - z + \Theta, \tag{1.29}$$

into the governing equations, where 1 - z is the basic temperature field. Refer to Appendix (page 23) for a detailed derivation of equation (1.29).

After considering that $|\Psi| \ll 1$ and $|\Theta| \ll 1$ and neglecting the products of perturbations with one another, the following partial differential system is obtained:

$$\Psi_{xx} + \Psi_{zz} = Ra\Theta_x, \tag{1.30a}$$

$$\Theta_t - \Psi_x = \Theta_{xx} - \Theta_{zz}, \tag{1.30b}$$

which are then transformed into ordinary differential eigenvalue form after substituting the following equations containing the exponential growth rate, λ:

$$\Psi = f(z)e^{\lambda t}\sin(kx) \text{ and } \Theta = g(z)e^{\lambda t}\cos(kx). \tag{1.31}$$

In this equations λ is the exponential growth rate and k is the wavenumber of the disturbance. Equations (1.30a) and (1.30b) then reduce to

$$f'' - k^2 f + Rakg = 0, \tag{1.32a}$$

$$g'' - k^2 g = kf + \lambda g, \tag{1.32b}$$

subject to the homogeneous boundary conditions $f = g = 0$ on $z = 0,1$. Equations (1.32) form an eigenvalue problem for λ in terms of k and Ra. In fact, equations (1.32) may be solved analytically in terms of sines:

$$f = -\frac{k^2 + n^2\pi^2 + \lambda}{k} A \sin n\pi z, \tag{1.33a}$$

$$g = A \sin n\pi z, \tag{1.33b}$$

is the solution for n convective rolls stacked above each other, where n is also known as the mode number and A is the amplitude which may take any value since this is an eigenvalue problem, and thus the amplitudes f and g are undetermined. The variation of λ with k and Ra may then be found and is given by $\lambda = \frac{Rak^2}{k^2 + n^2\pi^2} - \left(k^2 + n^2\pi^2\right)$. When λ (or more generally, the real part of λ) has the negative sign, it implies that disturbances will decay exponentially with time and therefore the system is said to be linearly stable. When the sign is positive this implies that disturbances are unstable due to the fact that disturbances now grow exponentially with time and eventually nonlinear effects take charge and suppress that growth. However, setting $\lambda = 0$ in the above expression gives the following relationship between Ra and k,

$$Ra = \frac{\left(k^2 + n^2\pi^2\right)^2}{k^2}, \tag{1.34}$$

which, when plotted yields the neutral stability curve or marginal stability curve. The dependence of Ra and k for the different values of n is illustrated in Figure 1.3 which shows the neutral curves for the first three modes $\left(n = 1,2,3\right)$ in the classical Darcy-Bénard problem, where n must be an integer in order that the upper boundary conditions are satisfied.

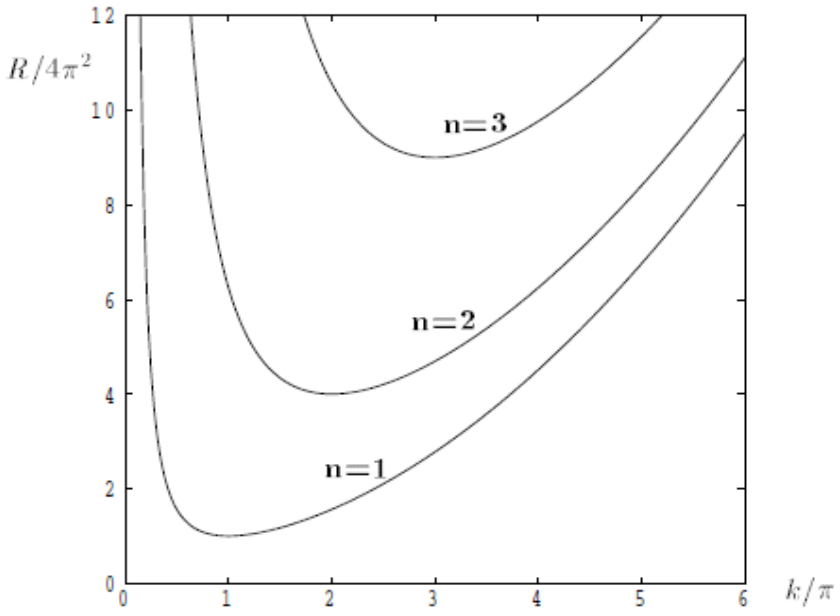

Figure 1.3: Neutral stability curves for the first three modes of the classical Darcy-Bénard problem (Rees, 2001).

The minimum value of *Ra* in (1.34) is called the critical Rayleigh number, Ra_c and it is equal to $4\pi^2$ when n=1. The corresponding critical wavenumber is $k_c = \pi$. Generally, the observation from Figure 1.3 is that, as n increases, the critical values of *Ra* and k also increase. The curve when $n=1$ (mode 1) is called the basic neutral stability curve of the classical Darcy-Bénard problem. Therefore, in an unbounded layer, all disturbances decay, i.e. are stable, when $Ra < 4\pi^2$, but when $Ra > 4\pi^2$, there is a range of values of k for which disturbance grow i.e they are unstable. The convection pattern of the first three modes are shown in Figure 1.4.

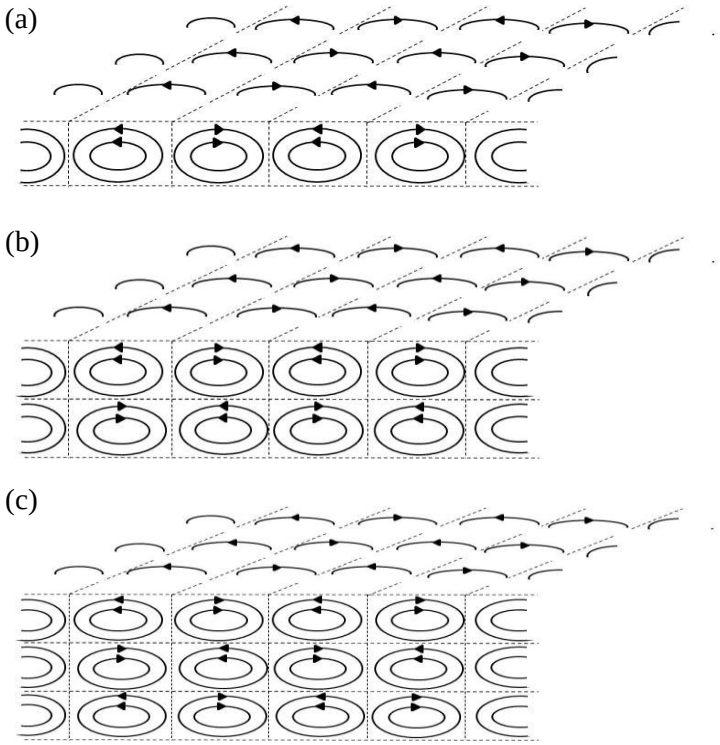

Figure 1.4: Convection cells corresponding to (a) $n = 1$, (b) $n = 2$, (c) $n = 3$

Note that, this detailed analysis of the Darcy-Bénard problem is illustrative of the various other analyses in the thesis such as the unsteady basic state discussed in chapter 2, layered medium considered in chapter 3 and 4, and a weakly nonlinear analysis of a case where local thermal nonequilibrium arises as reviewed in chapter 5, although the detailed analyses themselves are quite different.

1.7 Applications

This section explains the application of the works in this thesis. It is divided into (i) the general applications, (ii) the groundwater applications and (iii) the geothermal reservoir applications.

1.7.1 General applications

Nield and Bejan [1] have discussed some geophysical applications involving convection in porous media. The first application involves snow where in a dry snow cover, an unstable air density gradient is not uncommon, as the base is often warmer than the upper surface. Factors such as the geothermal heat flux, the heat release due to seasonal delay and the release of heat if the soil freezes tend to keep the snow cover near 0^oC at the bottom. By contrast, the upper boundary is commonly close to the ambient air temperature, which can be below 0^oC for long periods of time in cold climates. When the unsteady air density gradient within the snow becomes sufficiently large, convection happens and the rate of transport of both heat and vapour increases and the snow experiences metamorphosis of its crystalline structure.

The second application is with the formation of patterned ground. The ground in the arctic and mountainous regions give the appearance of regular patterns of circles, stripes or polygons, and processes such as the isolation of stones and fines resulting from diurnal, seasonal, or other repetitive freeze-thaw cycles in water-saturated soils make these shapes prominent. These patterns are also found submerged, in shallow lakes, or close to shores. The formation of patterned ground typically involves hexagonal cells within horizontal ground and roll cells or helical coils in sloped terrain when convection due to gravitation occurs (Ray et al [10]). These standard cellular flow designs can then be impressed on the underlying ice front, because in regions of down flow the hotter descending water causes additional melting, while in regions of up flow the rising cooler water prevents melting of the

ice front. Thus, the ice level is brought down beneath descending streams and raised over rising streams, relative to the mean level. In this way a design of routinely divided crests and troughs is shaped on the fundamental ice front that mirrors the cellular convection designs within the defrosted layer.

1.7.2 Groundwater application

When the rain falls and the snow melts into the ground, the water does not stop moving. Some of the water flows along the surface to the streams or lakes, some of it is used by plants, some evaporates and returns to the atmosphere and some is absorbed into the ground. The water that is found underground in the cracks and spaces in soil, sand and rock is called groundwater and the locations where it may be found are often called aquifers. The study of groundwater and its movement has become increasingly important as the world's population and industrial development expand, and the demand for water, particularly groundwater, will increase. Not only it is important to locate new groundwater sources, but once found, these sources must be protected from pollution and managed properly to ensure that users do not withdraw more water than can be replenished. Thus it is important to know and understand the behavior of the groundwater dynamics and solute distributions in many natural systems.

During the day, the sun will heat up the earth's ground and by night it will cool down. Questions such as how the rates of transfer of both heat and solute rates of transfer are affected during this natural mechanism? For example, should the water-bearing soil or rock contain a contaminant then the presence of a convective instability will cause that contaminant to spread, and therefore it is important to model these situations..

1.7.3 Geothermal reservoirs application

Since heat always moves from hotter regions to the colder regions, the earth's heat flows from its interior toward the surface. This flow drives convection motion in the mantle rock which in turn drives plate tectonics. When the plates move apart, a new crust is formed from magma rising into the rift. Whenever magma reaches the surface it can build volcanoes. However most magma stays well below ground and creates huge subterranean regions of hot rock. These shallow regions have high temperature gradients. In some regions with high temperature gradients, there are deep subterranean faults and cracks that allow rainwater and snowmelt to seep underground sometimes miles below. Down there the water is heated up and boiled by the hot rock and creates sources of hot water. This hot water produces steam which is trapped in permeable and porous rocks under a layer of impermeable rock. This is the formation of a geothermal reservoir.

As geothermal fluids rise to the surface, an exchange of heat from the liquid to the encompassing rocks takes place. By the time such a geothermal fluid reaches the Earth’s surface it is often cooled down by some amount, and may well be equal to the mean surface temperature of the region. Once more such circumstances, where heat is being supplied from below, can cause convection to take place. In addition dissolved salts accumulate at the surface due to a net upward flow caused by surface evaporation, and this also causes an increase in fluid density at the upper surface. In turn this may cause convective instabilities; such an instability is called the Wooding problem. The lost heat is transferred either by conduction process to the ground or to by convection to the air/surface. Like oil and gas stores, geothermal reservoirs can be overproduced in case not appropriately managed. Overproduction of a store leads to a critical shortening of its beneficial lifetime and a loss of pay. Thus, besides determining the rock and reservoir properties, this research also provided understanding in the flow and mechanism of steam and hot water through reservoir rocks where steam flows at different rate through a geothermal reservoir.

1.8 References

[1] Nield, D.A., Bejan, A. (2013). Convection in Porous Media, 4th edn. New York: Springer.

[2] Pop, I., Ingham, D.B. (2001). Convective Heat Transfer: Mathematical and Computational Modelling of Viscous Fluids and Porous Medium. Oxford: Pergamon.

[3] Brown, G. (2000). Summary of Darcy's experiment. Retrieved April 1, 2013, from biosystems.okstate.edu/darcy.

[4] Lage, J.L. (1998). The Fundamental theory of flow through permeable media from Darcy to turbulence. *Transport Phenomena in Porous Media*, 1-30. Oxford: Elsevier.

[5] Getling, A.V. (1998). Rayleigh-Bénard Convection: Structures and Dynamics. World Scientific Publishing.

[6] Tritton, D. J. (1988). Physical Fluid Dynamics, 2nd edn. Oxford: Clarendon Press.

[7] Horton, C.W., Rogers, F.T. (1945). Convection currents in a porous medium. *Journal of Applied Physics*, **16**, 367.

[8] Lapwood, E.R. (1948). Convection of a fluid in a porous medium. *Mathematical Proceedings of the Cambridge Philosophical Society*, **44**, 508-521.

[9] Rees, D.A.S. (2001). Stability Analysis of Darcy-Bénard Convection. Lecture Notes from the Summer School on Porous Medium Flows, Neptun, Constanta, Romania, June, 25-29.

[10] Wooding, R.A., Tyler, S.W., White, I. (1997). Convection in groundwater below an evaporating salt lake: 1. Onset of instability. *Water Resources Research*, **33**, 1199-1217.

[11] Ray, R.J, Krantz, W.B., Caine, T.N., Gunn, R.D. (1983). A model for sorted ground regularity. *J. Glaciology*, **29**, 317-337.

1.9 Appendix

Consider the two-dimensional flow that is governed by Darcy's law, conditions are taken to be such that the Boussinesq approximation is valid, and therefore the properties such as density, viscosity and thermal diffusivity are taken to be constant except within the buoyancy term. The porous matrix and the fluid are also assumed to be in local thermal equilibrium, and therefore only one heat transport equation is used to model the temperature variations in the two phases simultaneously. Thus the governing equations for the two-dimensional flow are given by:

$$\frac{\partial \bar{u}}{\partial \bar{x}} + \frac{\partial \bar{w}}{\partial \bar{z}} = 0, \tag{A1.1a}$$

$$\bar{u} = -\frac{K}{\mu}\frac{\partial \bar{p}}{\partial \bar{x}}, \tag{A1.1b}$$

$$\bar{w} = -\frac{K}{\mu}\frac{\partial \bar{p}}{\partial \bar{z}} + \frac{\rho \hat{g} \beta K}{\mu}\left(T - T_{\infty}\right), \tag{A1.1c}$$

$$\frac{\partial T}{\partial \bar{t}} + \bar{u}\frac{\partial T}{\partial \bar{x}} + \bar{w}\frac{\partial T}{\partial \bar{z}} = \kappa\left[\frac{\partial^2 T}{\partial \bar{x}^2} + \frac{\partial^2 T}{\partial \bar{z}^2}\right], \tag{A1.1d}$$

where κ is the thermal diffusivity of the saturated porous medium. These equations are subject to boundary conditions:

$$\begin{aligned} &\bar{z} = 0: \quad \bar{w} = 0, \quad T = T_h, \\ &\bar{z} = 1: \quad \bar{w} \to 0, \quad T \to T_c. \end{aligned} \tag{A1.2}$$

Equation (1.1a) - (1.1d) may be nondimensionalised using the following transformations:

$$\left(\bar{x}, \bar{z}\right) = d\left(x, z\right), \quad \left(\bar{u}, \bar{w}\right) = \frac{\kappa}{d}\left(u, w\right), \quad \bar{p} = \frac{\kappa \mu}{K} p, \quad \theta = \frac{T - T_c}{\left(T_h - T_c\right)}, \quad \bar{t} = \frac{d^2}{\kappa} t, \tag{A1.3}$$

where d is a lengthscale (the height of the layer). In addition, the streamfunction ψ is introduced according to:

$$u = -\frac{\partial \psi}{\partial \bar{z}}, \quad w = \frac{\partial \psi}{\partial \bar{x}}, \tag{A1.4}$$

which therefore satisfies the continuity equation in equation (A1.1a). After eliminating the pressure gradient in equations (A1.1b) and (A1.1c), now, the nondimensional forms of the equations (A1.1b) to (A1.1d) are:

$$\frac{\partial^2 \psi}{\partial x^2} + \frac{\partial^2 \psi}{\partial z^2} = Ra \frac{\partial \theta}{\partial x}, \tag{A1.5a}$$

$$\frac{\partial \theta}{\partial t} + \frac{\partial \psi}{\partial x}\frac{\partial \theta}{\partial z} - \frac{\partial \psi}{\partial z}\frac{\partial \theta}{\partial x} = \frac{\partial^2 \theta}{\partial x^2} + \frac{\partial^2 \theta}{\partial z^2}, \tag{A1.5b}$$

where the Darcy-Rayleigh number is

$$Ra = \frac{\rho \hat{g} \beta \left(T_h - T_c\right) Kd}{\mu \kappa}. \tag{A1.6}$$

and boundary condition (A1.2) becomes:

$$\begin{aligned} &z = 0: \ \psi = 0, \ \theta = 1, \\ &z = 1: \ \psi = 0, \ \theta = 0. \end{aligned} \tag{A1.7}$$

Given the above boundary condition, which are uniform in the x-direction, we expect the basic solution to be independent of x. The basic state, which consists of no flow and a linear temperature profile, are:

$$\psi = 0, \text{ and } \theta = 1 - z. \tag{A1.8}$$

These are the solutions for the basic state that we perturb in subsection 1.6, equation (1.29)

Chapter 2

The Onset of Convection in The Unsteady Thermal Boundary Layer Above a Sinusoidally Heated Surface Embedded in a Porous Medium.

2.1 Abstract

The linear stability of an unsteady thermal boundary layer in a semi-infinite porous medium is considered. This boundary layer is induced by varying the temperature of the horizontal boundary sinusoidally in time about the ambient temperature of the porous medium; this mimics diurnal heating and cooling from above in subsurface groundwater. On assuming that the heating varies sinusoidally with time, the basic state is essentially the thermal analogue of a Stokes wave, which is travelling wave which decays exponentially with depth. Thus if instability occurs, it will happen in those regions where cold fluid lies above hot fluid, and this is not necessarily a region which includes the bounding surface. A linear stability analysis is performed using small-amplitude disturbances of the form of monochromatic cells with wavenumber, k. This yields a parabolic system describing the time-evolution of small-amplitude disturbances which are solved using the Keller box method. The critical Darcy-Rayleigh number as a function of the wavenumber is found by iterating on the Darcy-Rayleigh number so that no mean growth occurs over one forcing period. It is found that the most dangerous disturbance has a period which is twice that of the underlying basic state. Cells which rotate clockwise at first tend to rise upwards from the heated lower surface and weaken, but they induce an

anticlockwise cell near the surface at the end of one forcing period which is otherwise identical to the clockwise cell found at the start of that forcing period. Therefore we find that the instability has twice the period of the thermal forcing itself.

2.2 Nomenclature

A	Amplitude
f	reduced streamfunction
g	reduced temperature
$\hat{g}$	gravity
k	wavenumber
k_c	critical wavenumber
K	permeability
L	length scale
p	pressure
$\bar{p}$	pressure (dimensional)
Ra, Ra_c	Darcy-Rayleigh number, critical Darcy-Rayleigh number
t	time
T	temperature (dimensional)
u	velocity in the x-direction
$\bar{u}$	velocity in the x-direction (dimensional)

w	velocity in the z-direction
$\bar{w}$	velocity in the z-direction (dimensional)
x	horizontal coordinate
$\bar{x}$	horizontal coordinate (dimensional)
z	vertical coordinate
$\bar{z}$	vertical coordinate (dimensional)

Greek letters

α	thermal diffusivity
β	thermal expansion coefficient
ΔT	temperature difference
θ	temperature (nondimensional)
Θ	temperature disturbance
λ	exponential growth rate
μ	dynamic viscosity
ρ	reference density
σ	heat capacity ratio
ψ	streamfunction
Ψ	streamfunction disturbance
ω	thermal forcing frequency

2.3 Introduction

The theoretical study of convection in a porous medium heated from below and cooled from above dates back to the pioneering stability analyses of Horton & Rogers [1] and Lapwood [2], and this forms the well-known Horton-Rogers-Lapwood or Darcy-Bénard problem. These authors showed that the critical parameters for the onset of convection are $Ra_c=4\pi^2$ and $k_c=\pi$ for a uniform horizontal porous layer heated from below. This porous medium analogue of the much older Rayleigh-Bénard problem shares many attributes of the latter. The neutral curve which describes the onset of convection is unimodal with one minimum in both cases, and weakly nonlinear analyses also show that two-dimensional rolls form the preferred pattern immediately post-onset (see Rees and Riley [3], Newell and Whitehead [4]). The porous medium configuration, as studied by Horton and Rogers [1] and Lapwood [2] also has the advantage that the analysis proceeds analytically even within the weakly nonlinear range, and therefore it forms a good pedagogical introduction to the study of weakly nonlinear theory.

This classical problem has been extended in a very large variety of ways. If the constant temperature surfaces are replaced by those with constant heat flux, then $Ra_c=12$ and $k_c=0$ (Nield [5]). If the porous medium is layered, then it is possible to have bimodal convection, where the neutral curve has two minima, and also to have convection with a square planform immediately post onset (McKibbin and O'Sullivan [6], Rees and Riley [7]). If the layer has a constant vertical through flow of fluid (Sutton [8]), then the bifurcation to convective flow is subcritical (Pieters and Schuttelaars [9], Rees [10]), meaning that strongly nonlinear flow exists at Rayleigh numbers below the linear threshold.

The present configuration belongs to a subgroup of papers which examines the stability properties of flows which are unsteady in time. Much is known about the system where the temperature of a bounding surface is raised or lowered suddenly, thereby causing an expanding basic temperature field to be described by the

complementary error function. Examples of these works include those by Elder [11], Caltagirone [12], Wooding et al. [13], Kim et al [14], Riaz et al. [15], Selim and Rees ([16], [17], [18], [19]) and Noghrehabadi et al. [20], and these and many others are reviewed in Rees et al. [21].

Substantially less attention has been paid to the onset properties when the boundary temperature of a semi-infinite domain varies sinusoidally with time about the ambient conditions. Such a configuration approximates natural heating processes of the earth's surface and the diurnal behavior of lakes and reservoirs (see Farrow and Patterson [22], Lei and Patterson [23]). Such problems also form a subset of the more general class of flows where boundary effects are time-dependent (see Otto [24], Hall [25] and Blennerhassett and Bassom [26]).

For convective instability to arise it is necessary for the critical Rayleigh number to be sufficiently large and positive. For the present case the boundary temperature rises above and falls below the ambient temperature in a periodic manner, and therefore the mean temperature difference between the boundary and the ambient is zero. This would suggest, perhaps, that all disturbances will decay. In detail, it is quite possible for a disturbance to grow in strength during the short phase when the boundary temperature is near its maximum, but that disturbance will also decay over a much longer period of time and hence one would expect overall stability. However, May and Bassom [27] presented detailed linear and nonlinear analyses of the analogous clear-fluid form of the present problem, demonstrating that the above *a priori* thinking is too simplistic, for it is possible to determine a minimum Rayleigh number above which disturbances will grow and achieve overall instability. Later, we shall discuss the physical mechanism by which this is possible.

Thus the present chapter comprises a first step within the context of porous media in acquiring an understanding of the manner in which instability develops when the boundary exhibits sinusoidal temperature variations in time. A detailed numerical analysis is presented, and it is found not only that the basic state may be

destabilised, but that convection cells move upwards and away from the surface and decay as time progresses; these cells are replaced by cells with the opposite circulation. It is also found that the period of the disturbances is twice that of the boundary forcing.

2.4 Governing equations

We study the linear stability of an unsteady thermal boundary layer in a semi-infinite porous medium which is bounded from below by a horizontal impermeable surface that is located at $z = 0$, as shown in Figure 2.1. This stability problem is identical mathematically to the one which arises when the upper surface of a water-bearing soil is subject to diurnal heating and cooling, and where ambient conditions exist at a sufficient depth. The temperature of the surface is assumed to vary sinusoidally in time according to $T = T_\infty + \Delta T \cos(\omega t)$, where T_∞ is the ambient temperature far from the heated surface. The normal velocity at the surface is zero.

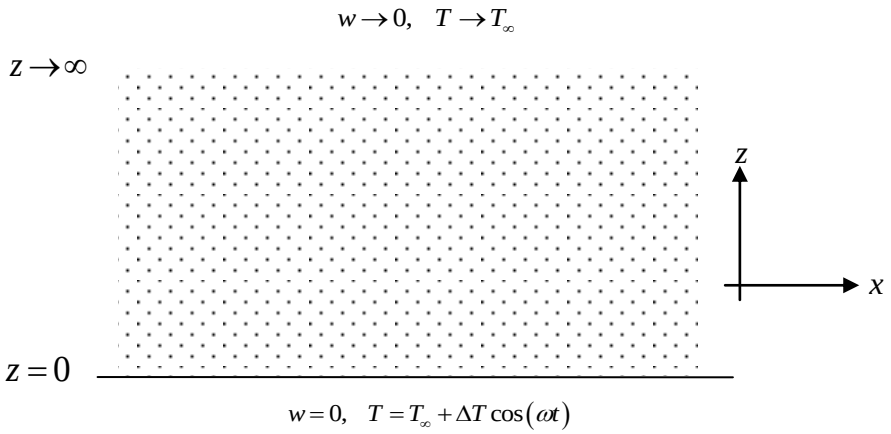

Figure 2.1**:** Depicting the semi-infinite porous medium and the imposed boundary conditions.

The porous medium is also assumed to be isotropic and homogeneous, the fluid to be Newtonian, and the flow to be governed by Darcy's law. In addition, conditions are taken to be such that the Boussinesq approximation is valid, and therefore material properties such as density, viscosity and thermal diffusivity are taken to be constant except within the buoyancy term. Finally, the porous matrix and the fluid are also assumed to be in local thermal equilibrium, and therefore only one heat transport equation is used to model the temperature variations in the two phases simultaneously. The governing equations for unsteady two-dimensional flow are given by:

$$\frac{\partial \bar{u}}{\partial \bar{x}} + \frac{\partial \bar{w}}{\partial \bar{z}} = 0, \tag{2.1a}$$

$$\bar{u} = -\frac{K}{\mu}\frac{\partial \bar{p}}{\partial \bar{x}}, \tag{2.1b}$$

$$\bar{w} = -\frac{K}{\mu}\frac{\partial \bar{p}}{\partial \bar{z}} + \frac{\rho \hat{g} \beta K}{\mu}\left(T - T_{\infty}\right), \tag{2.1c}$$

$$\sigma \frac{\partial T}{\partial \bar{t}} + \bar{u}\frac{\partial T}{\partial \bar{x}} + \bar{w}\frac{\partial T}{\partial \bar{z}} = \alpha\left[\frac{\partial^2 T}{\partial \bar{x}^2} + \frac{\partial^2 T}{\partial \bar{z}^2}\right]. \tag{2.1d}$$

These equations are subject to boundary conditions:

$$\bar{z} = 0: \quad \bar{w} = 0, \quad T = T_{\infty} + \Delta T \cos\left(\omega t\right),$$

$$\bar{z} \to \infty: \quad \bar{w} \to 0, \quad T \to T_{\infty}. \tag{2.2}$$

In these equations $\bar{x}$ and $\bar{z}$ are the dimensional horizontal and vertical coordinates, respectively, while $\bar{u}$ and $\bar{w}$ are the respective fluid flux velocities. Also, $\bar{p}$ is pressure, T the temperature, K permeability, μ the dynamic viscosity of the fluid, ρ the reference density (i.e. at $T = T_{\infty}$), $\hat{g}$ gravity, β the coefficient of cubical

expansion, σ the heat capacity ratio of the saturated medium to that of the fluid, and α the thermal diffusivity of the saturated medium. The heated surface has a spatially uniform but time-varying surface temperature distribution, $T = T_\infty + \Delta T \cos(\omega t)$, where ΔT is the maximum temperature difference between the wall and the ambient medium.

The resulting two-dimensional flow and temperature field may be studied by introducing the following transformations:

$$(\bar{x},\bar{z}) = L(x,z),\quad (\bar{u},\bar{w}) = \frac{\alpha}{L}(u,w),\quad L = \sqrt{2\alpha/\omega\sigma},\quad T = T_\infty + \Delta T\theta,\quad \bar{t} = \frac{2\pi t}{\omega}, \tag{2.3}$$

and a streamfunction, ψ, is defined according to,

$$u = -\frac{\partial\psi}{\partial\bar{z}},\quad w = \frac{\partial\psi}{\partial\bar{x}}. \tag{2.4}$$

It is to be noted that there is no physical lengthscale which can be used such as the depth of a layer, but the lengthscale, L, which is used here is one which arises naturally and is the thermal penetration depth due to the time-varying boundary temperature. Its nondimensional counterpart is, therefore, equal to precisely unity. On using Eqs. (2.3) and (2.4), Eqs. (2.1a) - (2.1d) are transformed into the following nondimensional form.

$$\frac{\partial^2\psi}{\partial x^2} + \frac{\partial^2\psi}{\partial z^2} = Ra\frac{\partial\theta}{\partial x}, \tag{2.5a}$$

$$\frac{1}{\pi}\frac{\partial\theta}{\partial t} + \frac{\partial\psi}{\partial x}\frac{\partial\theta}{\partial z} - \frac{\partial\psi}{\partial z}\frac{\partial\theta}{\partial x} = \frac{\partial^2\theta}{\partial x^2} + \frac{\partial^2\theta}{\partial z^2}, \tag{2.5b}$$

where the Darcy-Rayleigh number is

$$Ra = \frac{\rho\hat{g}\beta\Delta TKL}{\mu\alpha},$$

and the nondimensional forcing period is equal to 1.

2.5 Basic state

The continuity equation, (2.1a), is satisfied automatically by Eq. (2.4). Equations (2.5a) and (2.5b) now have to be solved subject to the boundary conditions:

$$z = 0 : \ \psi = 0, \ \theta = \cos\left(2\pi t\right); \quad z \to \infty : \ \psi \to 0, \ \theta \to 0. \tag{2.6}$$

These boundary conditions suggest that the basic temperature profile will be a function solely of z and t because there is no agency at the boundaries which would cause an x-variation, and if an initial condition were to be independent of x then the subsequent evolution remains independent. Given the form of Eq. (2.5a), this means that the basic state consists of a motionless state with ψ equal to a constant, which we may set to zero without a loss of generality. Therefore, the heat transport equation of the purely conducting state is:

$$\frac{1}{\pi}\frac{\partial \theta}{\partial t} = \frac{\partial^2 \theta}{\partial z^2}, \tag{2.7}$$

where we set $\theta = \cos(2\pi t)$ at $z = 0$, and $\theta \to 0$ as $z \to \infty$. The solution may be obtained by setting,

$$\theta = \mathrm{Re}\left[e^{2\pi i t} f\left(z\right)\right], \tag{2.8}$$

where $f(0)=1$ and $f(z) \to 0$ as $z \to \infty$. Therefore the basic streamfunction and temperature profiles are:

$$\psi = 0, \ \theta = e^{-z} \cos\left(z - 2\pi t\right). \tag{2.9}$$

The temperature field given in Eq. (2.9) is the thermal equivalent of the well-known Stokes layer which is induced by a plane surface executing sinusoidal movements parallel to itself in a Newtonian fluid. As has been noted already the basic state has a nondimensional period equal to unity. The rate of heat transfer at the surface is given by $\theta_z\left(z=0\right)$ and is;

$$\theta_z\left(z=0\right)=\sin 2\pi t-\cos 2\pi t \tag{2.10}$$

The main focus of the present chapter is on the stability of the time-dependent state given by Eq. (2.9) to disturbances of small amplitude which also exhibit an *x*-dependence. For now, it is worth noting that when *t* is close to an integer value, the surface is hotter than the fluid which lies immediately above it, and it is at these points in time that the porous medium is likely to be most susceptible to instability. At intermediate times, such as when *t* is an odd multiple of ½, the lower boundary is colder than the fluid above it, and we would expect those disturbances near to the surface (which occupy a relatively large region of cooler fluid sitting below warmer fluid) to decay. Therefore we have an *a priori* expectation that only those parts of each period which are close to integer values of *t* will be susceptible to instability. Figure 2.2 shows the graph of the temperature and rate of heat transfer at the surface a function of time, *t*, as given in Eq. (2.9). The temperature of the system takes the value of 1 when the lower surface is at the hottest and -1 at its coolest.

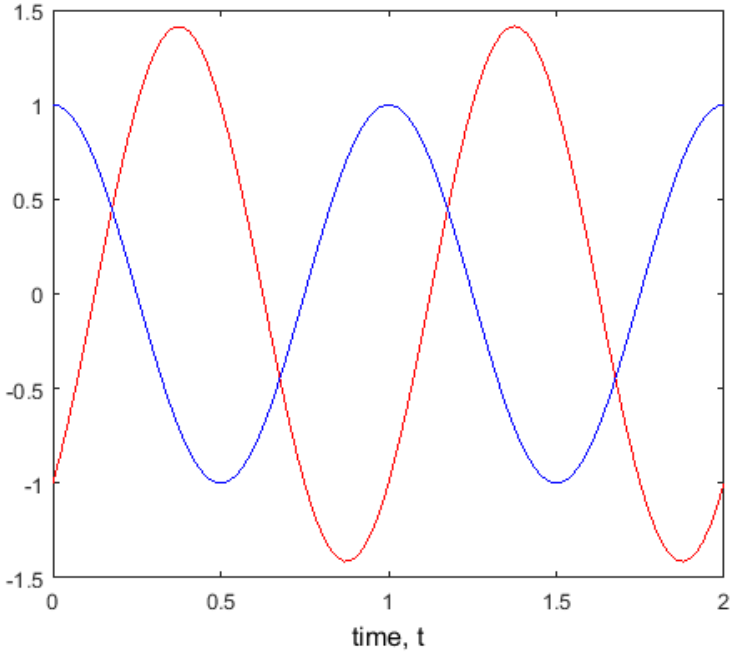

Figure 2.2: Variation of the surface temperature (blue line) and temperature gradient (red line) with time.

2.6 Basic Temperature Profile

Figure 2.3 shows the graph of the basic state as a function of distance in the *z*-direction. Ten profiles have been plotted, each at a different phase of the thermal forcing period. When the surface is hot, there is a relatively large region of hot fluid sitting beneath the relatively cold ambient fluid. Therefore we expect this phase to be more susceptible to instability. As the surface cools the region of potentially unstable fluid moves upwards and it also decays in time. After half a period the surface is now colder than the ambient and disturbances are expected to decay, although they remain weak and will eventually induce instability when the surface heats up again.

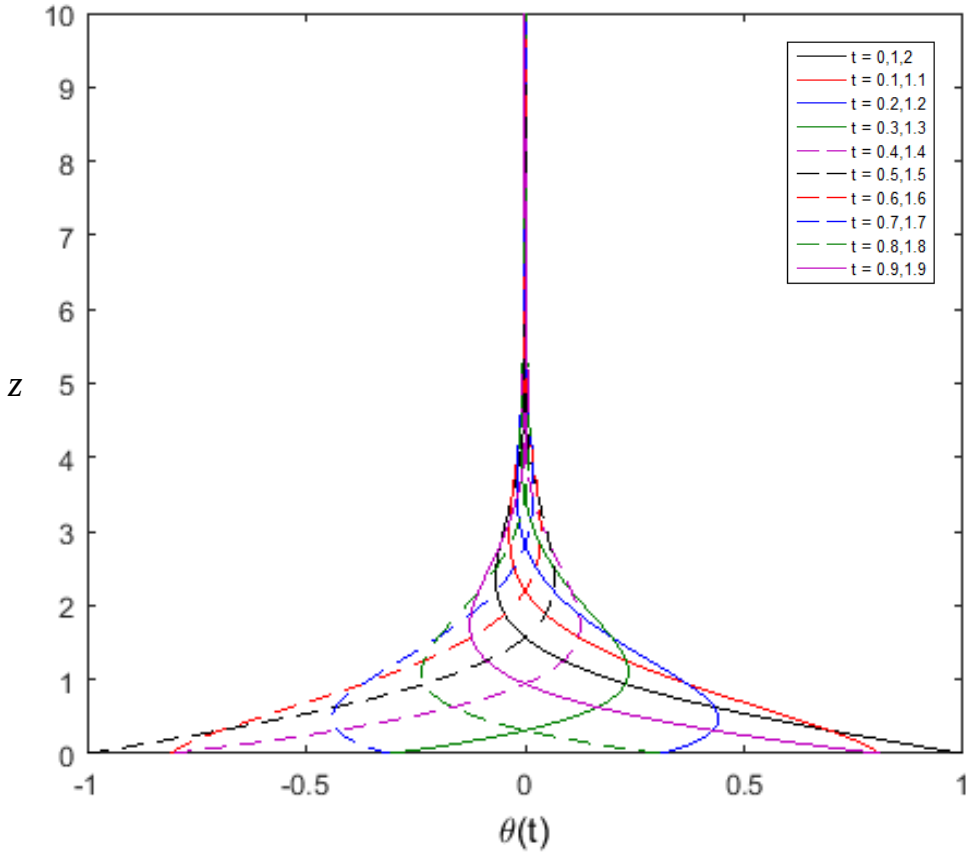

Figure 2.3: Graph of basic temperature profiles at different times

2.7 Linear stability analysis

Having the basic flow profile, linear stability theory may be used to determine the conditions under which the basic solution can be expected not to exist in practice, i.e. to be unstable to disturbances. More precisely, we aim to determine conditions for which disturbances are neutrally stable, i.e. they neither grow nor decay over multiples of the periodic forcing.

It may be shown (using the equivalent three-dimensional equations written in terms of primitive variables) that Squire's theorem holds, which means that it is

necessary only to consider two dimensional disturbances. Given that the governing equations and the basic state are independent of the orientations of the two horizontal coordinates, this is equivalent to saying that all three-dimensional disturbances are composed of sums or integrals of two-dimensional disturbances, and therefore it is sufficient only to consider two-dimensional disturbances.

A small-amplitude disturbance may now be introduced in order to perturb the solution given in Eq. (2.9) and therefore we set:

$$\psi = \Psi, \tag{2.11a}$$

$$\theta = e^{-z}\cos\left(z - 2\pi t\right) + \Theta, \tag{2.11b}$$

where both $|\Psi| \ll 1$ and $|\Theta| \ll 1$. On substituting Eqs. (2.11a) and (2.11b) into Eqs. (2.5a) and (2.5b) and neglecting those terms which are products of the disturbances, we obtain:

$$\Psi_{xx} + \Psi_{zz} = Ra\,\Theta_x, \tag{2.12a}$$

$$\frac{1}{\pi}\Theta_t - \Psi_x e^{-z}\left[\sin\left(z - 2\pi t\right) + \cos\left(z - 2\pi t\right)\right] = \Theta_{xx} + \Theta_{zz}, \tag{2.12b}$$

where subscripts denote partial derivatives. A closed system of disturbances may be obtained using the following substitutions:

$$\Psi = f\left(z,t\right)\sin\left(kx\right), \tag{2.13a}$$

$$\Theta = g\left(z,t\right)\cos\left(kx\right), \tag{2.13b}$$

which represent a monochromatic train of convection cells with an as-yet unknown vertical and temporal variation. This pattern, which is periodic in the horizontal direction, has the wavenumber, k, and hence its wavelength is $2\pi/k$. Using Equations (2.13a) and (2.13b), the reduced linearised disturbance equations take the form:

$$f'' - k^2 f + Ra\, kg = 0, \tag{2.14a}$$

$$g'' - k^2 g + kfe^{-z}\left[\sin\left(z - 2\pi t\right) + \cos\left(z - 2\pi t\right)\right] - \frac{1}{\pi} g_t = 0, \tag{2.14b}$$

and these have to be solved subject to the boundary conditions:

$$f\left(0,t\right) = 0,\ g\left(0,t\right) = 0 \text{ at } z = 0,$$

$$f\left(z,t\right) = 0,\ g\left(z,t\right) = 0 \text{ as } z \to \infty. \tag{2.15}$$

We have no need to specify the initial conditions at $t = 0$ because the neutral curves which we obtain are independent of these conditions, although it has been found that the time taken to converge to time-periodic solutions sometimes depends on the nature of these initial conditions.

2.8 Numerical solutions

2.8.1 Numerical method

The reduced linearised disturbance equations (2.14a) and (2.14b), which are subject to the boundary conditions (2.15), and which are parabolic in time, were solved numerically using a Keller box method. For each wavenumber, the value of the Darcy-Rayleigh number was adjusted until no mean growth occurred over one period of the boundary forcing, and this yields marginal stability.

The second order differential equations in equations (2.14a) and (2.14b) that are subject to boundary conditions in equation (2.15) are reduced to first order form by introducing the following variables, let:

$$V_1 = f,$$

$$V_2 = f',$$

$$V_3 = g, \tag{2.16a}$$

$$V_4 = g'.$$

Substituting these into equations (2.14a) and (2.14b), we obtain:

$$V_1' - V_2 = 0,$$

$$V_2' - k^2 V_1 + kRaV_3 = 0, \tag{2.17a}$$

$$V_3' - V_4 = 0,$$

$$V_4' - k^2 V_3 - kV_1 e^{-y}\left[\sin\left(y - 2\pi t\right) + \cos\left(y - 2\pi t\right)\right] - \frac{1}{\pi}\frac{\partial V_3}{\partial t} = 0,$$

and the boundary conditions become:

$$V_1(0) = 0, \quad V_3(0) = 0,$$

$$V_1(\infty) = 0, \quad V_3(\infty) = 0. \tag{2.17b}$$

The standard methodology of the Keller box method is used here, and so the parabolic governing equations in (2.14a) and (2.14b) are rewritten first as a system of four first order differential equations in (2.17a) by the introduction of the four new dependent variables defined in equations (2.16a) and (2.16b); details of how to do this are familiar to all practitioners of the Keller box method, and are omitted for the sake of brevity (see Keller and Cebeci [28]). Next, the new system in (2.17a) is approximated by a finite difference method. Central difference approximations based halfway between the grid points in the *z*-direction are used. For the time-stepping,

either central differences (second order, based halfway between timesteps) or backward differences (first order, based at the new timestep) were used to complete the finite difference approximations. In both cases there is an implicit system of difference equations to solve. Finally, the full set of discretised equations are solved using a multi-dimensional Newton-Raphson scheme, where the iteration matrix takes a block-tridiagonal form, and the block-Thomas algorithm is used to iterate towards the solution at each timestep. Although the system being solved is linear, a near-black-box user-written code which can solve nonlinear systems was used. The code also employs numerical differentiation to form the iteration matrix required by the Newton-Raphson method.

Points on the neutral curve were found in the following way. For a chosen wavenumber, the critical value of the Rayleigh number is guessed, and the evolution of the disturbance is computed over a sufficient number of periods of the boundary forcing. Although disturbances for most problems involving linear instability exhibit an exponential growth rate once transients have decayed sufficiently, it is not obviously so for the present configuration. This is because one may now have an interval of time during each forcing period within which the disturbance grows in amplitude and another interval wherein it decays. However, if the disturbance is sampled at the end of each period, then this sampled amplitude does exhibit an exponential behavior in time once the starting transients have decayed. We may define the amplitude, *A*, of the disturbance as follows,

$$A(t) = \sqrt{\left[\int_0^\infty V_3^{\,2} dz\right]} = \sqrt{\left[\int_0^\infty g^2 dz\right]}, \tag{2.18}$$

and then the sampled amplitudes satisfy the relation,

$$A(n+1) = A(n)e^{\lambda}, \tag{2.19}$$

where λ is the exponential growth rate and n is an integer. Therefore the code runs over as many periods as are necessary for the starting transients to decay. More specifically convergence is deemed to have taken place when

$$\left|\frac{A(n+1)}{A(n)}-\frac{A(n+2)}{A(n+1)}\right|<10^{-6} \tag{2.20}$$

is satisfied. In practice, f and g were rescaled at the end of each period so that $A = 1$ at the beginning of each period, but the scaling which was used is then substituted into a formula which is the equivalent of (2.20); this allows for the possibility of having exceptionally large or small values of A due to the value of Ra being too far from the sought-after value on the neutral curve. This process yields the value of λ for the chosen Ra. After that, the Rayleigh number is perturbed slightly and a new exponential growth rate found. Then these data are used as part of an outer single-variable Newton-Raphson loop in order to converge towards that value of Ra for which λ = 0. This overall scheme worked robustly in all cases, despite consisting of two nested iteration schemes.

Finally, it was also possible to enwrap the above algorithm by adding one more outer loop to allow the wavenumber to vary by a small amount from its previous value. In this way convergence was optimised by using the converged solution for the one wavenumber as the initial guess for the next wavenumber, and thus the neutral curve was built up point-by-point.

2.8.2 Numerical accuracy

In all numerical work it is vitally important that there is an accurate assessment of the accuracy of the computations. In first instance the spatial accuracy was assessed. The initial spatial grid which was chosen corresponded to $dz = 0.05$ with $z_{max} = 10$. It was found that further increases in z_{max} demonstrated that more than

six significant figures of accuracy had been achieved for the same spatial step, and therefore the disturbance was well-contained by the computational domain. In addition, at least four significant figures of accuracy were demonstrated by grid refinement (interval halving), and therefore there was no need to use either smaller spatial steps or a larger computational domain. With regard to the timestep and the two timestepping methods, we used dt = 0.02, 0.01 and 0.005 for a small set of values of k in order to determine the critical Rayleigh number. The results of these computations are shown in Table 2.1.

In Table 2.1 we see first of all that the formal order of accuracy of the methods is reflected faithfully in the numerical data. Thus the difference between the values of Ra for dt = 0.02 and 0.01 is roughly double that of the difference between those for dt = 0.01 and 0.005 for the first order method and four times that for the second order method. We may also perform Richardson's extrapolation on these data to obtain more accurate values (see appendix 2.11 for the example of Richardson's extrapolation method). Doing this for the dt = 0.02 and 0.01 data (for k = 1) for the second order method yields Ra = 41.1406, while the equivalent value for the dt = 0.01 and 0.005 data is Ra = 41.1407. Given this latter value of Ra, it is clear that the dt = 0.005 solution has a relative error of 1.6×10^{-4}. The equivalent error for the first order method is 1.0×10^{-2}. We therefore conclude that the use of the second order method with dt = 0.005 will give solutions of more than acceptable accuracy. It will be noticed that the accuracy of the solutions reduces a little when k takes greater values. This happens because the disturbance tends to occupy a smaller region when k takes larger values (so that the disturbance retains an approximately 1×1 aspect ratio) and therefore the spatial resolution decreases. It is will shown later that the smallest value of Ra is in the vicinity of k = 1 where the accuracy is very good indeed.

k	Order 1			Order 2		
	dt = 0.02	dt = 0.01	dt = 0.005	dt = 0.02	dt = 0.01	dt = 0.005
1.0	39.5114	40.2806	40.6998	41.0355	41.1143	41.1341
2.0	42.0992	44.9746	46.5697	47.8046	48.1649	48.2544
3.0	52.6382	59.2835	63.3727	66.0481	67.7715	68.1918

Table 2.1. Values of Ra for k = 1, 2 and 3 for different timesteps and for the two timestepping methods.

2.8.3 Neutral curves

Figure 2.3 shows the neutral curve as computed by each method and, for the second order method, for the three different timesteps. Even graphically it is clear that the accuracy of the first order method is unacceptably poor.

The shape of the neutral curve has the same qualitative features as that of the Darcy-Bénard problem in that it has a well-defined single minimum (which is marked by the solid circle in Figure 2.3 and Ra grows in an unbounded fashion as k reduces to zero or as k increases. But of most interest is the minimum of the neutral curve, and Table 2.2 gives this value as obtained using the different methods and timesteps. Once more a detailed analysis of these values shows that they reflect fully the order of accuracy which was used. The use of Richardson's extrapolation on the second order data yields the following as the values of the critical parameters:

$$k_c = 1.1878, \qquad Ra_c = 40.2889, \tag{2.21}$$

where if there is any error in the presented data,then we would expect at most a change of 1 in the last displayed decimal place.

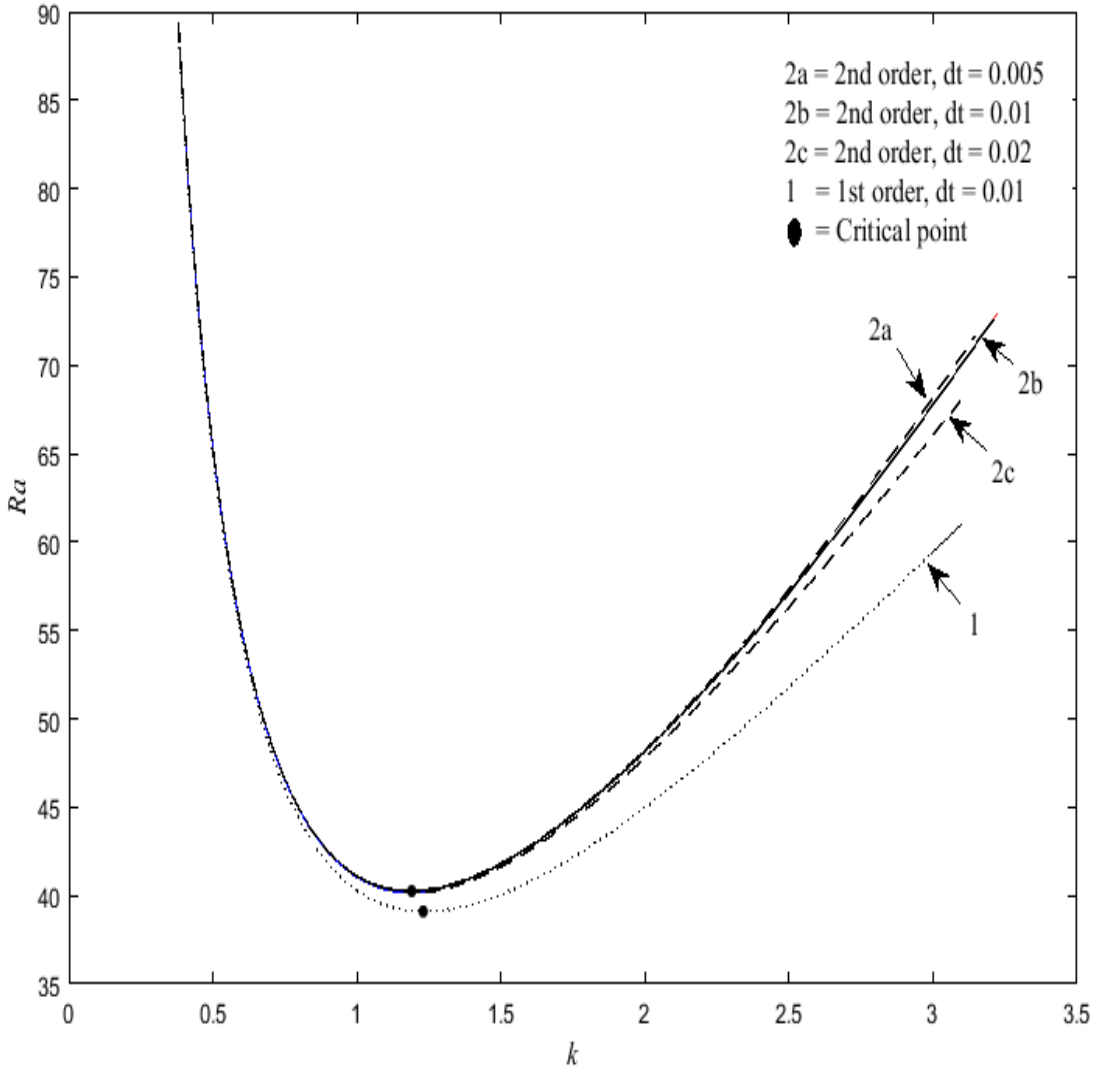

Figure 2.4: Neutral curves for the first and second order methods for different timesteps. The bullets denote the minima in each curve.

dt	1st order centred		2nd order	
	k_c	Ra_c	k_c	Ra_c
0.02	1.2912	37.9437	1.1923	40.1568
0.01	1.2356	39.1009	1.1889	40.2560
0.005	1.2109	39.6914	1.1881	40.2807

Table 2.2. The dependence of the critical wavenumber and Rayleigh number on the numerical method and the timestep.

2.8.4 Disturbance profiles

While undertaking the numerical simulations, quantities other than the amplitude (as defined in Eq. (2.18)) were monitored. If the values of $f_{\max}$ and $f_{\min}$ were to be plotted, then it will be clear that the disturbances have a period of 2, even though the basic state has a period of 1. Indeed it was found that $f_{\max}(t) = -f_{\min}(t+1)$ for all t. Even more clearly, the gradient of the reduced temperature disturbance, $g'(t)$, has a period of 2. It is therefore of great interest to determine physically why this should arise.

The disturbance temperature fields in the (x,y)-coordinates were created using Eq. (2.12b) and isotherms were plotted at discrete intervals of time over one period; these are displayed in Fig. 2.5 and Fig. 2.6 for the critical wavenumber, k_c and for $k = 3$, respectively. Red denotes that the fluid is hotter than the background basic state while blue denotes that it is cooler. Light green corresponds to disturbance amplitudes which are very small. In each frame the colours are scaled between $\pm|\Theta|_{\max}$, in order to indicate clearly where the disturbances are concentrated at each instant of time; the values of $\pm|\Theta|_{\max}$ may be found in Table 2.3. It is also worth noting that the associated streamfunction corresponds (for $t = 0$) to two whole counter-rotating cells centred in the vertical direction roughly where the temperature disturbances are.

The basic temperature field consists of a sequence of regions one above another which are characterised by having temperature gradients of alternating signs. When the sign is negative, then that region is potentially thermoconvectively unstable, but whether or not a local disturbance grows will depend on the value of a local Rayleigh number which may be defined in terms of (i) the height of the potentially unstable region and (ii) its associated temperature drop. Given that $t = 0$ corresponds to when the boundary is at its hottest, and to when the porous medium is at its most susceptible to convective instability, it is therefore not surprising that the thermal disturbance is centred close to the boundary.

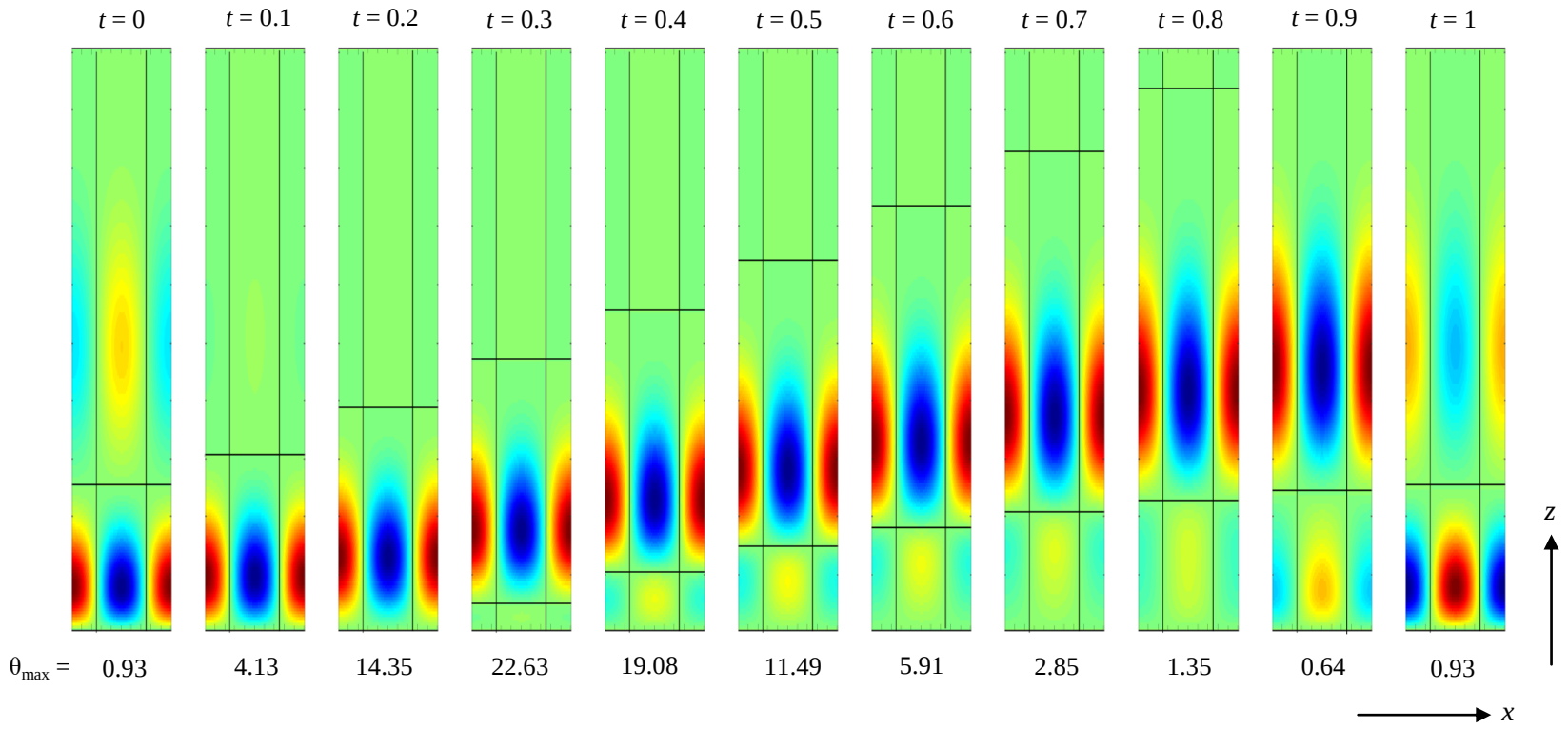

Figure 2.5: Disturbance isotherms corresponding to critical conditions, namely $k = k_c$ and $Ra = Ra_c$, and over one forcing period. The disturbances at $t = 0$ and $t = 1$ are identical apart from their signs.

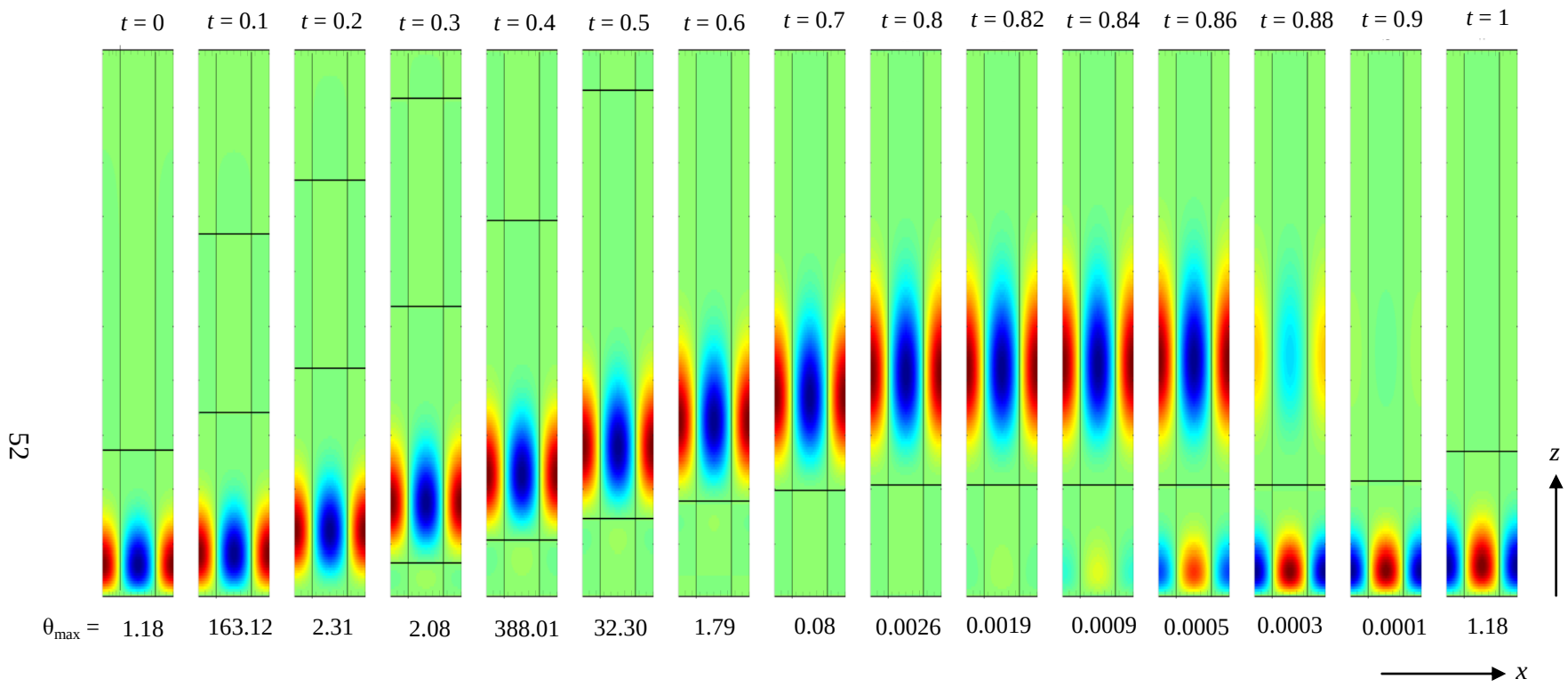

Figure 2.6: Disturbance isotherms corresponding to $k = 3$ and $Ra = 67.7715$, and over one forcing period.

time, t		0.0	0.1	0.2	0.3	0.4	0.5	0.6	0.7	0.8	0.9	1.0
$\lvert\Theta_{max}\rvert$	$k = k_c$	0.93	4.13	14.35	22.63	19.08	11.49	5.91	2.85	1.35	0.64	0.93
	$k = 3$	1.18	163.12	2.31	2.08	388.01	32.3	1.79	0.08	0.003	0.0001	1.18

Table 2.3: Values of $|\Theta|_{max}$ for each thermal disturbance field shown in Figure 5 and Figure 6 which for each subfigure are between their own respective maxima and minima because of the wide range in the orders of magnitude of $|\Theta|_{max}$.

For a short period of time after $t = 0$, the local Rayleigh number, which is reducing in magnitude, will be large enough to sustain further growth of the disturbance (see the amplitudes given in Table 2.3). In this interval of time the lower boundary is cooling, and therefore the lowest potentially unstable region rises away from the surface, and the disturbance follows its progress; see Fig. 2.5. Eventually the local Rayleigh number becomes too small and the disturbance begins to decay. In the meantime, the main convective cells have risen sufficiently far from the bounding surface that they have generated cells with the opposite circulation below them, i.e. an anticlockwise cell will generate clockwise cell below it and vice versa; it is these latter cells which then begin to grow as t approaches 1 and a new unstable region is then being born. Being of the opposite circulation, it means the upward flow which exists on the left hand side of $t = 0$ frame in Fig. 2.5 and which drags warm fluid upwards, is replaced by a downward flow on the left hand side of the $t = 1$ frame which drags cold fluid from above. Another reversal of direction is then obtained once t increases by another unit, and hence the natural period for the disturbance is double that of the basic state. The above-explained phenomena were also plotted in Figure 2.7 in the form of the z–dependent factor of the disturbance profile to show its evolution with time. The corresponding basic state profiles are also included to show that the location of the disturbance follows closely where the gradient of the basic state is at its most negative, and the amplitude corresponds to how negative the slope

is. We also see that cellular patterns which have risen above $z = 5$ decay extremely rapidly since the basic temperature field is almost perfectly uniform at this height.

An alternative view is provided by Fig. 2.8 which shows the variation of values of $g'(z = 0)$ as a function of time over two periods. The above comments about the period of growth of the disturbance being equal to 2 are seen clearly here. However, the surface rate of heat transfer is then dominated by the behavior of the disturbance at the surface, rather than by any potentially unstable region which has detached itself from the surface. However, the growth in the magnitude of $g'(z = 0)$ begins once t passes 0.75, which is when the surface temperature starts to rise again above zero. In the range $1 < t < 2$ it is very evident that the surface rate of heat transfer has exactly the opposite sign from that of the first unit period.

We also note that, for the larger values of k, the critical value of Ra is also larger, which means that both the growth and decay phases are more precipitous. This results in a much larger ratio between the maximum disturbance magnitude over a period and the minimum magnitude (c.f. Fig. 2.6 and Table 2.3 for $k = 3$). In Fig. 2.8 this results in quite a long apparently quiescent phase during the interval of time from $t = 0.4$ and $t = 1$.

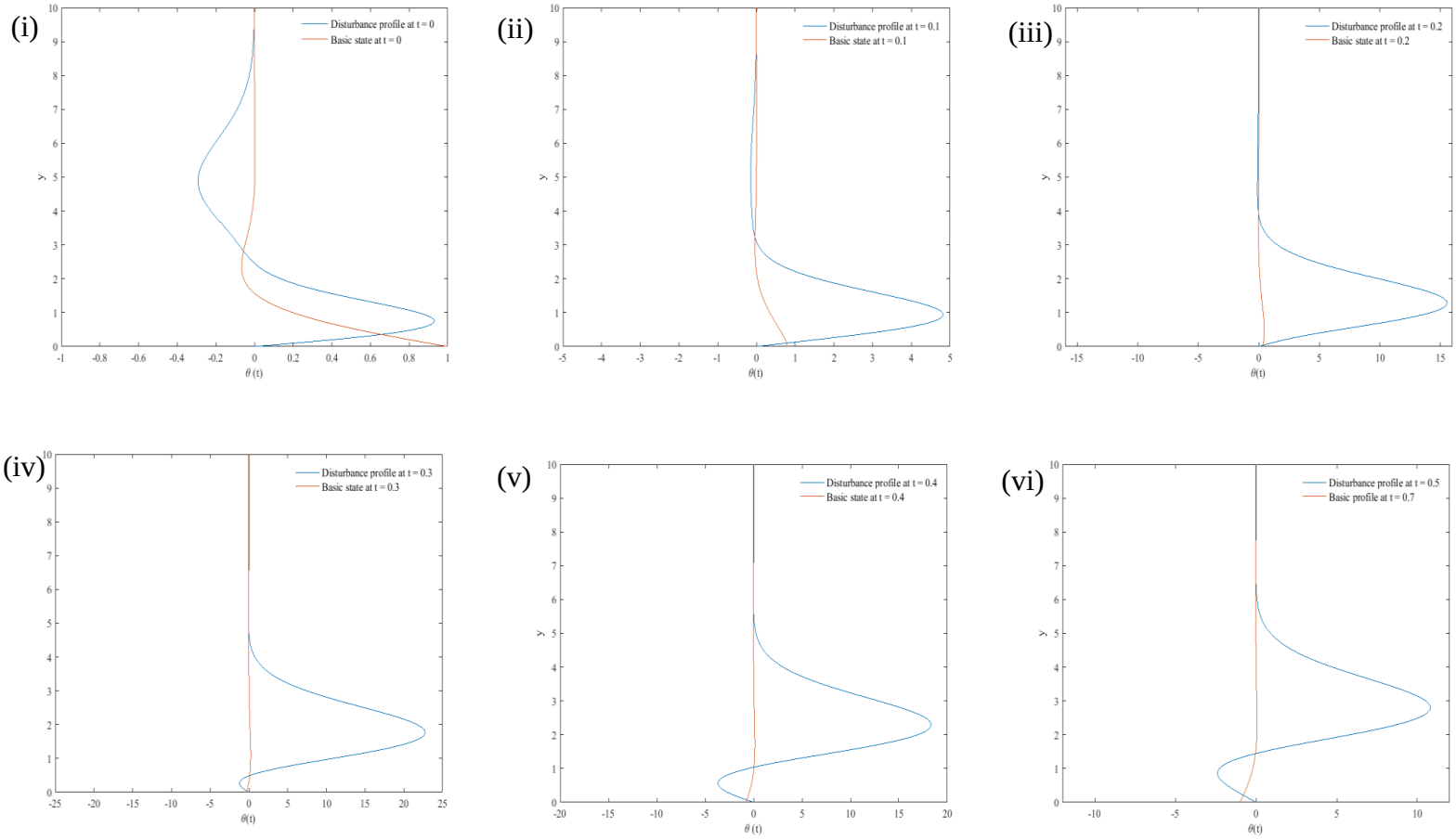
(i)
Disturbance profile at t = 0
Basic state at t = 0
y
θ (t)
(ii)
Disturbance profile at t = 0.1
Basic state at t = 0.1
y
θ(t)
(iii)
Disturbance profile at t = 0.2
Basic state at t = 0.2
y
θ(t)
(iv)
Disturbance profile at t = 0.3
Basic state at t = 0.3
θ(t)
(v)
Disturbance profile at t = 0.4
Basic state at t = 0.4
y
θ (t)
(vi)
Disturbance profile at t = 0.5
Basic profile at t = 0.7
y
θ(t)

(vii)

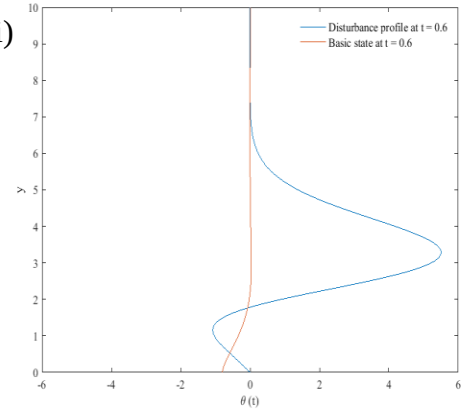

(viii)

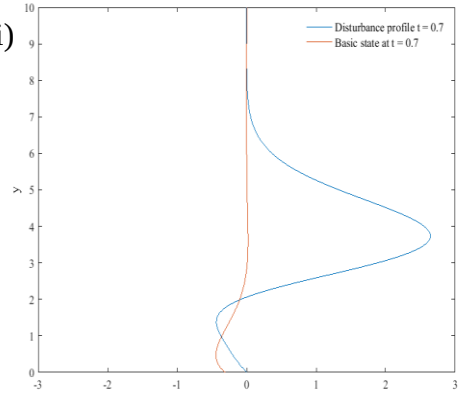

(ix)

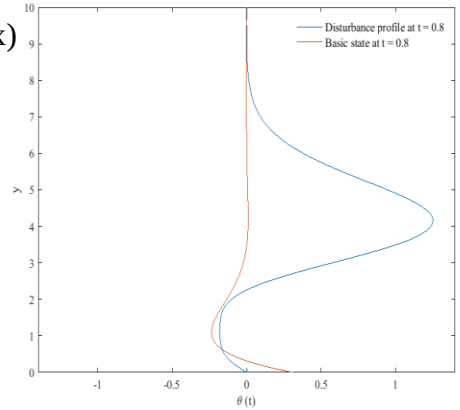

(x)

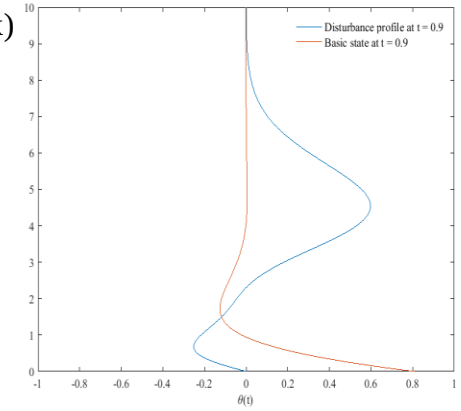

(xi)

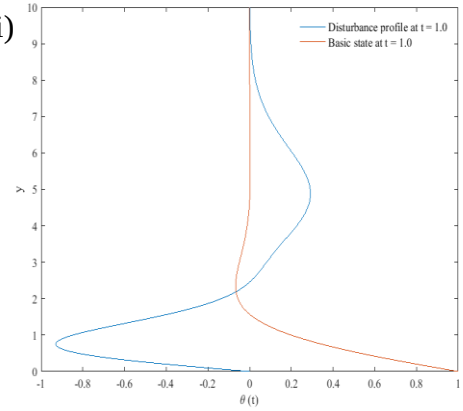

(xii)

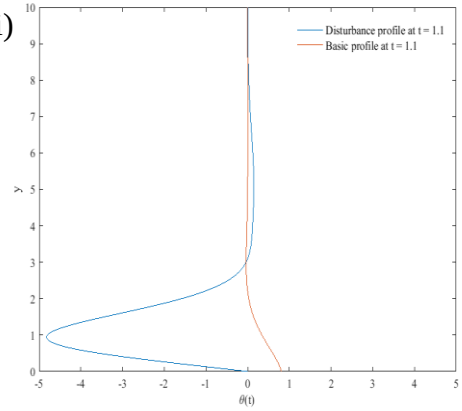

(xiii)

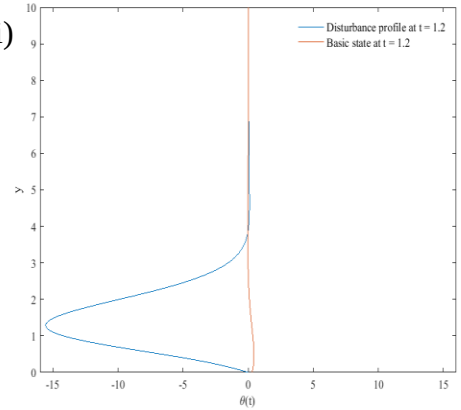

(xiv)

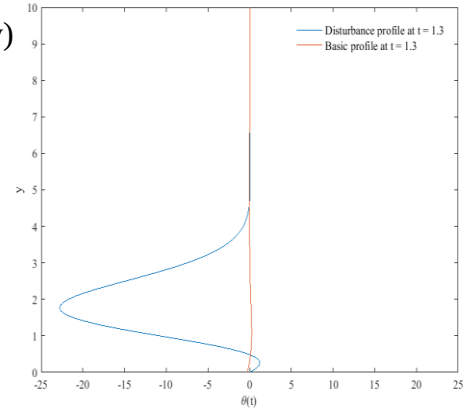

(xv)

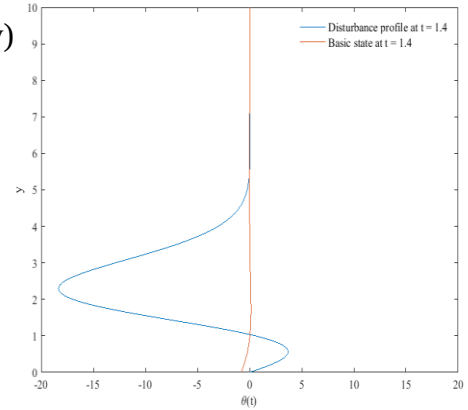

(xvi)

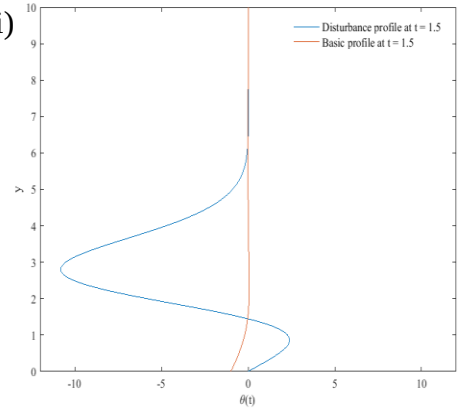

(xvii)

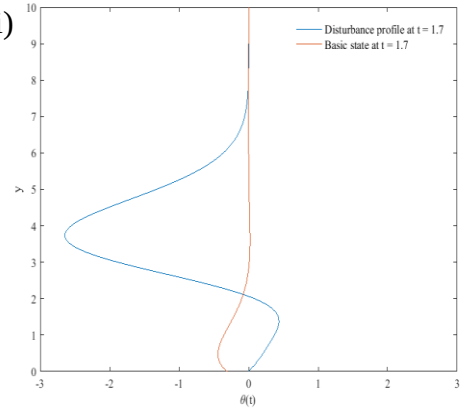

(xviii)

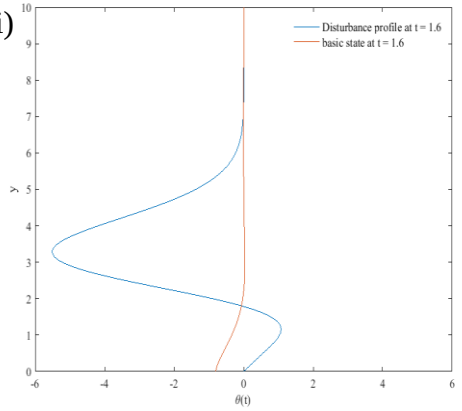

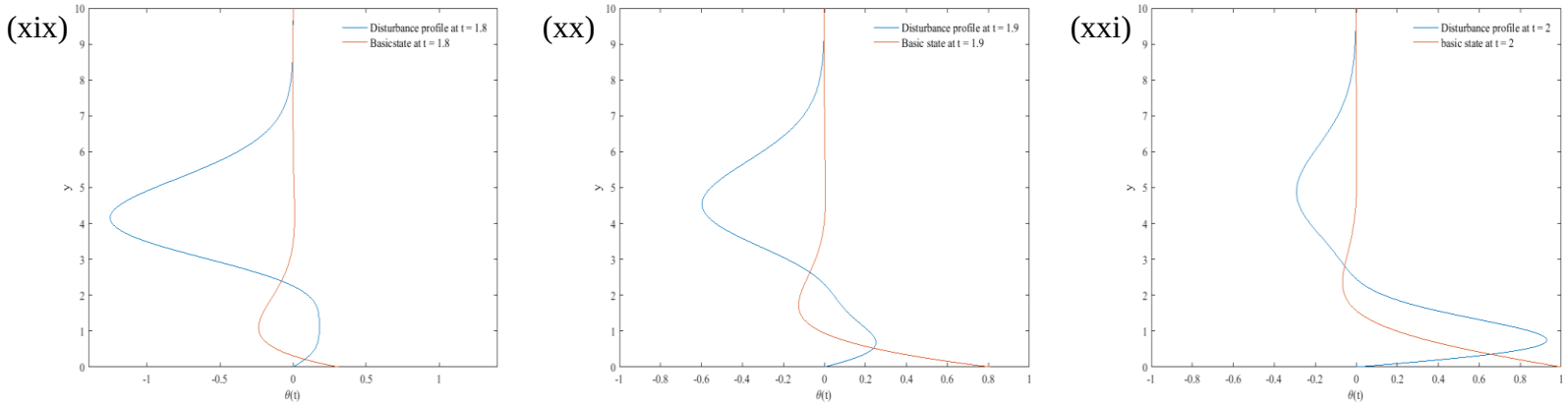

Figure 2.7: Graphs of basic temperature profile and disturbance profile in a cycle of one period.

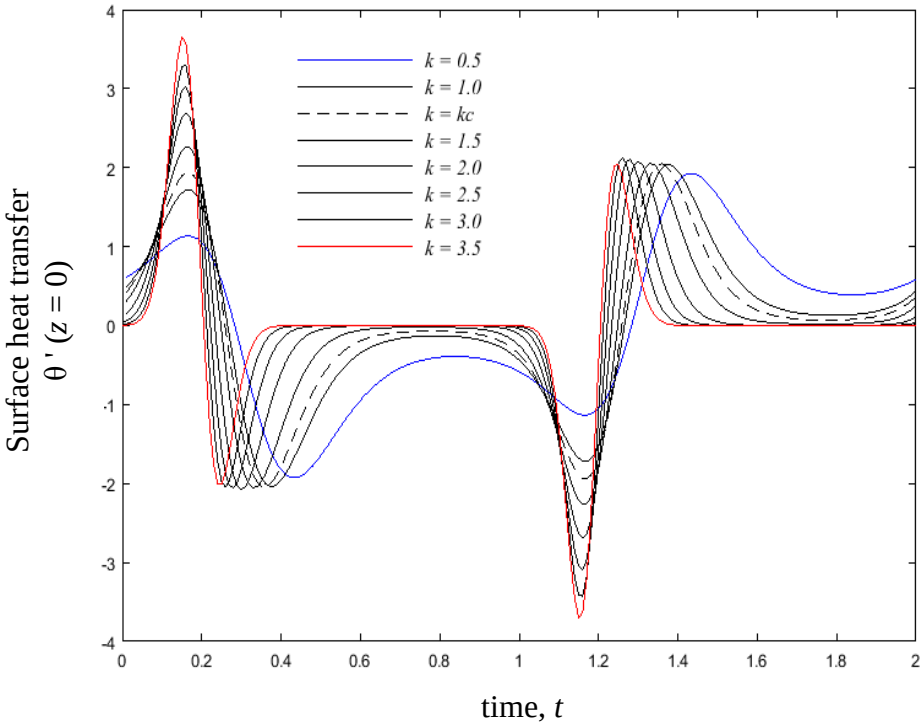

Figure 2.8: Variation with time of the surface rate of heat transfer of the disturbance over two forcing periods: $k = 0.5$ (blue); $k = 1$; $k = k_c$ (dashed); $k = 1.5$; $k = 2.0$; $k = 2.5$; $k = 3.0$; and $k = 3.5$ (red); where Ra takes the corresponding value from the neutral curve.

2.9 Conclusion

In this work, the onset of convection for a semi-infinite porous domain with a time-varying boundary temperature has been determined by using a numerical linear stability analysis. A Fortran code consisting of the Keller box method was written and internally validated, and onset criteria were obtained by (i) solving the time-evolution of the disturbances, and (ii) iterating towards the value of Ra which corresponds to zero growth over one forcing period. The computational results

showed that the second order method is substantially more accurate than the first order method in absolute terms.

The neutral curve was computed and the critical Darcy-Rayleigh number and the associated wavenumber were both computed accurately to four decimal places; these values are $Ra_c = 40.2889$ and $k_c = 1.1878$. Alongside the growth and decay of the disturbance over one forcing period, it was found that disturbances, having been generated at the bounding surface when it is relatively warm, then rise away from the surface and follow the motion of the potentially unstable regions of the basic state. This latter phenomenon provides the physical mechanism for cells to reverse direction after one period, and it yields a disturbance which has double the forcing period, a subharmonic instability.

2.10 References

[1] Horton, C.W., Rogers, F.T. (1945). Convection currents in a porous medium. *J. Appl. Phys*., **16**, 367–370.

[2] Lapwood, E.R. (1948). Convection of a fluid in a porous medium. *Math. Proc. Camb. Phil. Soc*., **44**, 508–521.

[3] Rees, D.A.S., Riley, D.S. (1989). The effects of boundary imperfections on convection in a saturated porous layer: near-resonant wavelength excitation. *J. Fluid Mech*., **199**, 133–154.

[4] Newell, A.C., Whitehead, J.C. (1969). Finite bandwidth, finite amplitude convection. *J. Fluid Mech*., **38,** 279–303.

[5] Nield, D.A. (1968). Onset of thermohaline convection in a porous medium. *Water Resour. Res*., **11**, 553–560.

[6] McKibbin, R., O'Sullivan, M.J. (1980). Onset of convection in a layered porous medium heated from below. *J. Fluid Mech*., **96**, 375-393.

[7] Rees, D.A.S., Riley, D.S. (1990). The three-dimensional stability of finite-amplitude convection in a layered porous medium heated from below. *J. Fluid Mech.*, **211,** 437–461.

[8] Sutton, F.M. (1970). Onset of convection in a porous channel with net through flow. *Phys. Fluids*, **13**, 1931–1934.

[9] Pieters, G.J.M., Schuttelaars, H.M. (2008). On the nonlinear dynamics of a saline boundary layer formed by throughflow near the surface of a porous medium. *Phys. D*., **237,** 3075–3088.

[10] Rees, D.A.S. (2009). The onset and nonlinear development of vortex instabilities in a horizontal forced convection boundary layer with uniform

surface suction. *Transp. Porous Media* [R.A.Wooding Special Issue], **77,** 243–265.

[11] Elder, J.W. (1967). Transient convection in a porous medium. *J. Fluid Mech*., **27,** 609–623.

[12] Caltagirone, J.P. (1980). Stability of a saturated porous layer subject to a sudden rise in surface temperature: Comparison between the linear and energy methods. *Q. J. Mech. Appl. Math*., **33,** 47–58.

[13] Wooding, R.A., Tyler, S.W., White, I. (1997). Convection in groundwater below an evaporating salt lake: 1. Onset of instability. *Water Res. Res*., **33**, 1199–1217.

[14] Kim, M.C., Kim, S., Chung, B.J., Choi, C.K. (2003). Convective instability in a horizontal porous layer saturated with oil and a layer of gas underlying it. *Int. Comm. Heat Mass Transfer*, **30**, 225–234.

[15] Riaz, A., Hesse, M., Tchelepi, H. A., Orr, F.M. (2006). Onset of convection in a gravitationally unstable diffusive boundary layer in porous media. *J. Fluid Mech*., **548,** 87–111.

[16] Selim, A., Rees, D.A.S. (2007a). The stability of a developing thermal front in a porous medium. I Linear theory. *J. Porous Media*, **10,** 1-15.

[17] Selim, A., Rees, D.A.S. (2007b). The stability of a developing thermal front in a porous medium. II Nonlinear theory. *J. Porous Media*, **10,** 17–23.

[18] Selim, A., Rees, D.A.S. (2010a). The stability of a developing thermal front in a porous medium. III Subharmonic instabilities. *J. Porous Media*, **13,** 1039–1058.

[19] Selim, A., Rees, D.A.S. (2010b). Linear and nonlinear evolution of isolated disturbances in a growing thermal boundary layer in porous media. Third

International Conference on Porous Media and its Applications in Science, Engineering and Industry, June 20-25, Montecatini, Italy. AIP Conference Proceedings *1254*, 47–52.

[20] Noghrehabadi, A., Rees, D.A.S., Bassom, A.P. (2013). Linear stability of a developing thermal front induced by a constant heat flux. *Transp. Porous Media,* **99**, 493–513.

[21] Rees, D.A.S., Selim, A., Ennis-King, J.P. (2008). The instability of unsteady boundary layers in porous media. In: "Emerging Topics in Heat and Mass *Transfer in Porous Media*" ed. P.Vadász. (Springer), 85–110.

[22] Farrow, D.E. & Patterson, J.C. (1993**).** On the response of a reservoir system to diurnal heating and cooling. *J. Fluid Mech*., **246**, 143–161.

[23] Lei, C.W., Patterson, J.C. (2006). Natural convection induced by diurnal heating and cooling in a reservoir with slowly varying topography. *J.S.M.E. International Journal Series B*, **49,** 605–615.

[24] Otto, S.R. (1992). On the stability of the flow around an oscillating sphere. *J. Fluid Mech.*, **239**, 47–63.

[25] Hall, P. (1984). On the stability of the unsteady boundary-layer on a cylinder oscillating transversely in a viscous fluid. *J. Fluid Mech*., **146,** 347–367.

[26] Blennerhassett, P.J., Bassom, A.P. (2002). The linear stability of flat Stokes layers. *J. Fluid Mech*., **464,** 393–410.

[27] May, A., Bassom, A.P. (2000). Nonlinear convection in the boundary layer ` above a sinusoidally heated flat plate. *J. Mech. Appl. Math*., **53**, 475–495.

[28] Keller, H.B., Cebeci, T. (1971). Accurate Numerical Methods for Boundary Layer Flow 1. Two Dimensional Laminar Flows. *Proc. Int. Conf. Numerical Methods in Fluid Dynamics*. Lecture Note in Physics 8, Springer, New York.

2.11 Appendix

Richardson Extrapolation.

The absolute accuracy of the data from the compution of integrals or the value of a variable at a given point having solved a system of ODEs or PDEs depends on the spacing between the grid points and that the approximation tends to the exact value as this spacing tends to zero. Let h be the step length for a uniform spacing and the approximation computed using the spacing h be denoted by $F(h)$. It follows that the exact value is given by $F(0)$, which we could denote by F_{exact}. Thus our approximation becomes:

$$F(h) = F_{\text{exact}} + Ah^2 + O(h^n), \tag{A2.1}$$

where $n > 2$. If we choose a value for h and then compute $F(h/2)$, we obtain:

$$F\left(\frac{h}{2}\right) = F_{\text{exact}} + \frac{Ah^2}{4} + O(h^n). \tag{A2.2}$$

Equation (A2.2) can be rearrange to:

$$4F\left(\frac{h}{2}\right) = 4F_{\text{exact}} + Ah^2 + O(h^n). \tag{A2.3}$$

We substract Equations (A2.2) and (A2.1) and neglect the higher order term, $O(h^n)$, thus the exact value, F_{exact} is given by:

$$F_{\text{exact}} = \frac{4F\left(h/2\right) - F(h)}{3} + O(h^n). \tag{A2.4}$$

This expression shows that the extrapolated value now has an n^{th} order error and is more accurate than the original data. Typically n will be equal to 3 or 4 depending on the nature of the numerical method. If we can describe the error in this approximation in the same way

that we describe the error in the original approximation, $F(h)$, we can repeat this process to obtain an approximation that is even more accurate. This process of extrapolating from $F(h)$ and $F(h/2)$ to approximate $F(0)$ is called Richardson extrapolation.

Chapter 3

The Linear Stability Of The Unsteady Thermal Boundary Layer In A Semi-Infinite Layered Porous Medium

3.1 Abstract

We consider a semi-infinite porous region bounded from below by an impermeable surface, where a porous sublayer with different physical properties is placed immediately next to the bounding surface. Initially the temperature is uniform and at the ambient value. When the temperature of the bounding surface is increased suddenly to a new constant value an evolving thermal boundary layer is formed which is potentially thermoconvectively unstable. The full disturbance equations form a parabolic system of PDEs and these equations are solved by employing the Keller box method to follow the evolution of small-amplitude disturbances in time. Thus the general aim is to provide a full understanding of the stability properties of this system. The temporal growth or decay of these disturbances is monitored by the computation of the thermal disturbance functional. Over a large part of parameter space the neutral curve displays the usual unimodal teardrop shape which is ubiquitous for boundary layers. However, there are regions of parameter space where the neutral curves have a double minimum, a property which hasn't yet been observed in systems with unsteady basic states; therefore the present chapter concentrates on this region of parameter space. We determine the locus in parameter space where two modes with different critical wavenumbers have simultaneous onset, and also find cases where the two minima and the intermediate maximum

merge to form a quartic minimum which heralds the return to the usual unimodal neutral curve.

3.2 Nomenclature

c	relative thickness
E	energy functional
$\hat{g}$	gravity
k	wavenumber
K	permeability
L	length scale
p	pressure
Ra	Darcy-Rayleigh number
t	time
T	temperature
u	horizontal velocity
v	vertical velocity
x	horizontal coordinate
y	vertical coordinate

Greek letters

α	thermal diffusivity

β	thermal expansion coefficient
δ	amplitude of disturbance
ΔT	temperature rise
η	similarity variable
θ	temperature profile
Θ	temperature disturbance
μ	dynamic viscosity
ρ	fluid density
τ	scaled time
ψ	streamfunction
Ψ	streamfunction disturbance

Superscripts and subscripts

$^{-}$, *	dimensional quantities
∞	ambient/ initial conditions
0	initial disturbance
1	lower interface
2	upper interface
b	basic state
c	critical values

3.3 Introduction

The theoretical study of the stability of convection in porous medium has been mentioned in the previous chapter (see: Horton and Rogers [1] and Lapwood [2]). Later, the finding from the work by Horton and Rogers [1] and Lapwood [2] has been supported experimentally by Katto and Masuoka [3]. In addition, the neutral curve is unimodal, in common with very many stability problems. It is also of interest to note that this classic problem may also be extended fully analytically even within the weakly nonlinear range, and therefore it forms a good pedagogical introduction to the study of weakly nonlinear theory. Rees and Riley [4], using the weakly nonlinear methods of Newell and Whitehead [5] showed that two-dimensional rolls form the preferred pattern immediately post-onset.

The Darcy-Bénard problem has since been developed greatly in a wide variety of ways including, non-Newtonian fluids, inhomogeneities, Local Thermal non-Equilibrium and layering. Since the onset and development of convection in homogeneous cases is well-known, we will consider the effect of layering as an example of a homogeneous system application particularly in geothermal systems. To the best of our knowledge the paper by Georghitza [6] was the very first to consider the effects of inhomogeneities on the Darcy-Bénard problem by considering variable permeability effects on single and two-layer porous media. Georghitza found that the marginal stability in inhomogeneous case whenever the upper medium is less permeable causes the critical temperature gradient to be greater than in the case of homogeneous case whereas a greater permeability in upper medium contributes to a smaller critical temperature gradient. It is now known that this observation may be explained simply by the manner in which the Rayleigh number is defined, i.e. which permeability is used as part of the nondimensionalisation. Donaldson [7] also was among the earliest researchers who studied the inhomogeneous medium mathematically and numerically in the simplest reservoir model including an experimental analysis. Donaldson concluded that the

size of the heated channel plays an important role beside the resistance of the connecting strata, the heat flux and parameter such as permeability. Afterwards, Rana, Horne and Cheng [8] studied the onset of natural convection in the Pahau geothermal reservoir which was modelled using three porous sublayers to investigate the consequence of layered structure of the rock formation. The outcomes of their study showed that the convection pattern changes substantially in the presence of layering and depends greatly on the value of permeability ratios and the thermal boundary conditions.

Prior to the 1980s no-one had studied the general case of a multilayered porous medium, but in 1980 McKibbin and O'Sullivan [9] became the first to develop a general analysis for any number of sublayers. Their comprehensive study of multilayered porous media showed that the common unimodal shape of the neutral curve for convection of the Bénard type isn't the sole possibility, but it could exhibit other shapes when the differences in permeability are large enough or are distributed appropriately, which means that double or multiple minima neutral curves are possible. Some of these were presented in [9]. Subsequently, McKibbin and O'Sullivan [10] extended the linear stability in [9] to look into the transportation of heat at supercritical Rayleigh numbers during convection by using a weakly nonlinear analysis. Their analysis, which used a streamfunction/temperature formulation was two dimensional. Afterwards, McKibbin and Tyvand [11] considered the effect of thin, low-permeability layers on the post-critical heat transfer, and McKibbin and Tyvand [12] studied thin but highly permeable layers. They conversely found that a crack in contact with an impermeable boundary tends to mimic a constant-pressure surface.

The bimodality found in [9] was studied in detail by Rees and Riley [13] whose primary concern was to determine whether the assumption of two-dimensionality in [10] is correct. In their three-dimensional analysis Rees and Riley [13] discovered regions in parameter space where bimodal neutral curves were found

to exist and that there are loci at which the two minima of the neutral curve correspond to the same value of the Darcy-Rayleigh number. They also found places in parameter space where the two minima and the intervening maximum merge to form a quartic minimum in the neutral curve. They also presented a trimodal case where three different modes have identical onset criteria. Similar neutral curves for a Darcy-Brinkman fluid sandwiched between two fluid layers were found by Shalbaf et. al [14] and these also exhibit bimodality for the case where the thickness of the lower fluid layer is varied.

In quite a different type of convecting system where solid outer boundaries of finite thickness were considered and where a horizontal pressure gradient was imposed within the porous layer, Rees and Mojtabi [15] found that neutral curves also no longer always formed a standard unimodal curve but also took more exotic shapes including bimodal and quartic ones, and some even displayed turning points. Another quite different system was considered by Rees and Patil [16] who considered a semi-infinite porous domain bounded below by a hot surface through which the fluid was drawn at a uniform rate. This forms a thermal boundary layer of finite thickness. They also considered the effect of Local Thermal non-Equilibrium (LTNE). Yet again, unimodal neutral curves arise in most cases, but there are a few where the LTNE effects are sufficiently finely tuned that the basic temperature profile splits into two well-defined regions, one which is relatively narrow but with a high temperature gradient, and the other which is much thicker but the temperature gradient is much less. In essence this is a natural layering where the local Rayleigh numbers of these sublayers are roughly equal, and this provides the conditions under which a bimodal neutral curve becomes possible. Once more bimodal and quartic neutral curves were obtained.

All the above-mentioned studies produce a similar qualitative behavior, namely the existence of bimodality, but apart from them being stability analyses these studies considered quite different configurations. However, a unifying feature

is that there was a layering effect present, one which is either physically imposed or else produced naturally by external effects. A second unifying feature is that the basic state, whose stability was considered, is steady in all cases. Therefore, in the present study, we shall consider removing the steady nature of the basic state and examine whether bimodality can arise when the basic state is unsteady.

So we shall consider the onset of convection in an inhomogeneous medium where the basic state varies with time, and this provides a layered extension to the work of Selim and Rees. [17]. Therefore we shall consider a semi-infinite domain with an impermeable lower bounding surface above which is a sublayer whose properties are different from the rest of the semi-infinite region. Everything is at a uniform ambient temperature at *t=0* but the temperature of the bounding surface is suddenly raised to a new constant value, and then heat diffuses upwards through the sublayer and into the porous region above. A full linear stability analysis is performed using the small-amplitude disturbance to perturb the basic state of this evolving temperature profile. We monitored the disturbance growth via the thermal energy of the disturbance, and instability is deemed to arise when disturbances begin to grow.

3.4 Governing equations

We are considering the evolution of small-amplitude disturbances within an evolving thermal boundary layer which occupies a layered semi-infinite system. The basic configuration is shown in Fig. 3.1, where $\bar{x}$ and $\bar{y}$ are horizontal and vertical coordinates, respectively, and $\bar{u}$ and $\bar{v}$ are the corresponding velocities. The porous medium, which lies above an impermeable surface at *y=0*, is initially at the temperature T_∞ and at time $t = 0$ the temperature of the bounding surface is raised suddenly to the value $T = T_\infty + \Delta T$. The evolving temperature field, which would normally be given analytically in terms of a complementary error function when the semi-infinite flow domain is uniform, is now more complicated because of the

presence of an interface at $y=L$ which separates two different but uniform and homogeneous porous media. The aims of this chapter are to determine the manner in which this boundary layer becomes unstable and, in particular, to determine if bimodal curves may be found.

The configuration which will be considered is shown in Figure 3.1.

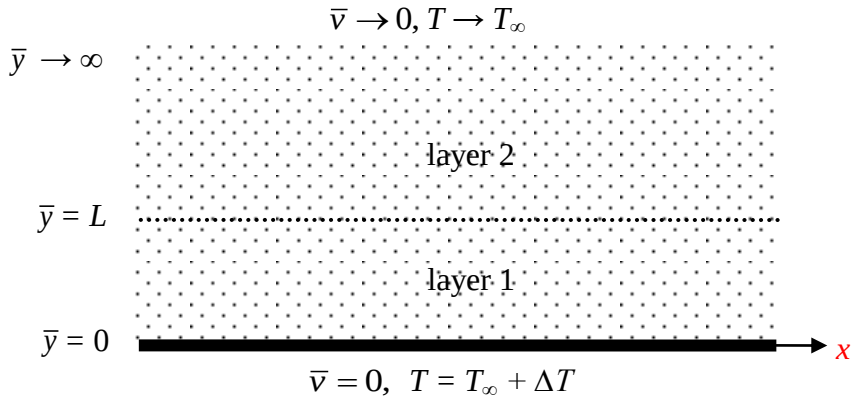

Figure 3.1: Depicting the semi-infinite porous medium and the imposed boundary conditions.

The two porous regions, which will be referred to as layer 1 (near the surface) and layer 2 (the remaining semi-infinite domain), are both assumed to be uniform and isotropic, but generally with different permeabilities, conductivities and diffusivities. In each layer, the flow is assumed to be governed by Darcy's law, and the Boussinesq approximation is also assumed to be valid. The porous matrix and the fluid are also assumed to be in local thermal equilibrium. Thus the governing equations for the unsteady two-dimensional free convective flow within the porous medium are given by:

$$\frac{\partial \bar{u}}{\partial \bar{x}} + \frac{\partial \bar{v}}{\partial \bar{y}} = 0, \tag{3.1}$$

$$\bar{u} = -\frac{K}{\mu}\frac{\partial \bar{p}}{\partial \bar{x}}, \tag{3.2}$$

$$\bar{v} = -\frac{K}{\mu}\frac{\partial \bar{p}}{\partial \bar{y}} + \frac{\rho \hat{g} \beta K}{\mu}\left(T - T_\infty\right), \tag{3.3}$$

$$\frac{\partial T}{\partial \bar{t}} + \bar{u}\frac{\partial T}{\partial \bar{x}} + \bar{v}\frac{\partial T}{\partial \bar{y}} = \alpha\left(\frac{\partial^2 T}{\partial \bar{x}^2} + \frac{\partial^2 T}{\partial \bar{y}^2}\right) + \frac{\partial \alpha}{\partial \bar{y}}\frac{\partial T}{\partial \bar{y}}. \tag{3.4}$$

These equations are subject to boundary conditions below:

$$\begin{aligned} &\bar{y} = 0: \quad \bar{v} = 0, \quad T = T_\infty + \Delta T, \\ &\bar{y} \to \infty: \quad \bar{v} \to 0, \quad T \to T_\infty. \end{aligned} \tag{3.5}$$

In these equations we have assumed that both K and α vary with $\bar{y}$, rather than to have a discrete interface at $\bar{y} = L$. While the ideal layered system has a distinct interface at $\bar{y} = L$ this will be replaced later by a rapidly varying interface region centred at the same location; this will be done in order to simplify the numerical modelling.

We may now rescale the variables in order to obtain a dimensionless system. Therefore we make the following transformations:

$$\left(\bar{x}, \bar{y}\right) = L\left(x, y\right), \ \left(\bar{u}, \bar{v}\right) = \frac{\alpha_2}{L}\left(u, v\right), \ T = T_\infty + \left(\Delta T\right)\theta, \ \ \bar{t} = \frac{L^2}{\alpha_2}t, \ \ \bar{p} = \frac{\alpha_2 \mu}{K_2}p, \tag{3.6}$$

where L is the height of layer 1 and α_2 and K_2 are the reference values, and where α_1 and K_1 may be associated with the lower layer. We note that time is scaled with respect to the natural diffusion time across layer 2. Given the above scalings, the governing equations take the form,

$$\frac{\partial u}{\partial x}+\frac{\partial v}{\partial y}=0, \tag{3.7}$$

$$u=-\left(\frac{K}{K_2}\right)\frac{\partial p}{\partial x}, \tag{3.8}$$

$$v=-\left(\frac{K}{K_2}\right)\frac{\partial p}{\partial y}+\left(\frac{K}{K_2}\right)Ra\theta, \tag{3.9}$$

$$\frac{\partial \theta}{\partial t}+u\frac{\partial \theta}{\partial x}+v\frac{\partial \theta}{\partial y}=\left(\frac{\alpha}{\alpha_2}\right)\left(\frac{\partial^2\theta}{\partial x^2}+\frac{\partial^2\theta}{\partial y^2}\right)+\frac{\partial\left(\alpha/\alpha_2\right)}{\partial y}\left(\frac{\partial \theta}{\partial y}\right), \tag{3.10}$$

and the boundary conditions are:

$$v=0, \quad \theta=1, \quad \text{at } y=0, \qquad v\to 0, \quad \theta\to 0, \quad \text{at } y\to\infty, \tag{3.11}$$

while $\theta = 0$ everywhere when $t < 0$. In the above the Darcy-Rayleigh number is defined as

$$Ra=\frac{\rho \hat{g}\beta\Delta T K_2 L}{\mu\alpha_2}. \tag{3.12}$$

The introduction of the streamfunction, ψ, as follows:

$$u=-\frac{\partial\psi}{\partial y} \text{ and } v=\frac{\partial\psi}{\partial y}, \tag{3.13}$$

allows us to eliminate the pressure *p*, and the continuity equation (3.7) is satisfied automatically. Thus the remaining equations (3.8) - (3.10) reduce to:

$$\frac{\partial^2\psi}{\partial x^2}+\frac{\partial^2\psi}{\partial y^2}-\frac{\left(\frac{K}{K_2}\right)_y}{\left(\frac{K}{K_2}\right)}\frac{\partial\psi}{\partial y}=\left(\frac{K}{K_2}\right)Ra\frac{\partial\theta}{\partial x}, \tag{3.14}$$

$$\frac{\partial\theta}{\partial t}+\frac{\partial\psi}{\partial x}\frac{\partial\theta}{\partial y}+\frac{\partial\psi}{\partial y}\frac{\partial\theta}{\partial x}=\left(\frac{\alpha}{\alpha_2}\right)\frac{\partial^2\theta}{\partial x^2}+\frac{\partial\left(\alpha/\alpha_2\right)}{\partial y}\left(\frac{\partial\theta}{\partial y}\right), \tag{3.15}$$

which are subject to boundary conditions

$$\begin{aligned}&\psi=0, \quad \theta=1, \quad \text{at } y=0,\\ &\psi\to 0, \quad \theta\to 0, \quad \text{at } y\to\infty,\end{aligned} \tag{3.16}$$

and the initial conditions are taken to be

$$\psi=\theta=0 \text{ at } t=0. \tag{3.17}$$

In the above, the interface at $y = 1$ is modelled using the following formulae,

$$K=\frac{1}{2}\left(K_2+K_1\right)+\frac{1}{2}\left(K_2-K_1\right)\tanh\left(\frac{y-L}{c}\right), \tag{3.18a}$$

$$\alpha=\frac{1}{2}\left(\alpha_2+\alpha_1\right)+\frac{1}{2}\left(\alpha_2-\alpha_1\right)\tanh\left(\frac{y-L}{c}\right), \tag{3.18b}$$

in dimensional terms, where the value of c determines the width of the interface region; a sufficiently good approximation to a discrete interface will correspond to sufficiently large values of c. After scaling, Eqs. (3.18) may be written in the form:

$$\frac{K}{K_2}=\frac{1}{2}\left(1+\frac{K_1}{K_2}\right)+\frac{1}{2}\left(1-\frac{K_1}{K_2}\right)\tanh\left(\frac{y-1}{c}\right), \tag{3.19a}$$

$$\frac{\alpha}{\alpha_2}=\frac{1}{2}\left(1+\frac{\alpha_1}{\alpha_2}\right)+\frac{1}{2}\left(1-\frac{\alpha_1}{\alpha_2}\right)\tanh\left(\frac{y-1}{c}\right). \tag{3.19b}$$

For simplification, from here onwards we shall replace K/K_2 by K and α/α_2 by α in equations 3.19(a) and 3.19(b). We shall now define the following constants: $K^* = K_1/K_2$ and $\alpha^* = \alpha_1/\alpha_2$ as permeability and diffusivity contrasts between the layers.

Note that the equations above allow for solutions that are uniform in the *x*-direction, and it is clear that an *x*-independent temperature profile in equation (3.14) suggests that there will be no flow. This is the basic state whose stability we will be assessing. When the two media have identical diffusivities this basic temperature profile may be found as the analytical solution of,

$$\frac{\partial \theta}{\partial t} = \frac{\partial^2 \theta}{\partial y^2}, \tag{3.20}$$

and it is

$$\theta_b = erfc(\eta) = \frac{2}{\sqrt{\pi}} \int_{\eta}^{\infty} e^{-\xi^2} d\xi . \tag{3.21}$$

However, in general, the basic temperature state is given by the solution of

$$\frac{\partial \theta}{\partial t} = \frac{\partial}{\partial y}\left(\frac{\alpha}{\alpha_2} \frac{\partial \theta}{\partial y} \right), \tag{3.22}$$

and the solution of this equation has to be obtained numerically. The form of the similarity solution given in (3.21) motivates the following transformation of the full governing equations (3.14) - (3.15) into the coordinate system (x, η, τ) where

$$\eta = \frac{y}{2\sqrt{t}} \text{ and } \tau = \sqrt{t} . \tag{3.23}$$

Thus the equations that govern the system are:

$$4\tau^2 \frac{\partial^2 \psi}{\partial x^2} + \frac{\partial^2 \psi}{\partial \eta^2} - \frac{K_\eta}{K} \frac{\partial \psi}{\partial \eta} = 4\tau^2 KRa \frac{\partial \theta}{\partial x}, \tag{3.24a}$$

$$2\tau \frac{\partial \theta}{\partial \tau} + 2\tau \left(\frac{\partial \psi}{\partial x} \frac{\partial \theta}{\partial \eta} - \frac{\partial \psi}{\partial \eta} \frac{\partial \theta}{\partial x} \right) = 4\alpha\tau^2 \frac{\partial^2 \theta}{\partial x^2} + \alpha \frac{\partial^2 \theta}{\partial \eta^2} + \alpha_\eta \frac{\partial \theta}{\partial \eta} + 2\eta \frac{\partial \theta}{\partial \eta}. \tag{3.24b}$$

and the boundary conditions are:

$$\psi = 0, \quad \theta = 1, \quad \text{at } \eta = 0,$$
$$\psi \to 0, \quad \theta \to 0, \quad \text{as } \eta \to \infty, \tag{3.24c}$$

3.5 Linear stability analysis

Having the basic flow profile, a linear stability theory can be used to determine the conditions under which the solution can be unstable. In other words, we endeavour to find out conditions for which disturbances neither grow nor decay. Thus, a small-amplitude disturbance is introduced to perturb the solution given in equation (3.21). We apply a small amplitude disturbance to perturb the basic solution given in equation (3.21), and therefore, we set:

$$\psi(\eta, x, t) = \delta\left[i\Psi(\eta, \tau)e^{ikx} + c.c\right], \tag{3.25}$$

$$\theta(\eta, x, t) = \theta_b(\eta, t) + \delta\left[\Theta(\eta, \tau)e^{ikx} + c.c\right], \tag{3.26}$$

where *c.c.* denotes complex conjugate, k is the wave number of the disturbance and δ is the small-amplitude of the disturbance and it is sufficiently small that higher order powers of δ may be omitted. Substitutions of equations (3.25) and (3.26) into the nonlinear governing equations (3.22) and (3.23) yield the following linear disturbance equations

$$\frac{\partial^2\Psi}{\partial\eta^2} - \frac{K_\eta}{K}\frac{\partial\Psi}{\partial\eta} - 4\tau^2k^2\Psi = 4\tau^2 KRak\Theta \tag{3.27}$$

$$2\tau\frac{\partial\Theta}{\partial\tau} - 2\tau k\Psi\frac{\partial\theta_b}{\partial\eta} = -4\tau^2\alpha k^2\Theta + \alpha\frac{\partial^2\Theta}{\partial\eta^2} + \alpha_\eta\frac{\partial\Theta}{\partial\eta} + 2\eta\frac{\partial\Theta}{\partial\eta}, \tag{3.28}$$

$$2\tau\frac{\partial\theta_b}{\partial\tau} = \alpha\frac{\partial^2\theta_b}{\partial\eta^2} + \alpha_\eta\frac{\partial\theta_b}{\partial\eta} + 2\eta\frac{\partial\theta_b}{\partial\eta}. \tag{3.29}$$

Due to the addition of equation (3.29), we need an additional boundary conditions for θ_b. Thus, Equations (3.27) – (3.29) are subject to boundary conditions:

$$\Psi = 0, \quad \Theta = 0, \quad \theta_b = 1 \quad \text{at } \eta=0,$$
$$\Psi \to 0, \quad \Theta \to 0, \quad \theta_b \to 0 \quad \text{at } \eta \to \infty. \tag{3.30}$$

3.6 Numerical method

The full system of governing equations (3.27) - (3.29), which are the equations for the disturbance and the basic state and which are subject to the boundary conditions (30), and are parabolic in time, were solved numerically using a modified Keller box method. The basic idea of the Keller box method is to rewrite the parabolic governing equations (a second order equation for the basic state and a fourth order system for the disturbances) as a system of six first order differential equations by introducing new dependent variables. Then the new system is approximated by means of a suitable finite difference method. We employed central difference approximations based halfway between the grid points in the η-direction and used either central differences (second order, based halfway between timesteps) or backward differences (first order, based at the new timestep) for the time stepping to complete the finite difference approximations. Finally, the full set of discretised equations are solved using a multi-dimensional Newton-Raphson scheme, where the iteration matrix takes a block-tridiagonal form, and the block-Thomas algorithm is used to iterate towards the solution at each timestep. Although the full system being solved is linear, we used a near-black-box user-written code which employs numerical differentiation to form the iteration matrix. This reduces substantially the code-development time, and the risk of incorrect programming.

The second order differential equations in equations (3.27) - (3.29) that are subject to boundary conditions in equation (3.30) are reduced to first order form by introducing the following variables, let:

$$V_1 = \Psi,$$

$$V_2 = \Psi',$$

$$V_3 = \Theta, \tag{3.31}$$

$$V_4 = \Theta',$$

$$V_5 = \theta_b,$$

$$V_6 = \theta_b',$$

After substitution of equation (3.21) into equations (3.17) – (3.20). we obtained:

$$V_1' - V_2 = 0, \tag{3.32i}$$

$$V_2' - \frac{K_\eta}{K} V_2 - 4\tau^2 k^2 V_1 = 4\tau^2 KRakV_3, \tag{3.32i}$$

$$V_3' - V_4 = 0, \tag{3.32iii}$$

$$2\tau \frac{\partial V_3}{\partial \tau} - 2\tau k V_1 V_6 - \alpha V_4' - \alpha_\eta V_4 - 2\eta V_4 + 4\tau^2 \alpha k^2 V_3 = 0, \tag{3.32iv}$$

$$V_5' - V_6 = 0, \tag{3.32v}$$

$$2\tau \frac{\partial V_5}{\partial \tau} = \alpha V_6' + \alpha_\eta V_6 + 2\eta V_6, \tag{3.32vi}$$

where the boundary conditions are:

$$V_1(0)=0,\ V_3(0)=0,\ V_5(0)=1 \text{ at } \eta=0, \tag{3.33i}$$

$$V_1(\infty)=0,\ V_3(\infty)=0,\ V_5(\infty)=0 \text{ at } \eta\to\infty. \tag{3.33ii}$$

In this chapter we are interested in studying the stability of the thermal boundary layer by introducing thermal disturbances into the system. The initial temperature profile, $\theta=9\eta e^{-3\eta}$ is introduced at $\tau_0=0.012$; while this might be considered to be an arbitrary shape and an arbitrary time, the detailed study by Selim and Rees [20] on the equivalent semi-infinite case in a uniform medium shows that the stability criterion is essentially independent of both the shape of the disturbance and its time of introduction as long as it is sufficiently early. In this study, the growth or decay of the disturbances is controlled by the computation of the thermal energy of the disturbance which is defined here as

$$E=-\frac{2\tau K^*}{\alpha^*}\int_0^\infty \theta d\eta. \tag{3.34}$$

It is important in every numerical work to determine an accurate assessment of the accuracy of the computations. In this numerical work, the initial spatial grid used was dy = 0.02 with η_{max} = 5. These values were tested and chosen based on the result that further increases in η_{max} shows that the first six significant figures do not change and therefore the disturbance was well-contained within the computational domain. The timestep used in the computation is $d\tau = 2\times10^{-3}$ and the chosen value of c was to be 0.05 which means that the porous medium properties vary over distance of 0.1 centred on the interface.

3.7 Numerical results and discussion

3.7.1 Neutral Curves

It is well-known that in the classical Darcy-Bénard problem, the minimum point on the neutral stability curve is when $Ra_c = 4\pi$ and $k_c = \pi$ and these are referred as critical Rayleigh number and critical wavenumber, respectively. When Ra is small, disturbances are damped by viscous friction, and therefore the system is always stable. But when Ra is large, disturbances grow since the buoyancy forces are greater than the restraining viscous forces, and therefore the system is unstable. Besides the values of Ra and *k*, parameters such as K^* and α^* play important roles in the onset of convection in layered problems. Thus, in this chapter, the general aim is to determine the time of onset of convection as a function of K^*, α^*, *Ra* and k using the temporal behavior of the energy functional defined in Equation (3.34), neutrality being defined to be when (i.e the value of τ at which) the functional takes its minimum value. Neutral curves will then be a function of K^*, α^* and *Ra*.

A large number of numerical simulations have been undertaken and, by incrementing *k* slowly and by determining when the energy functional ceases to decay, we are able to determine the time τ at when the disturbance is marginally stable. In general these neutral curves are unimodal with one minimum. Based on the fact that the double minimum cases which were found by Rees and Riley [16] generally had vertical disturbance profiles which were either global (i.e. occupied the whole porous layer, or at least two sublayers) or local (i.e. occupied only one layer) we were able to guess roughly where in parameter space that the present evolving basic state might yield the same type of neutral curves. Therefore an extensive set of computations were undertaken to determine the desired values of parameters Ra, K^* and α^* that produce double minimum neutral curves.

Initially, it is good to understand physically, and with reference to Selim and Rees [20] when convection might arise. In their work (which corresponds to both the present layers being identical, $\alpha^* = K^* = 1$, and with Ra = 1) they determined that convection begins when $\tau = 12.944$ and with the wavenumber $k = 0.0696$. The height of the disturbance is likely to be slightly more than the width of a cell, and therefore this is greater than $\pi/0.0696 \approx 45.1378$ height (in terms of y) or 6.3 (in terms of η) which is much larger than the width of layer 1 here. On referring to Eq. (3.24b) we see that the value α^* multiplies the diffusion term, and therefore large values (which correspond to strong thermal diffusion in layer 1) causes the thermal front to pass quickly through layer 1. This will bring forward the time for convection to happen. Correspondingly, small values of α will delay convection. In Eq. (3.24a), the Rayleigh number multiplies the buoyancy term, and therefore larger values of Ra will also bring the onset time earlier. This will also be true when K^* is large for it too multiplies the buoyancy term. If our aim is to try to determine suitable parameter values for bimodal convection to happen, then it will be essential have a large value of Ra so that convection can happen in layer 1. But at the same time a global pattern has to be formed which occupies both regions. Even with these ideas, it was difficult to find the appropriate region of parameter space.

Figures 3.2 and 3.3 are plotted to describe the behavior of the neutral curve when α is 0.2 and 0.5 at Ra = 200 and Ra = 800. These large values of Ra are consistent with the above physical argument. All the curves shown in Figure 3.2 are unimodal curves but there is clear evidence that there is a substantial change in the critical wavenumber as K^* decreases. For relatively large values of K^* the onset time is very early, and this is due to the large coefficient of the buoyancy term. Therefore convection has arisen in layer 1, well before the developing thermal field has reached layer 2. When K^* decreases, onset takes place later in layer 1 because of the reduced buoyancy. However, once the developing thermal field reaches layer 2, where both the permeability and diffusivity are much larger, convection switches suddenly to the region just above the interface. At the onset time, this thermally-varying region

region within layer 2 is very thin, and this accounts for the large wavenumber, since convection cells tend to be of roughly square cross-section. Similar arguments may be made for the curves shown in Figure 3.3. But now we see that each of the neutral curves shown does have two minima and, more importantly, it is easily seen that the onset time for the left hand minimum increases from below that of the right hand minimum to above it as K^* decreases. However, we are interested in investigating the onset of convection in double-minimum cases that occur simultaneously, i.e. that τ_c for both minima are equal. While the basic numerical scheme involving the Keller box method has already been described, the way in which the critical values of K^* which yield simultaneous onset also needs to be summarised. Once one is close to a parameter set for such a double minimum, there is one free parameter, which is K^* here. Each minimum is found using its own Newton-Raphson scheme. If the present iteration for the smaller of the two critical wavenumbers is k_1, then the onset time for this wavenumber may be denoted as $\tau(k_1)$. Then two further critical times are computed: $\tau(k_1+\delta k)$ and $\tau(k_1-\delta k)$ where δk is very small. Then a Newton-Raphson scheme is used to obtain the value for k_1 for which $\tau(k_1+\delta k)-\tau(k_1-\delta k) = 0$. The same scheme is used to obtain k_2. Then finally, an outer Newton-Raphson scheme is used which varies K^* until $\tau(k_1)-\tau(k_2) = 0$. Thus the double minima were found by using a Keller box scheme as a black box subroutine which outputs only the critical time, and then nested Newton-Raphson schemes to find both the minima in the neutral curves, and identical times for onset.

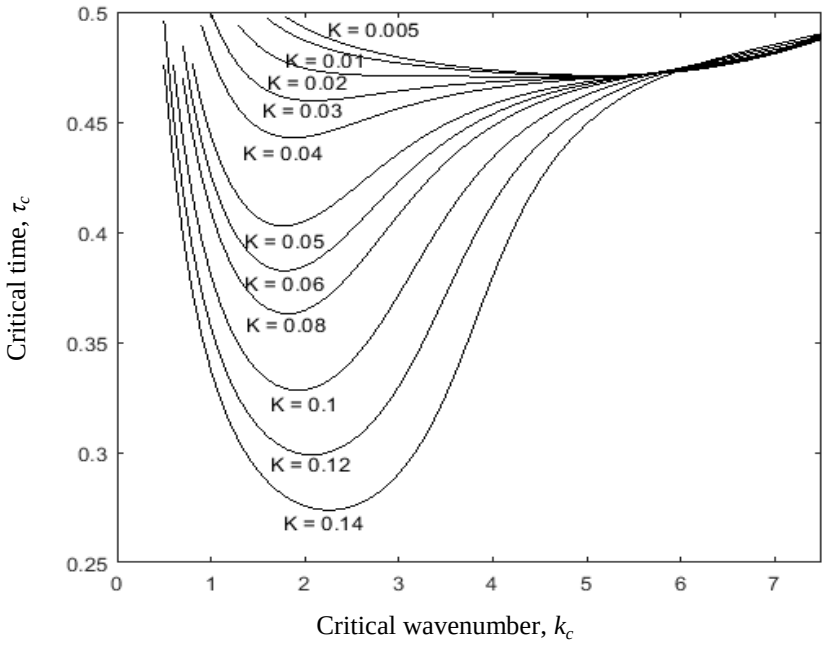

Figure 3.2: Neutral curves when Ra = 200, α^* = 0.5 and c = 0.05, and for K^* = 0.005, 0.01, 0.02, 0.03, 0.04, 0.05, 0.06, 0.08, 0.1, 0.12, 0.14.

(a)

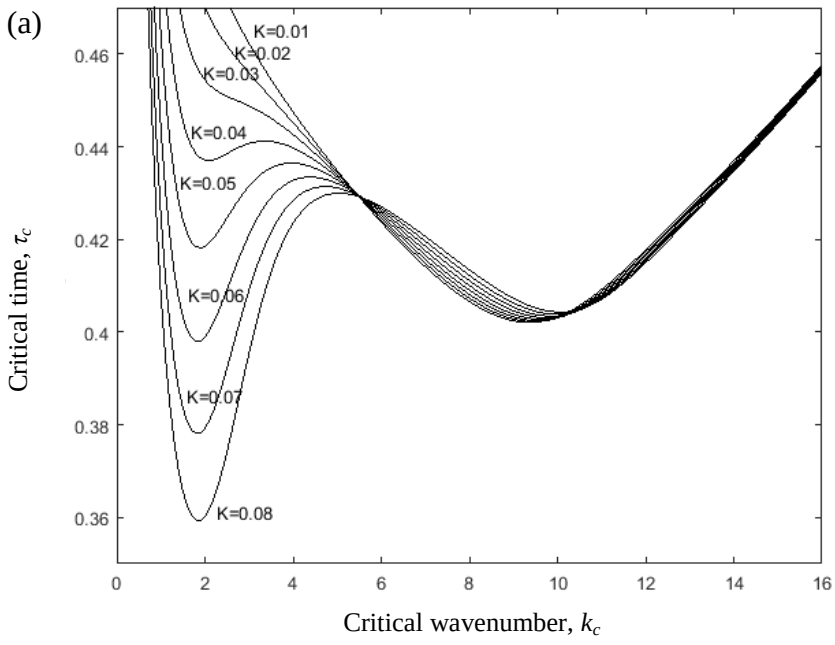

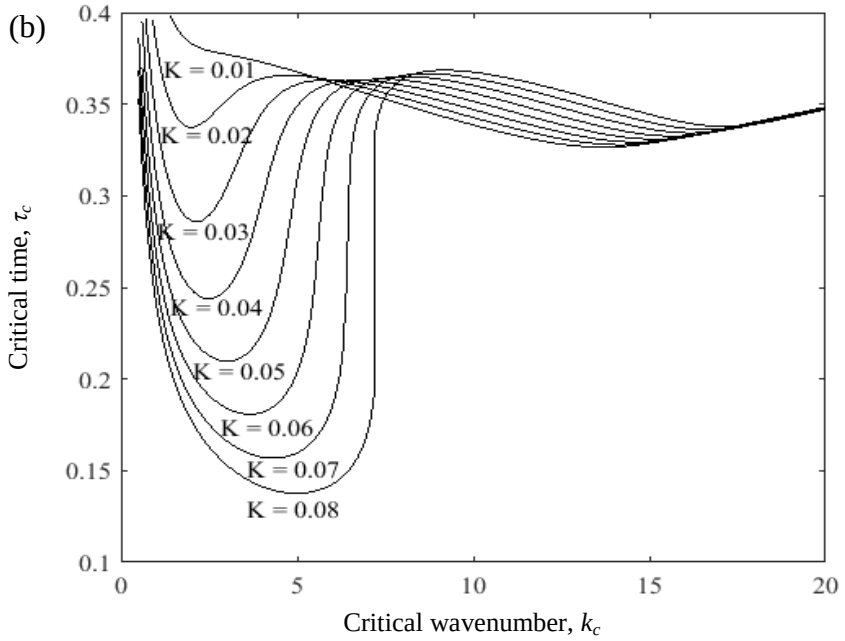

Figure 3.3: Neutral curves when (a) Ra = 200 and (b) Ra = 800, for $\alpha^* = 0.2$, c = 0.05 and for $K^* = 0.01, 0.02, 0.03, 0.04, 0.05, 0.06, 0.07, 0.08$.

As a result, we have recorded the data obtained into Table 3.1 and have plotted the resulting neutral curves in Figure 3.4. We note that the uppermost curve in Figure 3.4 is a standard unimodal neutral curve with a parabolic minimum where $\alpha^* = 0.51$ and the chosen value for Ra is extrapolated from the final two values in Table 3.1. From both Table 3.1 and Figure 3.4 we see that double minima exist only when $\alpha^* < 0.5061$ when $K^*=0.02$. The computation of this maximum value of α^* was by extrapolating to zero the values of $(k_{c1}-k_{c2})^2$; which are shown in Table 3.1.

Ra	K^*	α^*	k_{1c}	k_{2c}	τ_c
840.3921	0.02	0.2200	2.0049	14.1242	0.3307
627.7113	0.02	0.3400	2.0079	11.1867	0.3650
450.3012	0.02	0.4300	2.1209	8.6504	0.3984
352.4891	0.02	0.4700	2.2778	7.1338	0.4208
289.3099	0.02	0.4900	2.4698	6.0406	0.4383
246.4189	0.02	0.5000	2.7009	5.1827	0.4525
203.7273	0.02	0.5061	3.6182	3.6182	0.4691

Table 3.1: The values of critical double-minimum wavenumber, (k_{1c},k_{2c}), the critical time, τ_c, and the computed value of Ra for the given values of α^* when and $K^* = 0.02$.

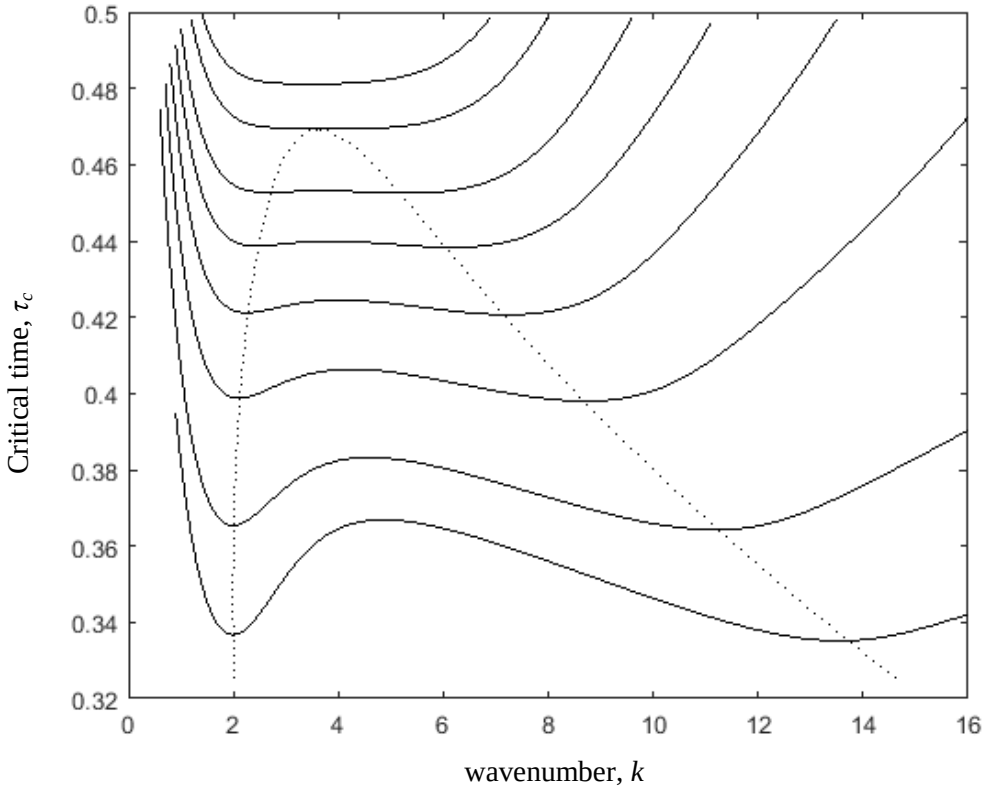

Figure 3.4: Neutral curves corresponding to different values of α^* for double-minimum cases when $K^* = 0.02$. The curves from the lowest upwards correspond to $\alpha^* =$ 0.22, 0.34, 0.43, 0.47, 0.49, 0.50, 0.5061 (quartic) and 0.51 (parabolic). For the corresponding values of Ra see Table 3.1 and Figure 3.5. The dotted line denotes the locus of the respective minimum points.

Figure 3.4 is incomplete in the sense that it doesn't display the corresponding values of Ra or α, which are also computed; these values are shown in Figures 3.5 and 3.6. The base of the *Ra* curve in Figure 3.5 corresponds to the quartic neutral curve which touches the top of the dotted curve in Figure 3.4. We see that, as the critical time reduces in Figure 3.4, the corresponding value of Ra increases.

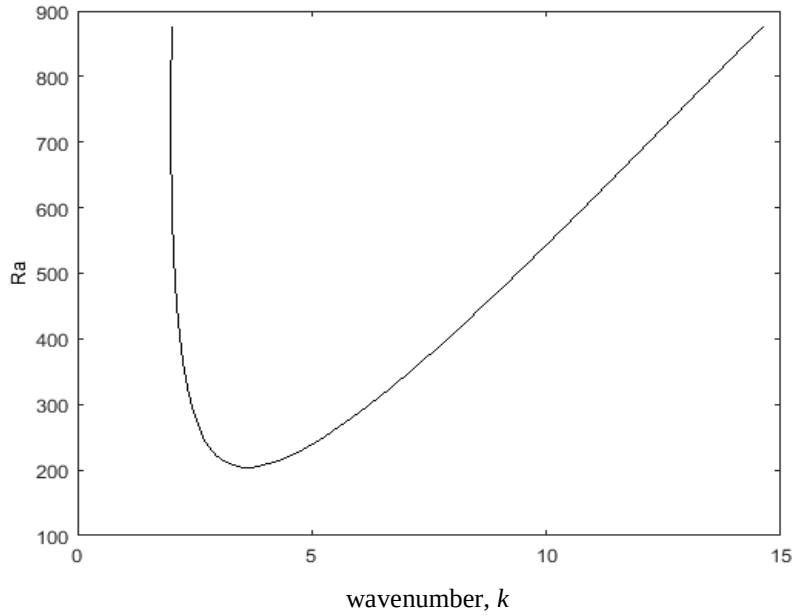

Figure 3.5: The variation of Ra at the double-minimum points for $K^* = 0.02$ and $c = 0.05$. This curves corresponds to the values of τ in Figure 3.4 and α in Figure 3.6.

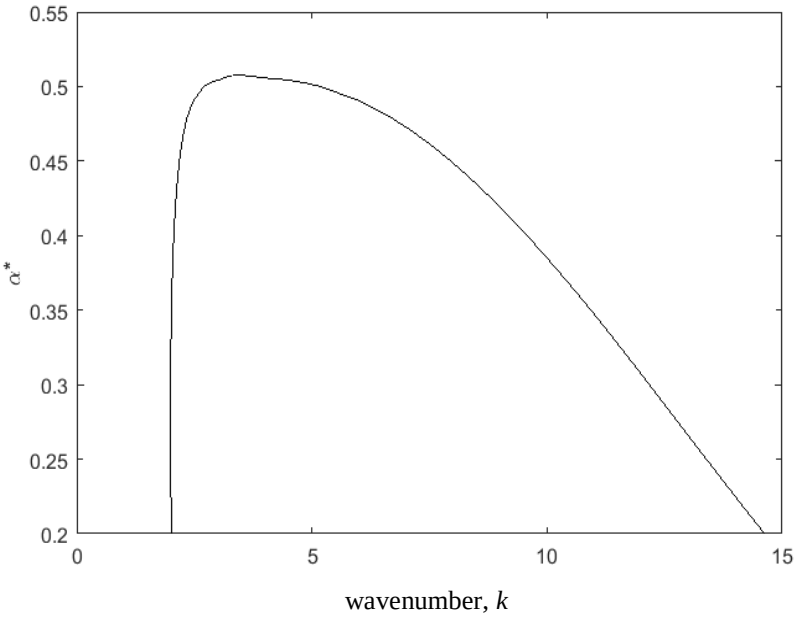

Figure 3.6: The variation of α^* at the double-minimum points for $K^* = 0.02$ and $c = 0.05$. This curve corresponds to the values of τ in Figure 3.4 and Ra in Figure 3.5.

There remains one free parameter, namely K^*, which means that there must also be neutral curves with a quartic minimum in the neighbourhood of the present value, $K^* = 0.02$. Therefore further numerical studies were performed for other values of K^* in order to find how the location of the quartic point varies in parameter space. Figure 3.7 shows how the value of α^* varies with K^*, and the trend appears to be roughly linear for the range of values of K^* which we have considered. Table 3.2 gives numerical information on how Ra_c, α^*, k_c and τ_c vary with K^*.

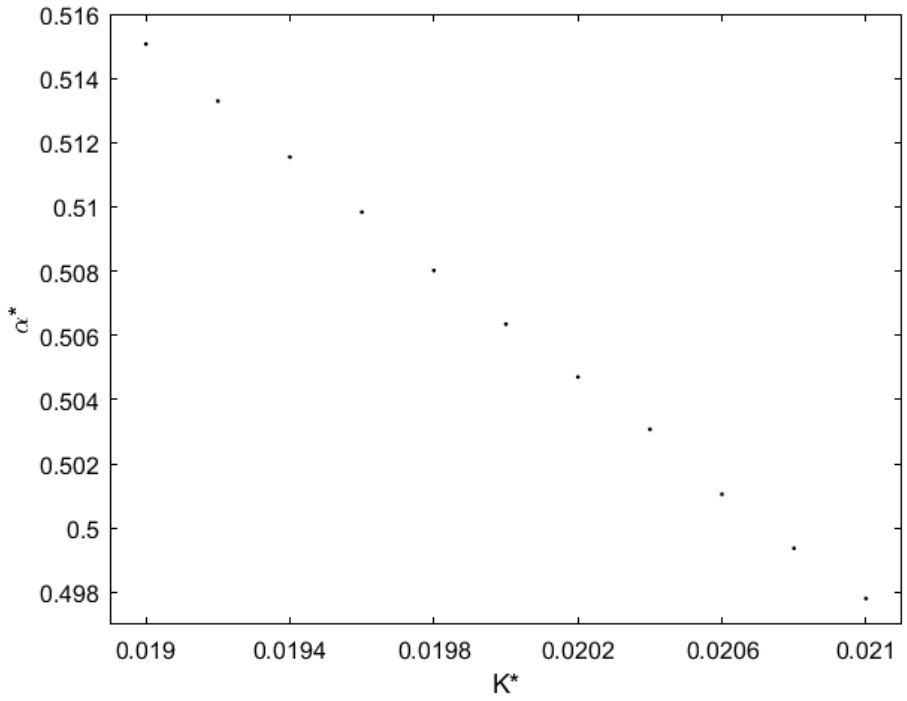

Figure 3.7: Graph of the relationship between the permeability ratio, K^* and the diffusivity ratio, α^* for $0.019 \leq K^* = 0.021$ for which a quartic minimum occurs. Table 3.2 gives further information.

Ra_c	K^*	α^*	k_c	τ_c
217.0312	0.0190	0.5151	3.6471	0.4648
214.3415	0.0192	0.5133	3.6419	0.4656
211.7510	0.0194	0.5116	3.6366	0.4664
209.2352	0.0196	0.5098	3.6316	0.4671
206.3223	0.0198	0.5080	3.6233	0.4683
203.7273	0.0200	0.5061	3.6182	0.4691
201.6217	0.0202	0.5047	3.6135	0.4698
199.3771	0.0204	0.5031	3.6090	0.4705
196.6533	0.0206	0.5011	3.5936	0.4718
195.2122	0.0208	0.4994	3.5868	0.4726
192.1798	0.0210	0.4978	3.5821	0.4735

Table 3.2: The values of the different government parameters on the locus of quartic minimum points..

3.7.2 Disturbance profiles at onset

In this subsection a small selection of instantaneous disturbance profiles will be shown in order to illustrate some of the previous comments about where the disturbances exist.

Figures 3.8 and 3.9 display the respective temperature and streamfunction profiles for those conditions where there is a double minimum, and where the critical parameters are given in Table 3.1. In both Figures the disturbances have been rescaled to have a maximum value of 1 simply so that each case may be compared easily. Concentrating first on the $\alpha^* = 0.22$, case in Figure 3.8 we see that the disturbance with the smaller critical wavenumber ($k_{1c} = 2.0049$) mainly occupies layer 1 while the disturbance with the larger critical wavenumber ($k_{2c} = 14.1242$) is closer to the interface but mostly above it. The Rayleigh number is roughly 840. Both the extent and location of these thermal disturbances model exactly the qualitative argument given earlier when discussing Figure 3.2.

As α^* increases towards 0.5061, the value corresponding to the quartic point, the critical wavenumbers become closer. In particular the upper critical wavenumber decreases quite rapidly, and, on assuming that convection cells remain of roughly the same aspect ratio in uniform media, this is confirmed by the increasing width of the disturbance temperature profile. By contrast, the lower critical wavenumber changes much more slowly and therefore that disturbance profile hardly changes.

Without exception, all the streamfunction profiles shown in Figure 3.9 are wider than their thermal counterparts in Figure 3.8. The mathematical reason for this is that the temperature profiles decrease superexponentially because of the presence of the $\eta\theta_\eta$ term in Equation (3.24b). On the other hand the streamfunction decreases exponentially, and will be proportional to $\exp[-k_c y]$, and therefore the decay of the two modes, whilst both being exponential, are at different rates. The disturbance with the lower critical wavenumber decays relatively slowly to that with the larger wavenumber.

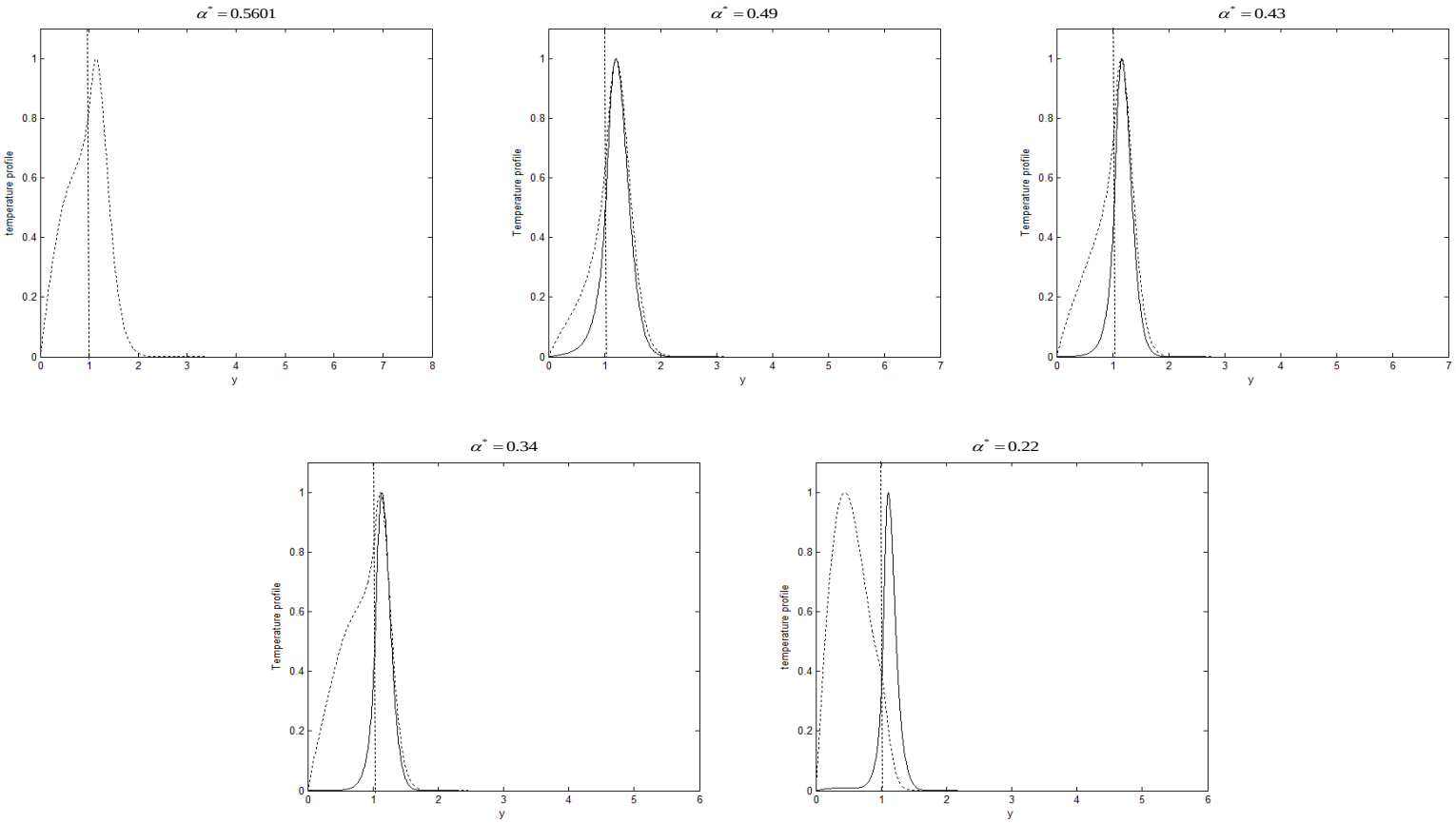

Figure 3.8: (From left) Temperature profiles at onset for $K^* = 0.02$ and for both the critical wavenumbers where $\alpha^* = 0.5601$ (quartic minimum), 0.49, 0.43, 0.34 and 0.22. Dashed lines correspond to profiles at $k = k_1$ and the continuous lines to $k = k_2$. Other numerical data may be found in Table 3.1.

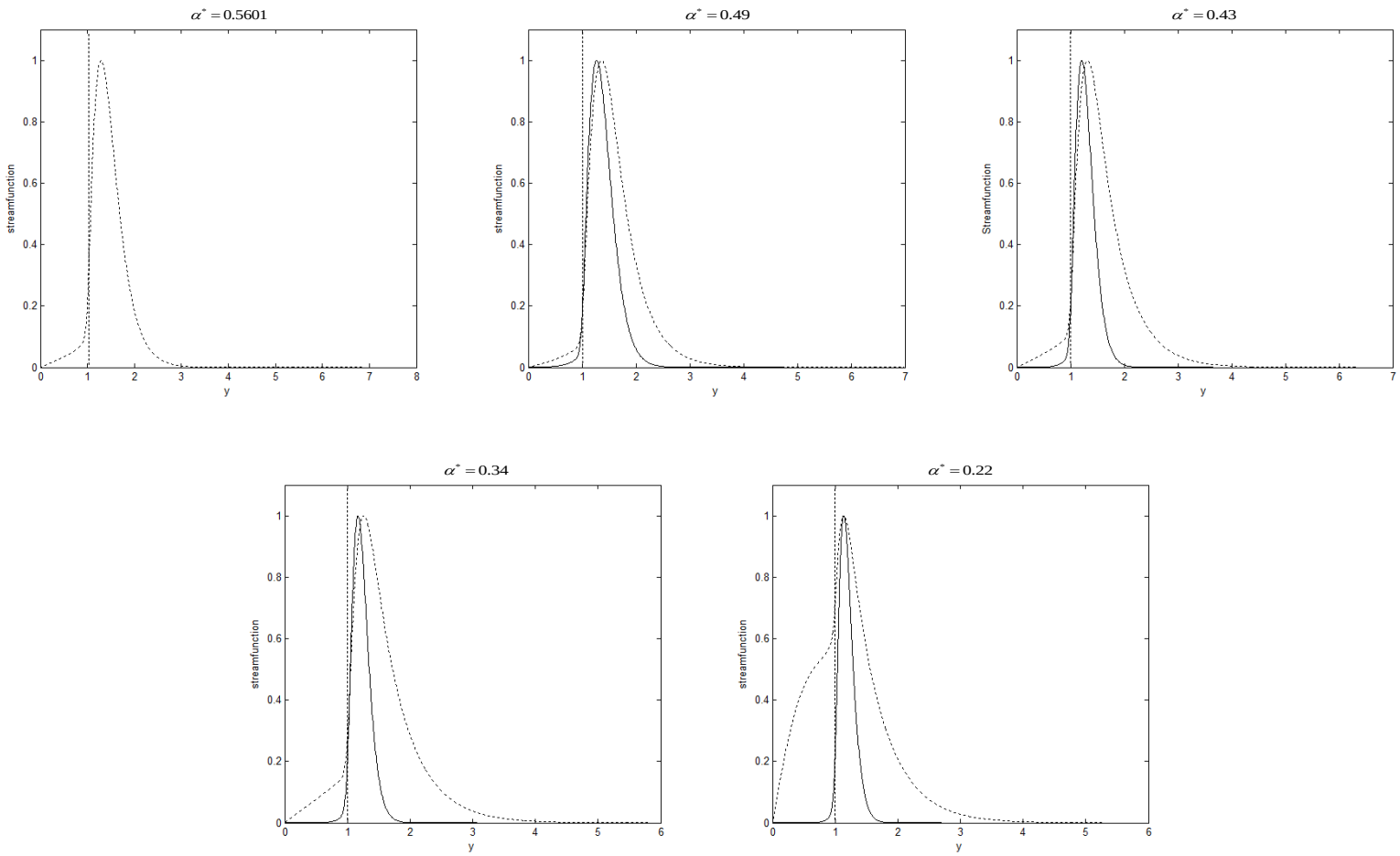

Figure 3.9: Reduced streamfunction profiles corresponding to the temperature profiles given in Figure 3.8.

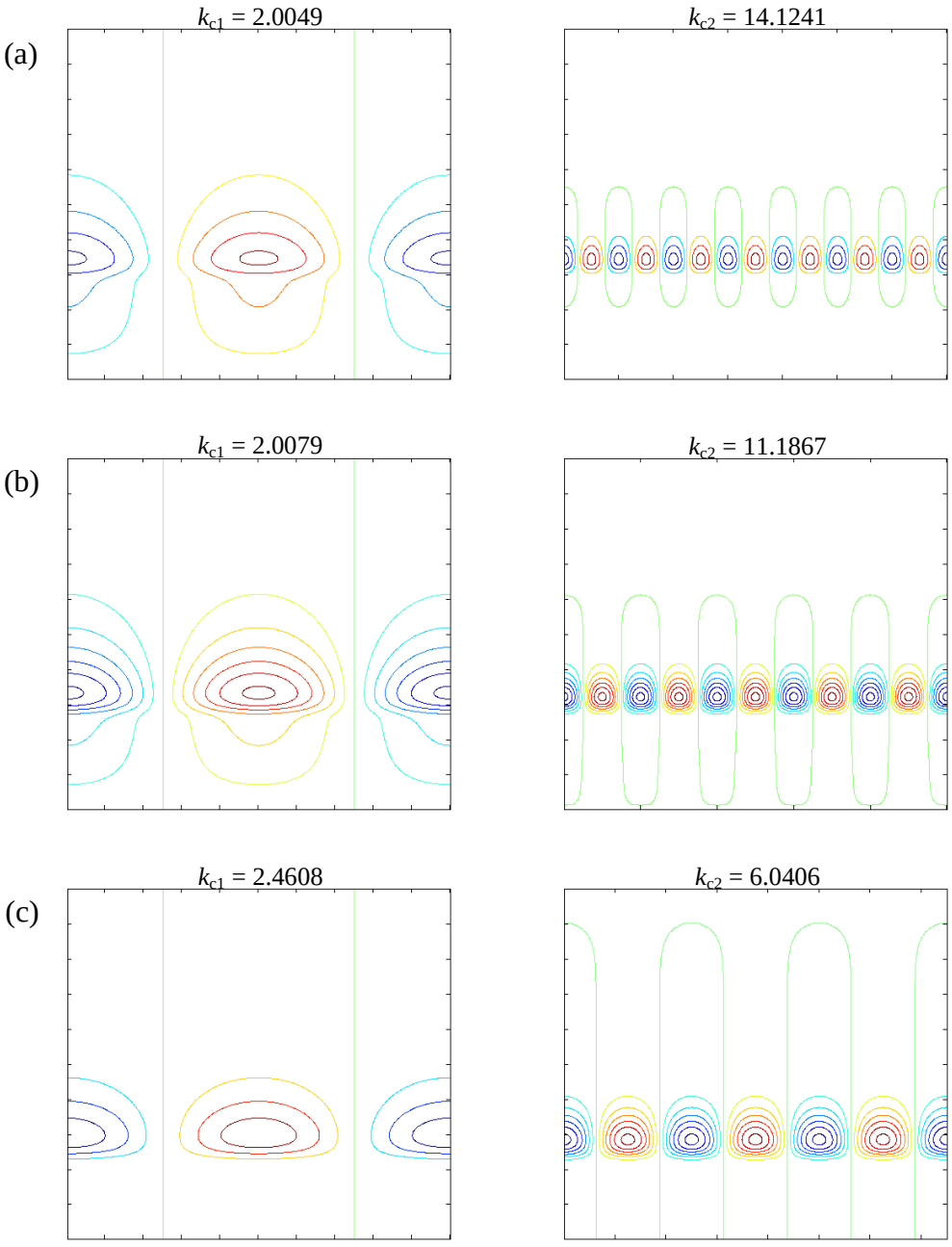

Figure 3.10: Two-dimensional mode shapes corresponding to the following three double minima (see Table 3.1) and at both minima: (a) $\alpha^* = 0.22$, (b) $\alpha^* = 0.34$ and (c) $\alpha^* = 0.49$. In all cases $K^* = 0.02$ and $c = 0.05$.

Figure 3.10 shows a reconstruction of the two-dimensional onset mode shapes at the critical times for the three double minimum points given by: (a) $\alpha^* = 0.22$, $k_1 = 2.0049$, $k_2 = 14.1241$, (b) $\alpha^* = 0.34$, $k_1 = 2.0079$, $k_2 = 11.1867$ and (c) $\alpha^* = 0.49$, $k_1 = 2.4608$, $k_2 = 6.0406$; in all cases $K^* = 0.02$ and $c = 0.05$. We have plotted the disturbance isotherms, Θ; see Equation 3.25. Figure 3.10(a) corresponds to a case when the critical wavenumbers are very well separated and are in a ratio of roughly 7. This contrast in ratio is seen clearly not only in the width of these cells but also in their vertical extent. In this case, for which $\alpha^* = 0.22$, a substantial part of the temperature disturbance lies in layer 1 for the smaller wavenumber, but is predominantly in layer 2 for the larger wavenumber; this is entirely consistent with the corresponding profiles shown in Figure 3.8.

As α^* decreases, seen in Figures 3.10(b) and 3.10(c), the modal shapes tend towards a common shape and the cells to a common width; the increase in the width of the disturbance for the larger wavenumber is particularly evident, which correlates with the reduction in k_{c2}.

3.7.3 Some examples of the evolution of disturbance profiles with time.

Figures 3.11 and 3.12 display some examples of how the temperature disturbance profiles vary with time. The cases chosen are essentially random but are nevertheless in the vicinity of cases which have already been presented. Thus, Figure 3.11 shows this variation for the case: $Ra = 900$, $K^* = 0.02$ and $k = 4$ for three different values of α^*. In this Figure and in Figure 3.12, all the profiles have been normalised to have a maximum of 1, and therefore information about the strength of the disturbance has been lost. The aim here is see how the disturbances pass through the interface and how this evolution is affected by changes in the thermal diffusivity of layer 1.

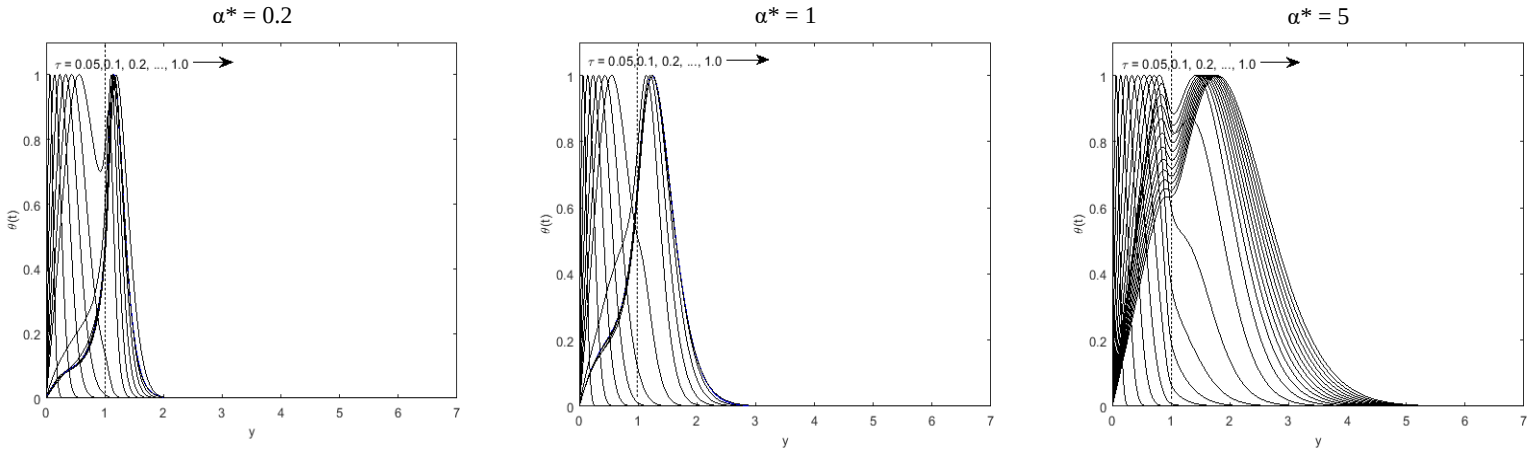

Figure 3.11: Evolution of the temperature profile over τ for the case Ra = 900, K^* = 0.02 and k = 4 with the given values of α^*.

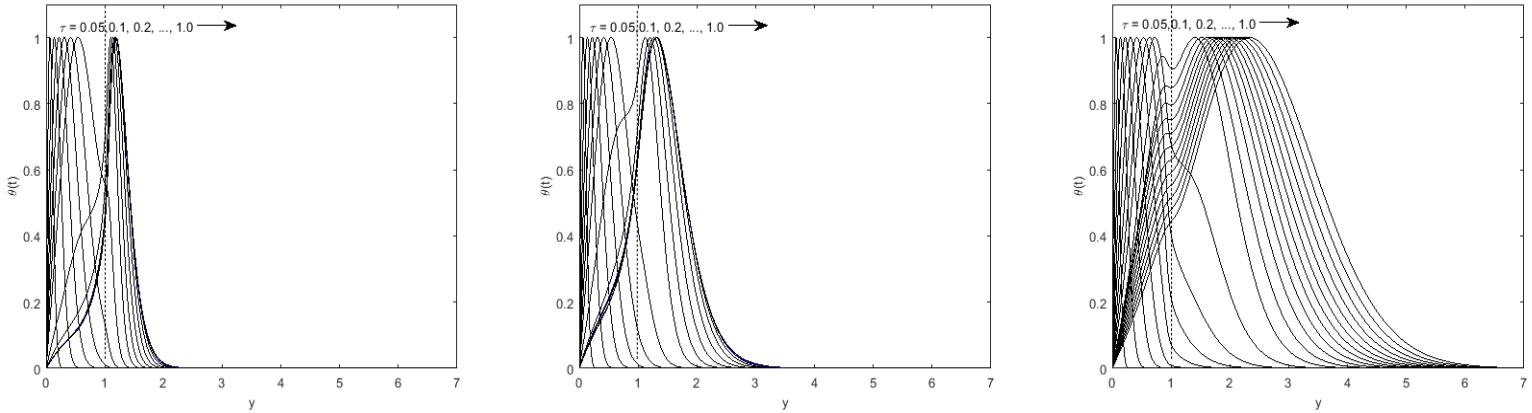

Figure 3.12: Evolution of the temperature profile over τ for the case Ra = 400, K^* = 0.02 and k = 3 with the given values of α^*.

When $\alpha^* = 0.2$ we see the disturbance growing width as time, as measured by τ, increases. In this early phase the magnitude of the disturbance is decaying. Very soon after this thickening profile enters layer 2, the profile very quickly develops a second maximum while the original is still well within layer 1. As both the permeability and the diffusivity of layer 2 are much larger than that of layer 1, the disturbance grows preferentially in layer 2, and therefore the maximum in layer 1 decays rapidly compared with the one in layer 2.

In the other cases shown in Figure 3.11, essentially the same scenario happens, except that, when $\alpha^* = 5$, the disturbance evolves much more rapidly in layer 1 than it does when $\alpha^* = 0.2$, and therefore the disturbance has penetrated much further in this case (note the different scales on the horizontal axes). Figure 3.12 appears to provide almost identical curves to those in Figure 3.11, but the chosen wavenumber and Rayleigh number are different. Therefore it is possible to conclude that, for small values of K^* but a wide range of values of α^*, there is a dramatic transition in the shape of the developing profile as the disturbance traverses the interface.

Finally, in Figure 3.13, we present an alternative view of the behavior of those temperature profiles which are depicted in Figure 3.11. In Figure 3.11 for $\alpha^* = 0.2$ there are profiles which either have one maximum, or else have two maxima and an intervening minimum. The values of y at which these extrema occur were also recorded as a function of τ, and it is these which are shown in Figure 3.13. In all three cases we see a range of times where three extrema exist. When $\alpha^* = 0.2$ and 1, this range is very limited, i.e. the transition from layer 1 dominating the profile to layer 2 doing so happens quickly. On the other hand, when $\alpha^* = 5$, this transition takes quite a long time to be achieved. Figure 3.13(c) also shows that the large-time location of the maximum quite obviously increases with time; such a phenomenon is related to the fact that the basic temperature profile, whose stability is being examined, continues to diffuse away from $y = 0$ into the ambient region beyond.

(a)

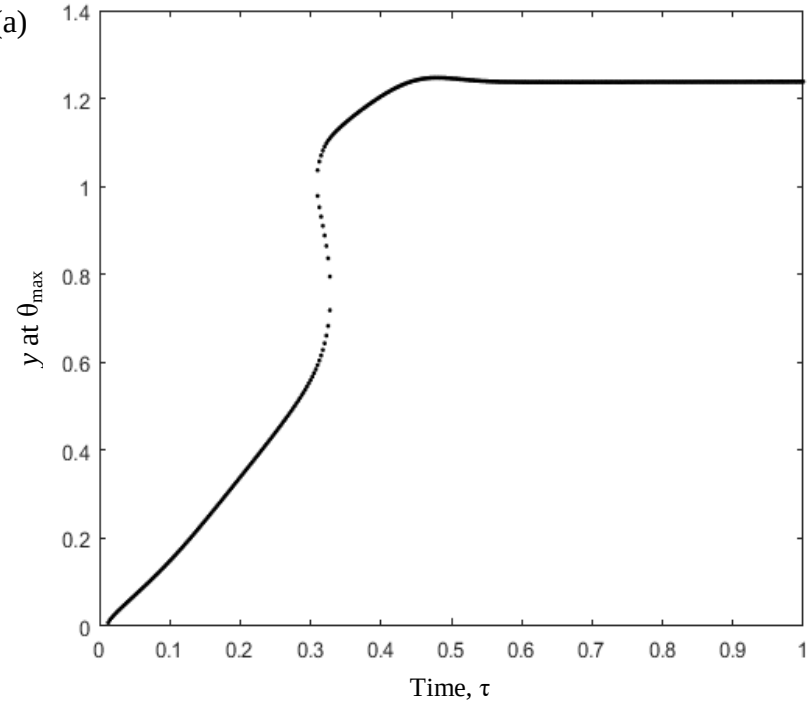
1.4
1.2
1
0.8
0.6
0.4
0.2
0
0
0.1
0.2
0.3
0.4
0.5
0.6
0.7
0.8
0.9
1
y at θmax
Time, τ

(b)

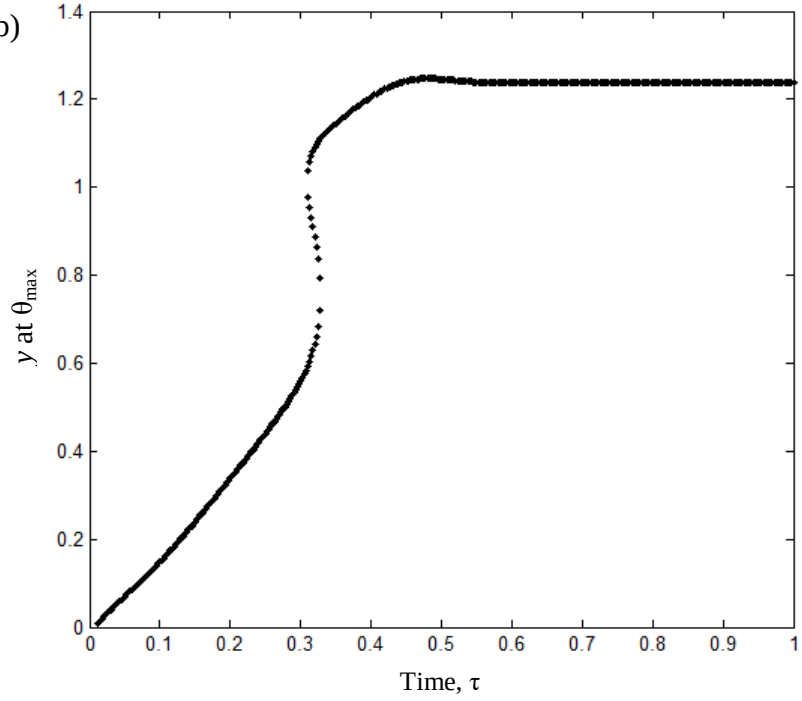
1.4
1.2
1
0.8
0.6
0.4
0.2
0
0
0.1
0.2
0.3
0.4
0.5
0.6
0.7
0.8
0.9
1
y at θmax
Time, τ

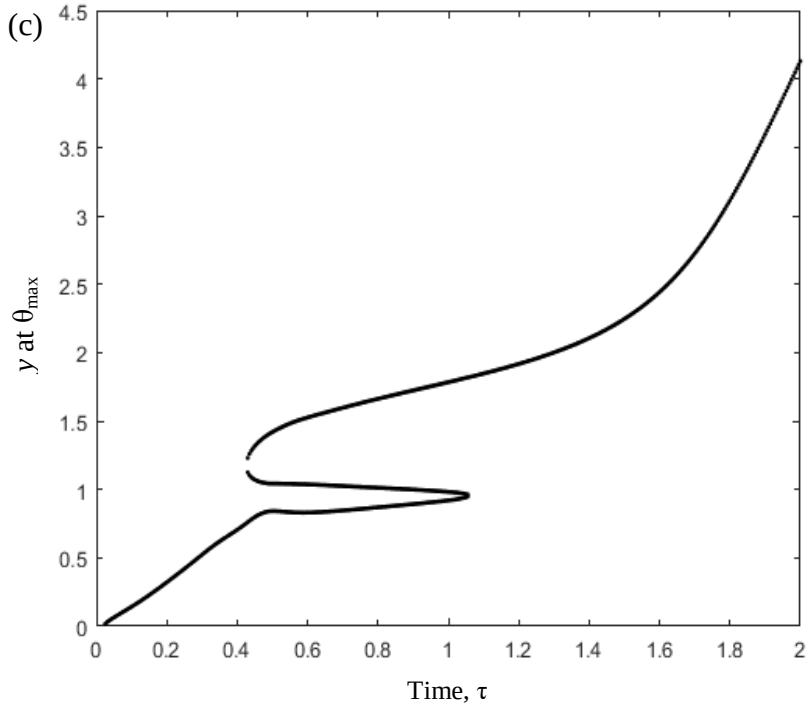

Figure 3.13: Graph of y at which the temperature profile achieves the local maximum θ_{max} (and minimum should there be two maxima), against time, τ, for the case Ra = 900, K^* = 0.02 and k_1 = 4 in variation of (a) α^* = 0.2, (b) α^* = 1 and (c) α^* = 5.

3.8 Conclusion

In this work, the onset of convection of the unsteady two-dimensional thermal boundary layer in a semi-infinite region of saturated porous medium consisting of two different homogeneous layers has been determined by employing a numerical linear stability analysis. When the temperature of the lower boundary is raised suddenly the resulting temperature field expands and eventually passes through the interface between the two porous media. We have studied the stability of this thermal boundary layer by introducing small-amplitude thermal disturbances, and then by monitoring the variation in time of the magnitude of a measure of the

thermal energy. The overall aim has been to investigate whether bimodal neutral curves (i.e with two minima corresponding to simultaneous onset times) can exist for this configuration. We have not only shown that such bimodal curves exist, but that the minima can coalesce to form a neutral curve with a single quartic minimum. Given that there remains one more free parameter to vary, we have also presented further parameter sets for which there exists a quartic minimum. We have also shown how the presence of the interface causes the shape of the disturbance profile to vary in unusual ways. When the two layers are identical, which is the case studied by Selim and Rees [20], the thermal disturbance has one well-defined maximum. While we would expect this to be true in general for the present problem, the range of parameters we have considered, where the properties of the two sublayers are very different from one another, yields disturbance profiles which can have two maxima for a short interval of time.

The present work has not been comprehensive because we have wished to seek out those conditions which can yield neutral curves with multiple minima. The work of Rees & Riley [16] suggests that a three layer system (with two sublayers of finite height) might be possible for a suitable choice of sublayer properties. We are also aware that we have approximated what would normally be a discrete discontinuity between the sublayers by a rapidly-varying smooth variation. Given that the variation is rapid, and given that the presence of bimodal curves occupies a large region of parameter space, we think it is very likely indeed that bimodal curves would also appear for the computationally more difficult case of discrete layering. Further work on this topic should also include nonlinear simulations.

3.9 References

[1] Horton, C.W., Rogers, F.T. (1945). Convection currents in a porous medium. *J. Appl. Phys*., **16**, 367–370.

[2] Lapwood, E.R. (1948).Convection of a fluid in a porous medium. *Math. Proc. Camb. Phil. Soc*., **44**, 508–521.

[3] Katto, Y., Masuoka, T. (1967). Criterion for the onset of convective flow in a fluid in a porous medium. *Intl J. Heat Mass Transfer*, **10**, 297-309.

[4] Rees, D.A.S., Riley, D.S. (1989). The effects of boundary imperfections on convection in a saturated porous layer: near-resonant wavelength excitation. *J. Fluid Mech*., **199**, 133–154.

[5] Newell, A.C., Whitehead, J.C. (1969). Finite bandwidth, finite amplitude convection. *J. Fluid Mech*., **38**, *38***,** 279–303.

[6] Georghitza. St.I. (1961). The marginal stability in porous inhomogeneous media. *Proc. Camb. Phil. Soc*., **57**, 871-877.

[7] Donaldson, I.G. (1970). The simulation of geothermal system with a simple convective model. Geothermics, **1**, 649-654.

[8] Rana, R., Horne, R.N., Cheng, P. (1979). Natural convection in a multi-layered geothermal Reservoir. *Trans. ASME C: J. Heat Transfer*, **101**, 411-416.

[9] McKibbin, R., O'Sullivan, M.J. (1980). Onset of convection in a layered porous medium heated from below. *J. Fluid Mech*., **96**, *96*, 375-393.

[10] McKibbin, R., O'Sullivan, M.J. (1981). Heat Transfer in a layered porous medium heated from Below. *J. Fluid Mech*., **111**, 141-173.

[11] McKibbin, R., Tyvand, P.A. (1983). Thermal convection in a porous medium composed of alternating thick and thin layers. *Intl. J. Heat Mass Transfer*. 26, 761-780.

[12] McKibbin, R., Tyvand, P.A. (1984). Thermal convection in a porous medium with horizontal cracks. *Intl. J. Heat Mass Transfer*. **27**, 1007-1023.

[13] Rees, D.A.S., Riley, D.S. (1990). The three-dimensional stability of finite-amplitude convection in a layered porous medium heated from below. *J. Fluid Mech*. **211,** 437–461.

[14] Shalbaf, S., Noghrehabadi, A., Assari, M. R., Dezfuli, A.D. (2013). Linear stability of natural convection in a multilayer system of fluid and porous layers with internal sources. *J. Acta Mech*. **224**, 1103-1114.

[15] Rees. D.A.S., Mojtabi, A. (2013). The effect of conducting boundaries on Lapwood-Prats convection. *Intl. J. Heat Mass Transfer*, **65**, 765-778.

[16] Rees, D.A.S., Patil, P.M. (2013). Linear instability of a horizontal thermal boundary layer formed by vertical throughflow in a porous medium: the effect of local thermal nonequilibrium. *J. Tansp Porous Med*., **99**, 207-227.

[17] Selim, A., Rees, D.A.S. (2007). The stability of a developing thermal front in a porous medium. I linear theory. *J. Tansp Porous Med*., **10**, 1-15.

Chapter 4

The effect of layering on unsteady conduction: an analytical solution method.

4.1 Abstract

The aim of this chapter is to present a mathematical study of the effect of layering on unsteady conduction in a layered solid. We have considered a semi-infinite solid domain which exhibits layering and where the boundary of that domain is suddenly raised to a new temperature. Each layer has its own thermal conductivity and diffusivity, and therefore the non-dimensional parameters are conductivity ratios and diffusivity ratios. The 2-layer and 3-layer systems are studied in detail over a wide range of variation of the governing non-dimensional parameters. The solution for the governing equations is obtained analytically by employing the Laplace transform. It is found that the general solution for the multilayer system may be expressed in terms of summations over different image systems and, when there are N layers, the solution will be comprised of $(N - 1)^2 - 1 = N^2+2N$ nested summations. It is also shown that multilayer systems reduce to a single layer system when the products of α and k are equal for all layers, where α is the square root of a diffusivity ratio and k is a conductivity ratio. On the other hand, when there are variations in α and k between the layers, it is concluded that those coefficients affect strongly the temperature drops and the overall thickness of the evolving boundary layer. Thus, the thermal diffusivity ratio and the thermal conductivity ratio are the coefficients that play the important role in determining the manner in which conduction occurs. In

particular, the thermal diffusivity ratio affects how quickly the temperature field evolves in time.

4.2 Nomenclature

A, B, C	constants
k	thermal conductivity ratio
L	thickness
Nu	Nusselt number
p	Laplace Transform variable
t	time
T	temperature
x	Cartesian coordinate

Greek letters

$\bar{\alpha}$	thermal diffusivity
$\alpha_n = \sqrt{\frac{\bar{\alpha}_{ref}}{\bar{\alpha}_n}}$	square root of a diffusivity ratio
θ	temperature profile
Θ	Laplace transform of the temperature
ρ	fluid density
ξ	quantities defined in (4.7)

Superscripts and subscripts

n	layer n
ref	reference value

∞	initial conditions
1	layer 1
2	layer 2
3	layer 3
$\bar{}$	denote dimensional variables

4.3 Introduction

The diffusion of matter and the conduction of heat in composite media has attracted attention from researchers in recent years, especially for systems involving multiple layers. The importance of multilayer diffusion has wide applications in area of heat transfer, such as in industrial applications, specifically in annealing steel coils (Barry and Sweatman [1] and McGuinness et. al [2]), biotechnological applications especially when studying the effectiveness of drug carriers inserted into living tissue (Pontrelli and Monte [3]) and last, but not least, in engineering applications such as in composite slabs; see Monte [4].

The first few studies in multilayer diffusion was presented by Ash, Barrer and Petropoulos [5] who studied theoretically the diffusion through a laminated membrane of n pairs of alternating materials labelled A and B and discussing the effect of diffusivity coefficients, permeability and time lags. In their work, they assumed the diffusivity coefficients of each layers is constant, and they were keen to find out the overall diffusivity coefficients for the laminated membrane by using the time-lag methods. Recently researchers have been fond of finding the exact and analytical solutions for the multilayer diffusion for various applications and geometries. For instance the exact solution for multilayer diffusion in cylindrical coordinates by Lu et. al [6] who developed an analytical method as the extension to the existing analytical approach derived to solve the heat conduction in a composite

slab. They used the separation of variables method to solve a system with time dependent boundary conditions. The result obtained for the *n*-layer closed form solution demonstrated a great accuracy and agreement with numerical result. Subsequently, Kayhani et. al [7] considered more complex boundary conditions which were based on the combination of conduction, convection as well as the internal and external radiation of the cylindrical laminate. Dalir and Nourazar [8], who have similar interests to Lu et. al [6] and Kayhani et. al [7], in solving for multilayer diffusion in cylindrical coordinates, have chosen to solve the three dimensional transient heat conduction equations with both homogeneous and inhomogeneous boundary conditions. On the other hand, there are a few other researchers who analytically solved multilayer diffusion in Cartesian coordinates, such as Monte [9], who considered unsteady heat conduction for a one dimensional multilayer where the boundaries are subjected to a convective heat flux. Later, Miller and Weaver [10] extended the work to more complex boundary conditions with a consideration of fully and partially unsteady convection boundary conditions as well as radiation boundary conditions. Hickson et. al [11] solved the steady state multilayer diffusion analytically for an insulated boundary condition.

In the analytical solution of these heat transfer problems, the most common mathematical method which is used is the method of separation of variables. However, in their paper Hickson et. al [12] applied a traditional averaging method to mark the critical times in multilayer diffusion, defined as the time required for the average temperature to reach a specified proportion of the average steady state. Hickson et. al have assumed the approximation of this critical time to be the ratio of the total length of the medium and the average diffusivity defined as the series-averaged diffusivity. The exact solution obtained by Hickson et. al for this steady-state multilayer diffusion with general boundary and interface conditions demonstrated that the implementation of the traditional averaged method however is restricted only to the steady state and for a large number of layers. Later, Hickson et. al [13] found that the results obtained from the employment of traditional averaging

methods previously was inaccurate when it failed to explain the behavior of the critical diffusion time defined such as the heating time of the material or the order of layer. Hickson et. al [13] then improved the weaknesses of the previous study by employing a perturbation expansion. It was found that as the number of layers increases, all the solutions approach to the single layer solution. In fact the manner in which the material is layered does not then affect the critical time of diffusion when the number of alternating layers is large.

While many studies have been devoted to the analytical methods mentioned above, there has been a lack of attention given to the possibility of using the Laplace transform, and this may be due to the complexity in finding the inverse transform, which frequently needs to be found numerically. Despite the complexity of the Laplace transform, Diard et.al [14] and Azeez and Vakakis [15] have used the method to solve other types of multilayer diffusion problems analytically and numerically. In Diard et.al's study in an Electrochemical impedance spectroscopy (EIS) of multilayer electrodes they concluded that a multilayer electrode cannot be assumed to be equivalent to any monolayer electrode and, most importantly, the order of the layering determines the electrochemical response of the system. While Azeez and Vakakis have chosen to apply the Laplace transform method in combination with the Hankel method to encounter any numerical instabilities that arise when the number of layers is infinite. However, the solution is unfortunately hard to employ due to the double numerical inversion of the transformed solution. This is among the reasons for not being the favorably chosen method among researchers to employ in their study.

Beside the analytical methods applied by the above mentioned researchers, in particular the separation of variables and traditional averaging methods, the common aim for all of the publications is the search for the critical time for multilayer diffusion where the critical time is subject to many different definitions, and these depend on the context defined by the researcher. The most common definition of

critical time is the time taken for the temperature to reach the steady state. and therefore it is a measure of how long the diffusive process takes. Another definition is the length of time taken for a change in temperature to be felt at a far boundary. Therefore, in the present paper, we do not compute critical times because we shall assume that the solid region is semi-infinite, but rather our aim is to use Laplace transforms to obtain an exact solution for unsteady heat diffusion in layered systems. Variations in the governing parameters are made in order to determine their effect on the diffusion process.

4.4 Governing equtions

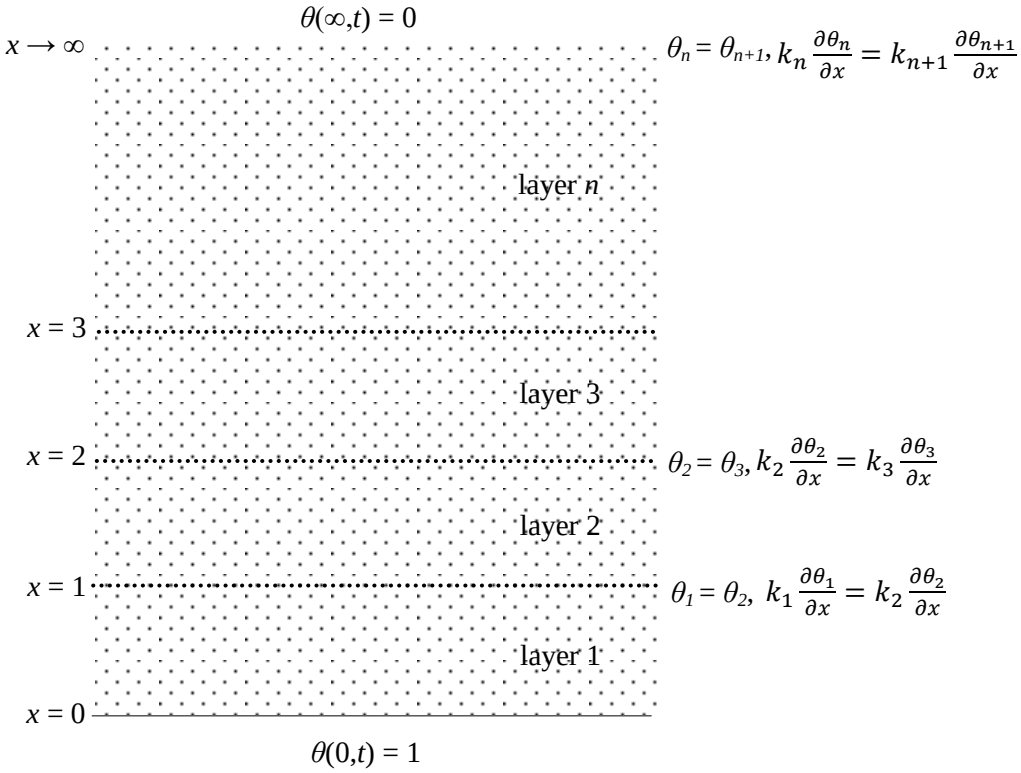

Figure 4.1: Depicting the semi-infinite medium and the imposed boundary and interface conditions in nondimensional form.

In this chapter we will consider the unsteady heat conduction which is induced by the sudden raising of the temperature of the plane boundary of a semi-infinite region from the ambient value to a new constant value. We will consider in turn and in detail, semi-infinite domains with zero, one or two uniform sublayers each of thickness, *L*, placed next to the heated surface. The region which is adjacent to the heated surface is labeled as layer 1, as shown in Figure 4.1. Layer *n* has thermal conductivity and thermal diffusivity equal to $\bar{k}_n$ and $\bar{\alpha}_n$, respectively.

For layer *n*, the dimensional form of Fourier's equations is

$$\frac{\partial \bar{\theta}_n}{\partial \bar{t}} = \bar{\alpha}_n \frac{\partial^2 \bar{\theta}_n}{\partial \bar{x}^2}. \tag{4.1}$$

At an interface between two neighbouring layers, we have the following continuity of temperature and continuity of heat flux conditions at $\bar{x} = nL$:

$$\bar{\theta}_n = \bar{\theta}_{n+1}, \text{ and } \bar{k}_n \frac{\partial \bar{\theta}_n}{\partial \bar{x}} = \bar{k}_{n+1} \frac{\partial \bar{\theta}_{n+1}}{\partial \bar{x}}. \tag{4.2}$$

At $\bar{t} = 0$ the temperature everywhere is at the ambient value $\bar{T} = \bar{T}_{\text{cold}}$, but the boundary at $\bar{x} = 0$ has its temperature raised suddenly to T_{hot}. This is an "impulsive" change in the thermal boundary condition at $\bar{x} = 0$.

We may now nondimensionalise the above equation and the boundary and initial conditions by using the following substitutions,

$$\bar{x} = Lx, \ \bar{t} = \frac{L^2}{\bar{\alpha}_{\text{ref}}} t, \qquad \bar{\theta} = \left(T_{\text{hot}} - T_{\text{cold}}\right)\theta + T_{\text{cold}}, \tag{4.3}$$

where the reference thermal diffusivity, $\bar{\alpha}_{\text{ref}}$, corresponds to one of the layers. Therefore Eq. (4.1) reduces to,

$$\alpha_n^2 \frac{\partial \theta_n}{\partial t} = \frac{\partial^2 \theta_n}{\partial x^2}, \tag{4.4}$$

where $\alpha_n^2 = \bar{\alpha}_{\text{ref}} / \bar{\alpha}_n$. This slightly unusual form of the heat diffusion equation makes for a simpler presentation of results later and the reference layer will always be the one of infinite extent. This definition of α_n means that the later physical descriptions have to account for the fact it relies on a negative power of the layer's diffusivity. The general interface conditions at $x = n$, are,

$$\theta_n = \theta_{n+1}, \quad \text{and} \quad k_n \frac{\partial \theta_n}{\partial x} = k_{n+1} \frac{\partial \theta_{n+1}}{\partial x}. \tag{4.5}$$

Finally, the initial condition is that we have $\theta = 0$ everywhere at $t < 0$, while the boundary condition is that we set $\theta_1 = 1$ at $x = 0$ and for $t > 0$.

4.5 Analytical solutions

4.5.1 The single layer analysis

When the whole of the region in $0 \le x < \infty$ has constant physical properties we have to choose region 1 to be the reference region, and hence we solve,

$$\frac{\partial \theta}{\partial t} = \frac{\partial^2 \theta}{\partial x^2}, \tag{4.6}$$

where the subscripts have been dropped for this uniform case. This is the classical sudden heating problem which is very often taught to students at undergraduate level. The solution may be obtained quite quickly by means of a similarity analysis. This solution is,

$$\theta = \text{erfc}\left(\frac{x}{2\sqrt{t}} \right) = \frac{2}{\sqrt{\pi}} \int_{x/2\sqrt{t}}^{\infty} e^{-\xi^2} d\xi. \tag{4.7}$$

For the purposes of the present chapter we shall solve the same problem using the Laplace Transform, $\mathscr{L}$.

$$\Theta(x,t) = \mathscr{L}\left[\theta(x,t)\right] = \int_0^\infty \theta(x,t) e^{-pt}\, dt. \tag{4.8}$$

Therefore Eq. (4.6) transforms to,

$$\frac{\partial^2 \Theta}{\partial x^2} - p\Theta = 0, \tag{4.9}$$

and this has to be solved subject to $\Theta = 1/p$ at $x = 0$ as this is the Laplace transform with respect to time of the boundary condition, $\theta = 1$, at $x = 0$. Hence the solution is,

$$\Theta = \frac{e^{-\sqrt{p}x}}{p}, \tag{4.10}$$

because the final solution cannot grow exponentially with x for physical reasons. The following formula will be used very frequently in the rest of the paper, and therefore it is quoted here for easy reference:

$$\mathscr{L}\left[\operatorname{erfc}\left(\frac{x}{2\sqrt{t}}\right)\right] = \frac{e^{-\sqrt{p}x}}{p}. \tag{4.11}$$

4.5.2 The two-layer analysis

In this subsection we consider the two-layer case, which means that the domain is comprised of a layer of unit thickness next to the heated surface, and the rest of the domain is semi-infinite. The uniform layer which is adjacent to the heated surface is denoted as layer 1, while the rest of the semi-infinite domain is layer 2. The governing equations are,

$$\alpha_1^2 \frac{\partial \theta_1}{\partial t} = \frac{\partial^2 \theta_1}{\partial x^2}, \quad (0 \le x \le 1),$$
$$\alpha_2^2 \frac{\partial \theta_2}{\partial t} = \frac{\partial^2 \theta_2}{\partial x^2}, \quad (1 \le x), \tag{4.12}$$

while the boundary and interface conditions are,

$$x = 0: \quad \theta_1 = 1,$$
$$x = 1: \quad \theta_1 = \theta_2, \; k_1 \frac{\partial \theta_1}{\partial x} = k_2 \frac{\partial \theta_2}{\partial x}, \tag{4.13}$$
$$x \to \infty: \; \theta_2 \to 0.$$

We note that α_2 = 1 here because layer 2 is the reference layer, but the following solutions display their symmetries much better when we retain the general notation. The Laplace transforms of Eqs. (4.12) yield the Ordinary Differential Equations,

$$\frac{\partial^2 \Theta_1}{\partial x^2} - \alpha_1^2 p \Theta_1 = 0,$$
$$\frac{\partial^2 \Theta_2}{\partial x^2} - \alpha_2^2 p \Theta_2 = 0, \tag{4.14}$$

and their solutions may be written as,

$$\Theta_1 = A_1 e^{\alpha_1 \sqrt{p} x} + B_1 e^{-\alpha_1 \sqrt{p} x},$$
$$\Theta_2 = A_2 e^{\alpha_2 \sqrt{p} (x-1)} + B_2 e^{-\alpha_2 \sqrt{p} (x-1)}. \tag{4.15}$$

The boundary and interface conditions given in Eqs. (4.13) may also be Laplace-transformed, given that they are steady in time, and therefore they become,

$$A_1 + B_1 = \frac{1}{p},$$

$$A_1 e^{\alpha_1 \sqrt{p}} + B_1 e^{-\alpha_1 \sqrt{p}} = A_2 + B_2, \tag{4.16}$$

$$k_1 \alpha_1 \left(A_1 e^{\alpha_1 \sqrt{p}} - B_1 e^{-\alpha_1 \sqrt{p}} \right) = k_2 \alpha_2 \left(A_2 - B_2 \right),$$

$$A_2 = 0.$$

Given that $A_2 = 0$, it is clear that A_1 and B_1 may be written in terms of B_2:

$$\begin{aligned} A_1 &= \frac{1}{2}\left(1-\frac{k_2\alpha_2}{k_1\alpha_1}\right)B_2 e^{-\alpha_1\sqrt{p}}, \\ B_1 &= \frac{1}{2}\left(1+\frac{k_2\alpha_2}{k_1\alpha_1}\right)B_2 e^{\alpha_1\sqrt{p}}. \end{aligned} \tag{4.17}$$

Substitution of these expressions into the first line of Eq. (4.16) gives,

$$B_2 = \frac{2}{p}\left[\left(1-\frac{k_2\alpha_2}{k_1\alpha_1}\right)e^{-\alpha_1\sqrt{p}} + \left(1+\frac{k_2\alpha_2}{k_1\alpha_1}\right)e^{\alpha_1\sqrt{p}}\right]^{-1}. \tag{4.18}$$

For what follows, it proves advantageous to rewrite B_2 in the following manner,

$$B_2 = \left(\frac{2}{p}\right)\left(\frac{k_1\alpha_1}{k_1\alpha_1+k_2\alpha_2}\right)e^{-\alpha_1\sqrt{p}}\left[1+\left(\frac{k_1\alpha_1-k_2\alpha_2}{k_1\alpha_1+k_2\alpha_2}\right)e^{-2\alpha_1\sqrt{p}}\right]^{-1}, \tag{4.19}$$

and then the term in square brackets may be expanded as a binomial series:

$$B_2 = \left(\frac{2}{p}\right)\left(\frac{k_1\alpha_1}{k_1\alpha_1+k_2\alpha_2}\right)e^{-\alpha_1\sqrt{p}}\sum_{n=0}^{\infty}(-1)^n\left(\frac{k_1\alpha_1-k_2\alpha_2}{k_1\alpha_1+k_2\alpha_2}\right)^n e^{-2n\alpha_1\sqrt{p}}. \tag{4.20}$$

We also find that,

$$\begin{aligned} A_1 &= \left(\frac{1}{p}\right)\left(\frac{k_1\alpha_1-k_2\alpha_2}{k_1\alpha_1+k_2\alpha_2}\right)e^{-2\alpha_1\sqrt{p}}\sum_{n=0}^{\infty}(-1)^n\left(\frac{k_1\alpha_1-k_2\alpha_2}{k_1\alpha_1+k_2\alpha_2}\right)^n e^{-2n\alpha_1\sqrt{p}}, \\ B_1 &= \left(\frac{1}{p}\right)\sum_{n=0}^{\infty}(-1)^n\left(\frac{k_1\alpha_1-k_2\alpha_2}{k_1\alpha_1+k_2\alpha_2}\right)^n e^{-2n\alpha_1\sqrt{p}}. \end{aligned} \tag{4.21}$$

The expressions for A_1, B_1, A_2 and B_2 may now be substituted back into Eqs. (4.15), and the result given in Eq. (4.11) applied. Therefore we obtain the following solution in the two layers:

$$\theta_1 = \frac{1}{\left(k_1\alpha_1 + k_2\alpha_2\right)} \sum_{n=0}^{\infty} (-1)^n \left(\frac{k_1\alpha_1 - k_2\alpha_2}{k_1\alpha_1 + k_2\alpha_2} \right)^n \left[\begin{array}{l} \left(k_1\alpha_1 + k_2\alpha_2\right) \operatorname{erfc}\left(\dfrac{\left(2n + x\right)\alpha_1}{2\sqrt{t}} \right) + \\ \left(k_1\alpha_1 - k_2\alpha_2\right) \operatorname{erfc}\left(\dfrac{\left(2n + 2 - x\right)\alpha_1}{2\sqrt{t}} \right) \end{array} \right], \tag{4.22}$$

$$\theta_2 = \frac{2k_1\alpha_1}{\left(k_1\alpha_1 + k_2\alpha_2\right)} \sum_{n=0}^{\infty} (-1)^n \left(\frac{k_1\alpha_1 - k_2\alpha_2}{k_1\alpha_1 + k_2\alpha_2} \right)^n \operatorname{erfc}\left(\frac{\left(x-1\right)\alpha_2 + \left(2n+1\right)\alpha_1}{2\sqrt{t}} \right).$$

Each of the above expressions reduce to $\theta = \operatorname{erfc}\left(\alpha_1 x / 2\sqrt{t}\right)$ when the two layers are identical (i.e. when both $k_1 = k_2$ and $\alpha_1 = \alpha_2$); which is equivalent to the 1-layer case. These expressions also simplify in the slightly more general case when $k_1\alpha_1 = k_2\alpha_2$, and we have,

$$\theta_1 = \operatorname{erfc}\left(\alpha_1 x / 2\sqrt{t}\right), \quad \theta_2 = \operatorname{erfc}\left(\frac{\left(x-1\right)\alpha_2 + \alpha_1}{2\sqrt{t}} \right). \tag{4.23}$$

It is clear that the solutions for θ_1 for the 1-layer case and when $k_1\alpha_1 = k_2\alpha_2$ for the 2-layer case are identical, but the solutions for θ_2 are different. This is of interest because it means that the measurement of heat flux at the x = 0 surface will not give any information about the precise nature of the structure of the solid. However, it is not clear what this "conservation-of-$k\alpha$" condition means physically since α is the reciprocal of the square root of a diffusivity ratio.

We also note that the arguments of the complementary error functions in Eqs. (4.22) and (4.23) may be regarded as a series of images brought about by the combined presence of the interface and the boundary at x = 0.

4.5.3 Summary of the three-layer analysis

The semi-infinite heat-conducting solid domain is now characterised by having two sublayers, each with a unit nondimensional thickness, and placed next to the heated surface, while the third region is infinitely wide. The three regions have nondimensional thermal conductivities, k_1, k_2 and k_3, respectively, while the reciprocals of the square roots of the corresponding thermal diffusivity ratios are, α_1, α_2 and α_3. The governing equations are,

$$\begin{aligned}
&\alpha_1^2 \frac{\partial \theta_1}{\partial t} = \frac{\partial^2 \theta_1}{\partial x^2}, \quad (0 \le x \le 1), \\
&\alpha_2^2 \frac{\partial \theta_2}{\partial t} = \frac{\partial^2 \theta_2}{\partial x^2}, \quad (1 \le x \le 2), \\
&\alpha_3^2 \frac{\partial \theta_3}{\partial t} = \frac{\partial^2 \theta_3}{\partial x^2}, \quad (2 \le x),
\end{aligned} \tag{4.24}$$

while the boundary and interface conditions are,

$$\begin{aligned}
&x = 0: \quad \theta_1 = 1, \; x = 1: \quad \theta_1 = \theta_2, \; k_1 \frac{\partial \theta_1}{\partial x} = k_2 \frac{\partial \theta_2}{\partial x}, \\
&x \to \infty: \; \theta_3 \to 0 x = 2: \quad \theta_2 = \theta_3, \; k_2 \frac{\partial \theta_2}{\partial x} = k_3 \frac{\partial \theta_3}{\partial x}.
\end{aligned} \tag{4.25}$$

The same Laplace Transform technique that was used for the two-layer system is used here to modify Eqs. (4.24). The solutions of the transformed equations may be written in the forms,

$$\begin{aligned}
&\Theta_1 = A_1 e^{\alpha_1 \sqrt{p} x} + B_1 e^{-\alpha_1 \sqrt{p} x}, \\
&\Theta_2 = A_2 e^{\alpha_2 \sqrt{p} (x-1)} + B_2 e^{-\alpha_2 \sqrt{p} (x-1)}, \\
&\Theta_3 = A_3 e^{\alpha_3 \sqrt{p} (x-2)} + B_3 e^{-\alpha_3 \sqrt{p} (x-2)}.
\end{aligned} \tag{4.26}$$

Application of the transformed versions of Eqs. (4.25) result in the following equations for the *A* and *B* coefficients:

$$A_1 + B_1 = \frac{1}{p},$$

$$A_1 e^{\alpha_1\sqrt{p}} + B_1 e^{-\alpha_1\sqrt{p}} = A_2 + B_2,$$

$$k_1\alpha_1\left(A_1 e^{\alpha_1\sqrt{p}} - B_1 e^{-\alpha_1\sqrt{p}}\right) = k_2\alpha_2\left(A_2 - B_2\right), \tag{4.27}$$

$$A_2 e^{\alpha_2\sqrt{p}} + B_2 e^{-\alpha_2\sqrt{p}} = A_3 + B_3,$$

$$k_2\alpha_2\left(A_2 e^{\alpha_2\sqrt{p}} - B_2 e^{-\alpha_2\sqrt{p}}\right) = k_3\alpha_3\left(A_3 - B_3\right),$$

$$A_3 = 0.$$

First, we may find A_2 and B_2 in terms of B_3:

$$\begin{aligned} A_2 &= \frac{1}{2}\left(1 - \frac{k_3\alpha_3}{k_2\alpha_2}\right) B_3 e^{-\alpha_2\sqrt{p}}, \\ B_2 &= \frac{1}{2}\left(1 + \frac{k_3\alpha_3}{k_2\alpha_2}\right) B_3 e^{\alpha_2\sqrt{p}}. \end{aligned} \tag{4.28}$$

and, in turn, we may find A_1 and B_1 in terms of A_2 and B_2:

$$\begin{aligned} A_1 &= \frac{1}{2}\left[\left(A_2 + B_2\right) + \frac{k_2\alpha_2}{k_1\alpha_1}\left(A_2 - B_2\right)\right] e^{-\alpha_1\sqrt{p}}, \\ B_1 &= \frac{1}{2}\left[\left(A_2 + B_2\right) - \frac{k_2\alpha_2}{k_1\alpha_1}\left(A_2 - B_2\right)\right] e^{\alpha_1\sqrt{p}}. \end{aligned} \tag{4.29}$$

Hence,

$$A_1 = \left(\frac{1}{4}\right)\left[\left(1+\frac{k_2\alpha_2}{k_1\alpha_1}\right)\left(1-\frac{k_3\alpha_3}{k_2\alpha_2}\right)B_3 e^{(-\alpha_1-\alpha_2)\sqrt{p}} + \left(1-\frac{k_2\alpha_2}{k_1\alpha_1}\right)\left(1+\frac{k_3\alpha_3}{k_2\alpha_2}\right)B_3 e^{(-\alpha_1+\alpha_2)\sqrt{p}}\right],$$
$$B_1 = \left(\frac{1}{4}\right)\left[\left(1-\frac{k_2\alpha_2}{k_1\alpha_1}\right)\left(1-\frac{k_3\alpha_3}{k_2\alpha_2}\right)B_3 e^{(\alpha_1-\alpha_2)\sqrt{p}} + \left(1+\frac{k_2\alpha_2}{k_1\alpha_1}\right)\left(1+\frac{k_3\alpha_3}{k_2\alpha_2}\right)B_3 e^{(\alpha_1+\alpha_2)\sqrt{p}}\right], \tag{4.30}$$

Substitution of these latest two expressions into Eq. (4.27) with a little rearrangement yields,

$$B_3 = \left(\frac{4}{p}\right)\left(\frac{\left(k_1\alpha_1\right)\left(k_2\alpha_2\right)}{\left(k_1\alpha_1+k_2\alpha_2\right)\left(k_2\alpha_2+k_3\alpha_3\right)}\right)e^{-(\alpha_1+\alpha_2)\sqrt{p}}\left[1+\xi_1+\xi_2+\xi_3\right]^{-1}, \tag{4.31}$$

where

$$\xi_1 = \left(\frac{k_1\alpha_1-k_2\alpha_2}{k_1\alpha_1+k_2\alpha_2}\right)e^{-2\alpha_1\sqrt{p}},$$
$$\xi_2 = \left(\frac{k_1\alpha_1-k_2\alpha_2}{k_1\alpha_1+k_2\alpha_2}\right)\left(\frac{k_2\alpha_2-k_3\alpha_3}{k_2\alpha_2+k_3\alpha_3}\right)e^{-2\alpha_2\sqrt{p}}, \tag{4.32}$$
$$\xi_3 = \left(\frac{k_2\alpha_2-k_3\alpha_3}{k_2\alpha_2+k_3\alpha_3}\right)e^{(-2\alpha_1-2\alpha_2)\sqrt{p}}.$$

The term in square brackets in Eq. (4.31) may now be expanded in the form,

$$\sum_{n=0}^{\infty}\left(-1\right)^n\left(\xi_1+\xi_2+\xi_3\right)^n, \tag{4.33}$$

where each term within this sum may be expanded using the standard trinomial expansion. Eventually, after some fairly extensive manipulations, it is possible to show that,

$$B_3 = \left(\frac{4}{p}\right)\frac{\left(k_1\alpha_1\right)\left(k_2\alpha_2\right)}{\left(k_1\alpha_1+k_2\alpha_2\right)\left(k_2\alpha_2+k_3\alpha_3\right)}\sum_{n=0}^{\infty}\sum_{i=0}^{n}\sum_{j=0}^{n-i}C_{i,j,n}e^{-\left[\alpha_1(1+2n-2j)+\alpha_2(2n-2i+1)\right]\sqrt{p}}, \tag{4.34}$$

where

$$C_{i,j,n} = (-1)^n \left(\frac{n!}{i!\,j!(n-i-j)!} \right) \left(\frac{k_1\alpha_1 - k_2\alpha_2}{k_1\alpha_1 + k_2\alpha_2} \right)^{i+j} \left(\frac{k_2\alpha_2 - k_3\alpha_3}{k_2\alpha_2 + k_3\alpha_3} \right)^{n-i} \tag{4.35}$$

and where the second bracket on the right hand side of (4.35) is a trinomial coefficient. The coefficients, A_2 and B_2 are,

$$A_2 = \left(\frac{2}{p} \right) \frac{(k_1\alpha_1)(k_2\alpha_2 - k_3\alpha_3)}{(k_1\alpha_1 + k_2\alpha_2)(k_2\alpha_2 + k_3\alpha_3)} \sum_{n=0}^{\infty} \sum_{i=0}^{n} \sum_{j=0}^{n-i} C_{i,j,n} e^{-\left[\alpha_1(1+2n-2j)+\alpha_2(2n-2i+2)\right]\sqrt{p}}, \tag{4.36}$$

and

$$B_2 = \left(\frac{2}{p} \right) \frac{(k_1\alpha_1)(k_2\alpha_2 + k_3\alpha_3)}{(k_1\alpha_1 + k_2\alpha_2)(k_2\alpha_2 + k_3\alpha_3)} \sum_{n=0}^{\infty} \sum_{i=0}^{n} \sum_{j=0}^{n-i} C_{i,j,n} e^{-\left[\alpha_1(1+2n-2j)+\alpha_2(2n-2i)\right]\sqrt{p}}. \tag{4.37}$$

Clearly some cancellation may take place between the numerator and the denominator in (4.37), but the cancellation is not made for the sake of clarity and consistency in the appearance of the denominators.. The coefficients, A_1 and B_1, are now,

$$A_1 = \left(\frac{1}{p} \right) \sum_{n=0}^{\infty} \sum_{i=0}^{n} \sum_{j=0}^{n-i} C_{i,j,n} \left[\begin{array}{l} \left(\dfrac{k_2\alpha_2 - k_3\alpha_3}{k_2\alpha_2 + k_3\alpha_3} \right) e^{-\left[\alpha_1(2n-2j+2)+\alpha_2(2n-2i+2)\right]\sqrt{p}} \\ + \left(\dfrac{k_1\alpha_1 - k_2\alpha_2}{k_1\alpha_1 + k_2\alpha_2} \right) e^{-\left[\alpha_1(2n-2j+2)+\alpha_2(2n-2i)\right]\sqrt{p}} \end{array} \right], \tag{4.38}$$

$$B_1 = \left(\frac{1}{p} \right) \sum_{n=0}^{\infty} \sum_{i=0}^{n} \sum_{j=0}^{n-i} C_{i,j,n} \left[\begin{array}{r} \left(\dfrac{k_1\alpha_1 - k_2\alpha_2}{k_1\alpha_1 + k_2\alpha_2} \right) \left(\dfrac{k_2\alpha_2 - k_3\alpha_3}{k_2\alpha_2 + k_3\alpha_3} \right) e^{-\left[\alpha_1(2n-2j)+\alpha_2(2n-2i+2)\right]\sqrt{p}} \\ + e^{-\left[\alpha_1(2n-2j+2)+\alpha_2(2n-2i)\right]\sqrt{p}} \end{array} \right]. \tag{4.39}$$

The final solutions for the three layers may now be found. The expressions given in Eqs. (4.34) and (4.36) to (4.40) are substituted into Eqs. (4.26), and use is again made of the formula given in Eq. (4.11). We have,

$$\theta_3 = 4(k_1\alpha_1)(k_2\alpha_2)\sum_{n=0}^{\infty}\sum_{i=0}^{n}\sum_{j=0}^{n-i} C^*_{i,j,n}\,\mathrm{erfc}\left(\frac{\alpha_1(2n-2j+1)+\alpha_2(2n-2i+1)}{2\sqrt{t}}\right), \tag{4.40}$$

$$\theta_2 = 2(k_1\alpha_1)\sum_{n=0}^{\infty}\sum_{i=0}^{n}\sum_{j=0}^{n-i} C^*_{i,j,n}\left[\begin{array}{l}(k_2\alpha_2 - k_3\alpha_3)\,\mathrm{erfc}\left(\dfrac{\alpha_1(2n-2j+1)+\alpha_2(2n-2i+1)-\alpha_2(x-1)}{2\sqrt{t}}\right)\\ +(k_2\alpha_2 + k_3\alpha_3)\,\mathrm{erfc}\left(\dfrac{\alpha_1(2n-2j+1)+\alpha_2(2n-2i)-\alpha_2(x-1)}{2\sqrt{t}}\right)\end{array}\right], \tag{4.41}$$

and

$$\theta_1 = \sum_{n=0}^{\infty}\sum_{i=0}^{n}\sum_{j=0}^{n-i} C^*_{i,j,n}\left[\begin{array}{l}(k_1\alpha_1 + k_2\alpha_2)(k_2\alpha_2 - k_3\alpha_3)\,\mathrm{erfc}\left(\dfrac{\alpha_1(2n-2j+2-x)+\alpha_2(2n-2i+2)}{2\sqrt{t}}\right)\\ +(k_1\alpha_1 - k_2\alpha_2)(k_2\alpha_2 + k_3\alpha_3)\,\mathrm{erfc}\left(\dfrac{\alpha_1(2n-2j+2-x)+\alpha_2(2n-2i)}{2\sqrt{t}}\right)\\ +(k_1\alpha_1 - k_2\alpha_2)(k_2\alpha_2 - k_3\alpha_3)\,\mathrm{erfc}\left(\dfrac{\alpha_1(2n-2j+x)+\alpha_2(2n-2i+2)}{2\sqrt{t}}\right)\\ +(k_1\alpha_1 + k_2\alpha_2)(k_2\alpha_2 + k_3\alpha_3)\,\mathrm{erfc}\left(\dfrac{\alpha_1(2n-2j+x)+\alpha_2(2n-2i)}{2\sqrt{t}}\right)\end{array}\right], \tag{4.42}$$

where

$$C^*_{i,j,n} = \frac{C_{i,j,n}}{(k_1\alpha_1 + k_2\alpha_2)(k_2\alpha_2 + k_3\alpha_3)}. \tag{4.43}$$

For three layers, the image system mentioned earlier is now much more complicated and it involves three summations. Given the manner in which the trinomial appeared earlier in Eq. (4.33), it is straightforward to predict that a configuration which has four sublayers will yield similar expressions with eight summations, and in general, that *N* sublayers will yield $(N-1)^2 - 1$ summations. Therefore it would appear that this analytical technique rapidly becomes very unwieldy as the number of layers increases, although the solutions obtained in this way remain exact.

Finally, we note that when $k_n\alpha_n$ takes the same values in all three layers, then the solution in layer 1 reduces to the single term given in Eq. (4.23). More specifically, we obtain,

$$\theta_1 = \text{erfc}\left(\frac{\alpha_1 x}{2\sqrt{t}}\right),$$
$$\theta_2 = (k_1\alpha_1)\,\text{erfc}\left(\frac{\alpha_1 + \alpha_2(x-1)}{2\sqrt{t}}\right), \qquad (4.44)$$
$$\theta_3 = (k_1\alpha_1)(k_2\alpha_2)\,\text{erfc}\left(\frac{\alpha_1 + \alpha_2 + \alpha_3(x-2)}{2\sqrt{t}}\right).$$

Therefore, this special case also yields a situation where the properties of layers 2 and 3 cannot be inferred from the variation in Nu, given that it is independent of the diffusivities of layers 2 and 3. Finally, it is clear that all three expressions reduce to the form given in Eq. (4.7) when all three layers have identical properties and thus we have, $k_1 = \alpha_1 = k_2 = \alpha_2 = k_3 = \alpha_3 = 1$.

4.6 Temperature profiles

4.6.1 Purpose

We are interested in determining the effect of varying the thermal diffusivity parameter, α, and the thermal conductivity parameter, *k*, on the temperature profile of the heat transport equations of the multilayer system. Therefore, the evolution with time of the temperature profiles will be presented. It is generally assumed that the semi-infinite domain for the two-layer and three-layer systems forms the reference layer and hence that $k_2 = \alpha_2 = 1$ and $k_3 = \alpha_3 = 1$ in those two cases, respectively. We will begin with the two-layer system case and consider in turn those subcases when $k\alpha$ is the same in all layers, and then consider those subcases where $k = \alpha$. Then we shall consider similarly configured three layer systems.

In the following figures, which show the evolving profiles, the location of each interface is shown by a dotted line at $x = 1$, and, for the three-layer case, a second one at $x = 2$.

4.6.2 Two layers: Identical values of $k\alpha$

We choose to consider this case first because of the observation arising from Eq. (4.23) that solutions in layer 1 are comprised of a single complementary error function solution. Given that we choose to use layer 2 as the reference layer when there are two layers present, this means that $k_1\alpha_1 = 1$. Figure 4.2 is typical of later Figures of the same type by showing the detailed temperature profiles as a function of x at unit times between 0 and 10.

Figure 4.2 shows the evolution with time of the temperature profile of seven cases where $k_1 = 0.1$, 0.25, 0.5, 1, 2, 4 and 10, and hence α_1 takes the respective values, 10, 4, 2, 1, 0.5, 0.25 and 0.1. In practice this means that both the conductivity and the diffusivity of layer 1 increase together, although the definition of α means that heat capacity doesn't remain constant.

We may observe from this Figure that the temperature profiles are well-behaved in the sense that there is a monotonic variation in the general shape of the profiles as k_1 increases. Thus when k_1 takes large values (and α_1 takes correspondingly small values) then there is a very slow evolution of the temperature field towards the interface due to the low diffusivity. And, due to very high thermal conductivity in layer 1, the slope in the isotherms just to the right of the interface is correspondingly small in magnitude. As the diffusivity of layer 1 increases (α_1 decreases) and the conductivity increases, we see an increasingly rapid spreading of heat towards the interface, and an increasing temperature on the interface (and for larger values of x) at any fixed point in time.

4.6.3 Two layers: The $k = \alpha$ case

We shall consider now the case where all the layers satisfy the condition that $k_n = \alpha_n$ in all layers. In practice, this means that, should a layer have a large diffusivity (i.e. if $\alpha_n << 1$ and hence $k_n << 1$ also), it remains difficult for heat to be transferred into the next layer.

Figure 4.3 shows the evolution with time of the temperature profile of such two-layer systems for the following cases: $k_1 = 0.1, 0.25, 0.5, 1, 2, 4, 10$. The single-layer uniform medium case corresponds to when $k_1 = \alpha_1 = 1$, and this again serves as a reference.

At early times, usually those which are well in advance of $t = 1$, the evolving boundary layer is self-similar and is contained well within layer 1. The speed of spread of the profile away from $x = 0$ depends on the value of α_1, large values corresponding to a low thermal diffusivity and hence a slow evolution. When $\alpha_1 = 10$ the temperature field has penetrated only as far as the interface by the time $t = 5$, whereas it is clear that the boundary layer spreads faster for smaller values of α_1. After this time ($t = 5$ for $\alpha_1 = 10$) heat spreads into the layer 2 but does so slowly because k_1 is small, and therefore very little heat is transferred across the interface. Graphically this is equivalent to the almost horizontal profiles of θ_1 immediately to the left of the interface.

In more detail, when we have for small values of α_1, the temperature field will evolve relatively quickly in layer 1, but the small conductivity means that little of this heat is able to escape into layer 2. Thus the extreme case of small values of k_1 and α_1 means that the temperature profile in layer 1 adjusts extremely rapidly to the slowly varying interface temperature. This is why the temperature profile is almost precisely linear when $k_1 = \alpha_1 = 0.1$. It should be possible, therefore, to replace layer 1 by an equivalent Robin boundary condition when k_1 and α_1 are sufficiently small.

As k_1 and α_1 begin to increase from small values it is very clear that the temperature field evolves more quickly in layer 1 even though the diffusivity is increasing. However, the increasing value of k_1 means that heat is more able to penetrate through the interface, and that the overall shape of the profile may be said to rise as these parameters increase. However, at some point close to the case where, $k_1 = \alpha_1$=4, the profiles have begun to descend once more; this is due to the rapidly decreasing diffusivity in layer 1. This phenomenon may be seen in the following Table 4.1 which shows the values of the temperature at the interface at t = 0.1, 1.0 and 10.

$k_1 = \alpha_1$	$\theta(t = 0.1)$	$\theta(t = 1)$	$\theta(t = 10)$
10	0.000000	0.000000	0.050193
4	0.000000	0.008805	0.686431
2	0.000012	0.251658	**0.889038**
1	0.025347	**0.479500**	0.823063
0.5	**0.105612**	0.371125	0.689257
0.25	0.077974	0.227918	0.507194
0.1	0.034392	0.103439	0.276387

Table 4.1: Table of values of the temperature at the interface (x = 1) at different times, and for a selection of values of $k_1 = \alpha_1$. The bold data correspond to the largest values in the given column.

.

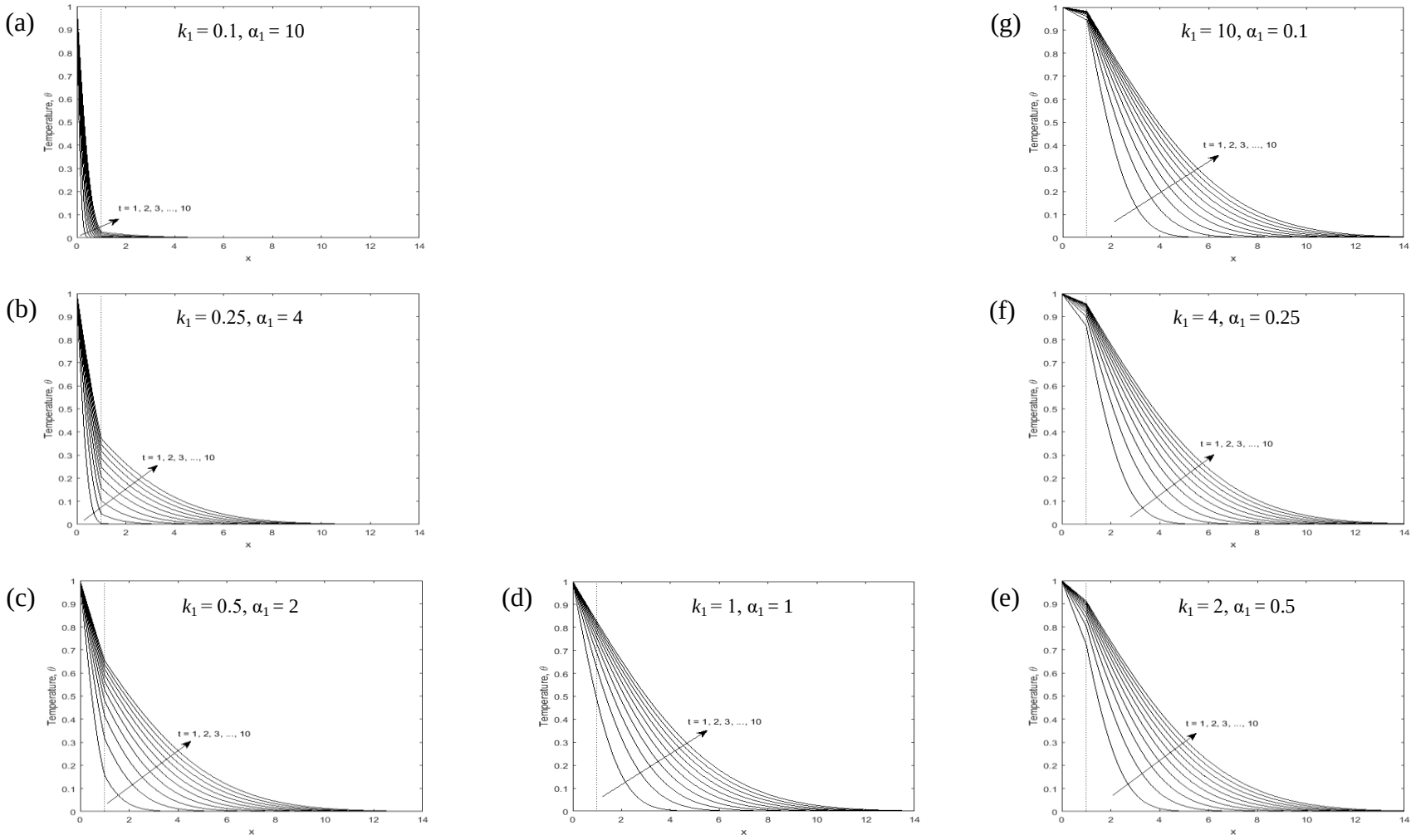

Figure 4.2: Evolution with time of the temperature profiles for $k_1\alpha_1 = 1$ with the semi infinite domain as the reference layer hence that $k_2 = \alpha_2 = 1$ (Two-layer case). Note that the dotted vertical line is the location of the interface.

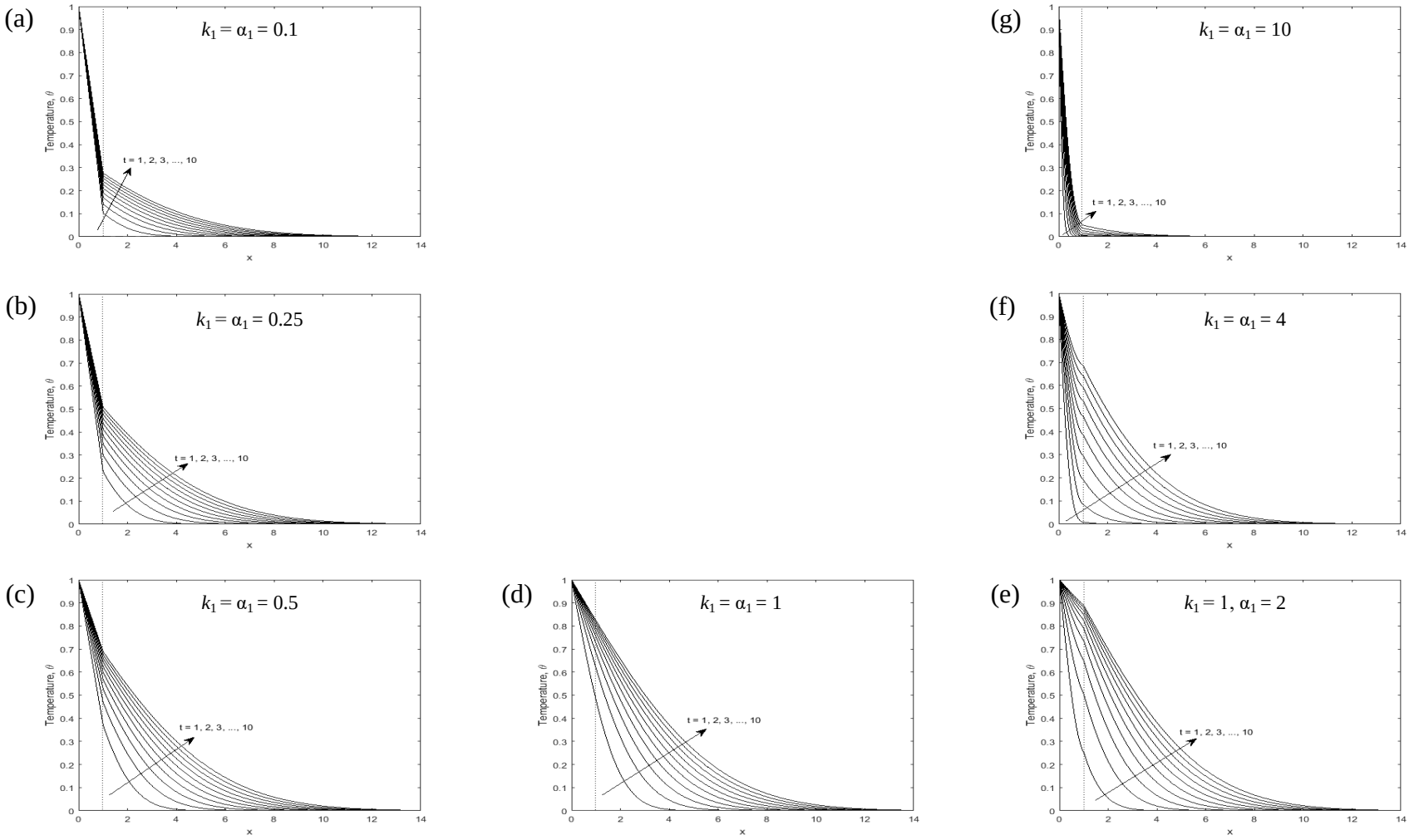

Figure 4.3: Evolution with time of the temperature profiles for $k_1 = \alpha_1$ with the semi infinite domain as the reference layer hence that $k_2 = \alpha_2 = 1$ (Two-layer case). Note that the dotted vertical line is the location of the interfaces.

4.6.4 Three layers: Identical values of $k\alpha$.

This is the three-layer equivalent of what was considered in section 4.6.2. We shall assume that layers 1 and 3 have identical properties and form the reference case, and that layer 2 has different values of the diffusivity and the conductivity. The temperature profiles are shown in Figures 4.4. and 4.5.

Figure 4.4 shows those cases where the sandwiched sublayer satisfies the relation, $k_2\alpha_2 = 1$. As for the corresponding two-layer case, we find that these curves also vary monotonically at all chosen values of x and t as the conductivity of the non-reference layer 2 increases. When $k_2 = 0.1$ (low conductivity and low diffusivity) then the very large slope of the isotherms in layer 2 shows how difficult it is for heat to pass through this layer. As both the conductivity and diffusivity increase, heat is able to penetrate more rapidly through layer 2 and through into layer 3. At the opposite extreme, namely when the conductivity and diffusivity are high, then it appears that the speed at which heat diffuses into layer 3 has reached a limiting state. The high diffusivity of layer 2 allows heat to pass through extremely quickly, and it is possible to infer that the large-k_2, small-α_2 state is essentially same as that of a uniform semi-infinite domain, but with layer 2 excised.

We also note that the solutions in layer 1 are independent of k_2 and α_2, which is in accord with the solution given in Eq. (4.23). Given that layer 1 is the reference layer here, this means that all the cases shown in Fig. 4.4 have identical solutions in layer 1, as may be seen. Therefore, if the sole information one has about this conducting system are the properties of layer 1, then it is only possible to infer that the medium has a uniform value of $k\alpha$. In making this statement, we have assumed that there could be either two or three layers present− although the present analysis is confined to these configurations, it is suspected that this may also be true for more than three sublayers.

4.6.5 Three layers: The $k = \alpha$ case.

The first statement about this type of configuration is that solutions at very early times, i.e. substantially earlier than $t = 1$, all the temperature profiles are independent of the values of k_2 and α_2 given that the temperature profile is still well within layer 1. As time progresses and the first interface is encountered, the profiles then become dependent on the properties of layer 2.

If we consider first the $k_2 = \alpha_2 = 0.1$ case, which corresponds to a high diffusivity but low conductivity, then we see that layer 1 has heated up rapidly by the time $t = 1$ when compared with that of the uniform medium for which $k_2 = \alpha_2 = 1$, or any of the other cases considered. Although these two cases will have identical self-similar profiles at very early times, once the evolving thermal boundary layer spreads as far as the interface between layers 1 and 2, heat is transmitted very slowly into layer 2 when $k_2 = \alpha_2 = 0.1$. This allows layer 1 to heat up relatively rapidly, as may also be seen in Fig. 4.5. Using a similar idea, heat is lost from layer 2 very slowly into layer 3, but there is an extensive spreading of the thermal field even though the temperature is not large. This is a counter-intuitive case because a slowly-varying temperature field with a large drop in temperature is generally associated with a small diffusivity, whereas here the diffusivity of layer 2 is $\sqrt{10}$ times that of layers 1 and 3. The evolution of the temperature field in layer 2 is being dominated by its low conductivity and the slow transfer of heat through the interfaces. As a consequence the temperature profile in layer 2 is essentially linear.

At the opposite extreme, $k_2 = \alpha_2 = 10$, the diffusivity of layer 2 is small, which means that heat spreads very slowly from the interface between layers 1 and 2, and a linear temperature profile is set up in layer 1. Passage of heat into layer 3 has only just started to happen when $t = 10$. As the governing parameters vary between these two extremes, the shapes of the profiles also vary but do so in a manner which is to be expected given the shapes of the profiles at those extremes.

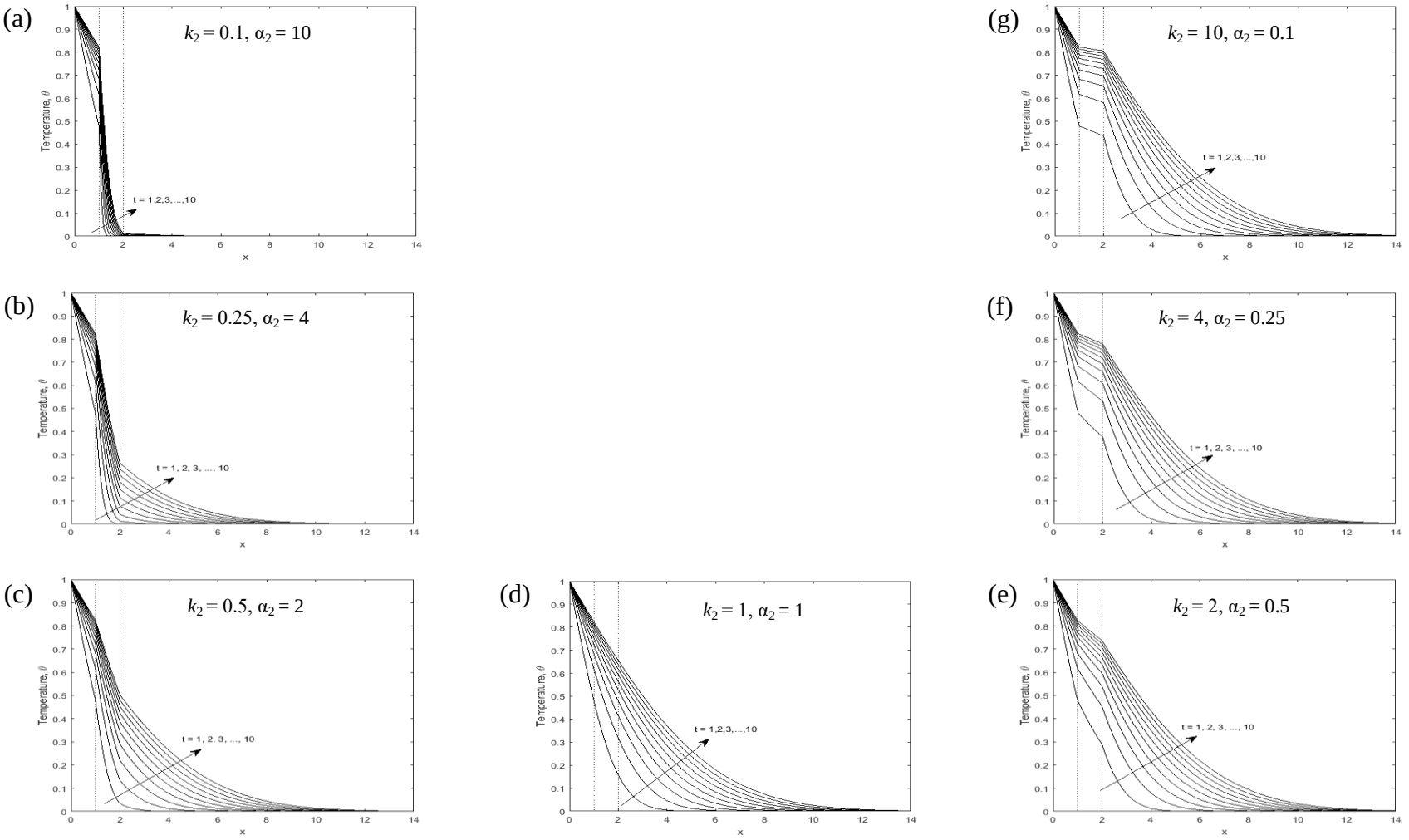

Figure 4.4: Evolution with time of the temperature profiles for $k_2\alpha_2 = 1$ with the semi infinite domain as the reference layer hence that $k_1 = \alpha_1 = 1$ and $k_3 = \alpha_3 = 1$ (Three-layer case). Note that the dotted vertical lines are the locations of the interfaces.

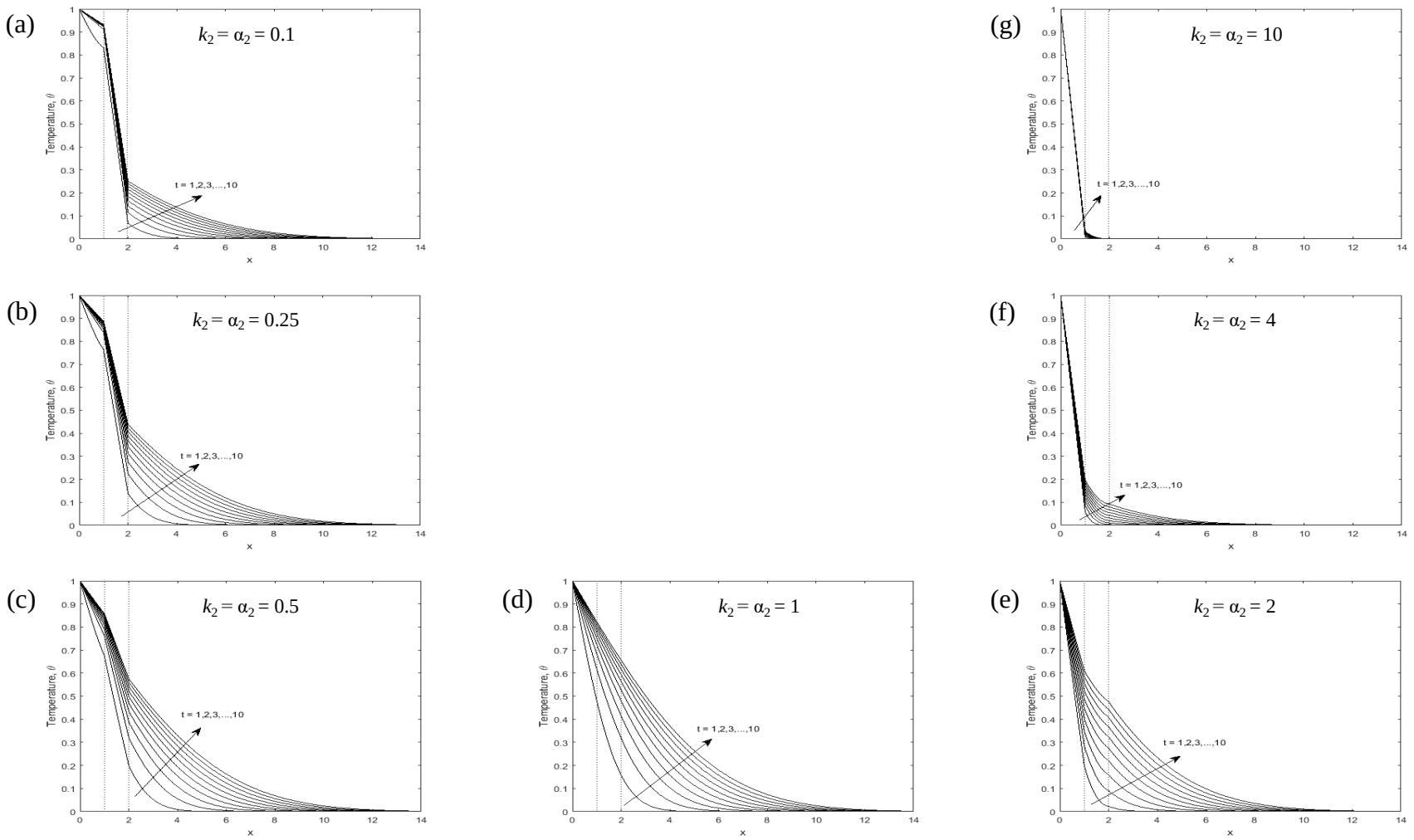

Figure 4.5: Evolution with time of the temperature profiles for $k_2 = \alpha_2$ with the semi infinite domain as the reference layer hence that $k_1 = \alpha_1 = 1$ and $k_3 = \alpha_3 = 1$ (Three-layer case). Note that the dotted vertical lines are the locations of the interfaces.

4.7 Heat Transfer and the dimensionless heat flux number

4.7.1 The single layer

For the single-layer case where the solid is uniform, Equation (4.7) gives the classical complementary error function solution for the developing temperature profile. The nondimensional rate of heat transfer at $x = 0$ is given by

$$\left.\frac{\partial \theta_1}{\partial x}\right|_{x=0} = -\frac{1}{\sqrt{\pi t}}, \tag{4.45}$$

and the variation of this with time is shown in Figure 4.6.

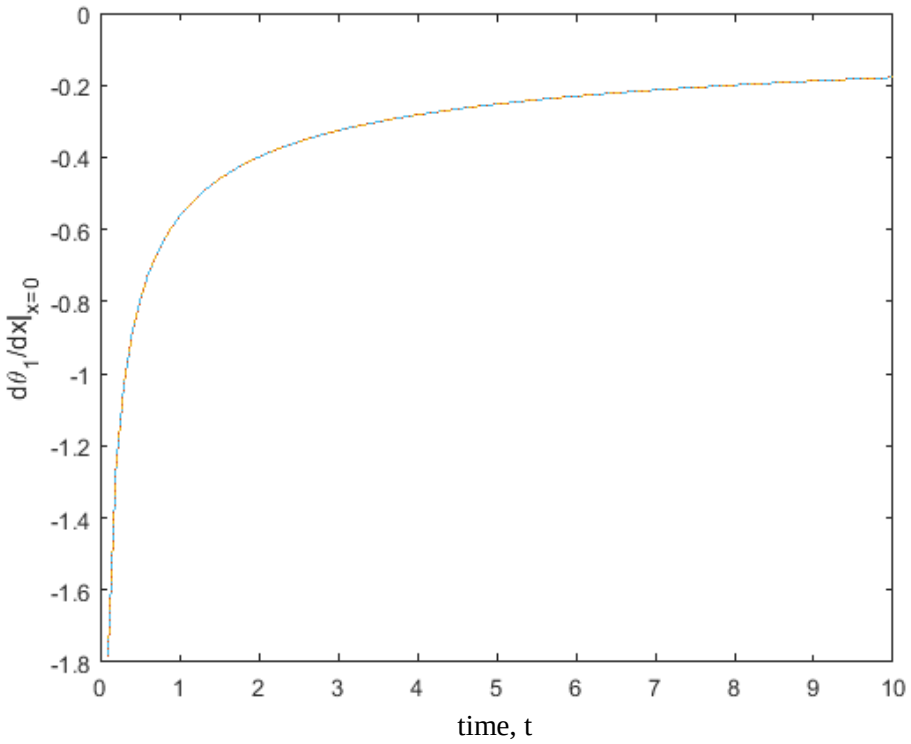

Figure 4.6: Evolution of the surface rate of heat transfer in the range, $0 < t < 10$ for the uniform case.

Given that the rate of heat transfer is infinite when $t = 0$ (which reflects the infinitesimal width of the developing boundary layer) and tends to zero as time progresses, it proves more convenient to use a dimensionless heat flux denoted and defined as Nu:

$$\mathrm{Nu} = -\sqrt{\pi t}\left.\frac{\partial \theta_1}{\partial x}\right|_{x=0}. \tag{4.46}$$

Given the definition of Nu in (4.46), the uniform case yields a unit dimensionless heat flux and therefore it will be straightforward to compare the multilayer cases with this. It is now of interest to consider how layering affects the dimensionless heat flux. In particular, the question of whether the presence of a finite-thickness layer is detectable from the evolution of Nu with time.

4.7.2 The two-layer case

For the two-layer case $\dfrac{\partial \theta_1}{\partial x}$ at x=0 is given as follows:

$$\frac{\partial \theta_1}{\partial x} = \frac{1}{\left(k_1\alpha_1 + k_2\alpha_2\right)}\left(-\frac{\alpha_1}{\sqrt{\pi t}}\right)\sum_{n=0}^{\infty}\left(-1\right)^n\left(\frac{k_1\alpha_1 - k_2\alpha_2}{k_1\alpha_1 + k_2\alpha_2}\right)^n\begin{bmatrix}\left(k_1\alpha_1 + k_2\alpha_2\right)\mathrm{e}^{-\left(\frac{\alpha_1(2n+x)}{2\sqrt{t}}\right)^2} \\ -\left(k_1\alpha_1 - k_2\alpha_2\right)\mathrm{e}^{-\left(\frac{\alpha_1(2n+2-x)}{2\sqrt{t}}\right)^2}\end{bmatrix}, \tag{4.47}$$

and Nu is given as

$$\mathrm{Nu} = -\sqrt{\pi t}\left.\frac{\partial \theta_1}{\partial x}\right|_{x=0} = \frac{\alpha_1}{\left(k_1\alpha_1 + k_2\alpha_2\right)}\sum_{n=0}^{\infty}\left(-1\right)^n\left(\frac{k_1\alpha_1 - k_2\alpha_2}{k_1\alpha_1 + k_2\alpha_2}\right)^n\begin{bmatrix}\left(k_1\alpha_1 + k_2\alpha_2\right)\mathrm{e}^{-\left(\frac{2\alpha_1 n}{2\sqrt{t}}\right)^2} \\ -\left(k_1\alpha_1 - k_2\alpha_2\right)\mathrm{e}^{-\left(\frac{\alpha_1(2n+2)}{2\sqrt{t}}\right)^2}\end{bmatrix}. \tag{4.48}$$

Figures 4.7 to 4.9 show how the evolution of Nu with time depends on the governing parameters. In each case we use α_1 = 0.1, 0.25, 0.5, 1, 2, 4, 10, and the three Figures correspond to k_1= 0.1, 1 and 10, respectively. We plot $\log_{10}$Nu against $\log_{10}t$ because of the large variation in the magnitude of these parameters.

Figure 4.7 is very much representative of the general behavior of the Nusselt number with time for two-layer systems, and these values move monotonically between the small-time and the large-time asymptotic states. Thus when $t = 10^{-4}$, the value of Nu is essentially equal to α_1. This is in accord with the expression for Nu given in Eq. (4.48). When $t << 1$, all the exponential terms, except for one, are superexponentially small, and it is straightforward to show that

$$\mathrm{Nu} \sim \alpha_1 \text{ as } t \to 0. \tag{4.49}$$

On the other hand, all the curves in Fig. 4.7 approach the value Nu = 0.1 as $t \to \infty$. Once more, this may be shown to be correct by allowing t to tend towards infinity in Eq. (4.48). In this case all the exponential terms tend towards unity, and the resulting geometric series may be summed to yield,

$$\mathrm{Nu} \sim \frac{k_2\alpha_2}{k_1} \text{ as } t \to \infty. \tag{4.50}$$

For the two-layer system we set k_2 = 1 and α_2 = 1, therefore Eqs. (4.49) and (4.50) are clearly reproduced in all three of Figs. 4.7 to 4.9.

The only other feature shown in Figs 4.7 to 4.9 which requires some explanation is the length of the delay before the value of Nu begins to deviate from its small-t value and begins its evolution towards the large-t value. This is found to be directly related to the value of α_1. When α_1 is small, the diffusivity of layer 1 is large, and therefore temperature diffuses quickly from the hot surface towards the interface, which causes the delay to be short, and vice-versa.

Finally, we note that the constant $k\alpha$ cases which were referred to earlier, and which are shown in these Figures when (i) $k_1 = 0.1$ and $\alpha_1 = 10$, (ii) $k_1 = 1$ and $\alpha_1 = 1$, and (iii) $k_1 = 10$ and $\alpha_1 = 0.1$, correspond to the constant curves in Figs. 4.7 to 4.9, respectively.

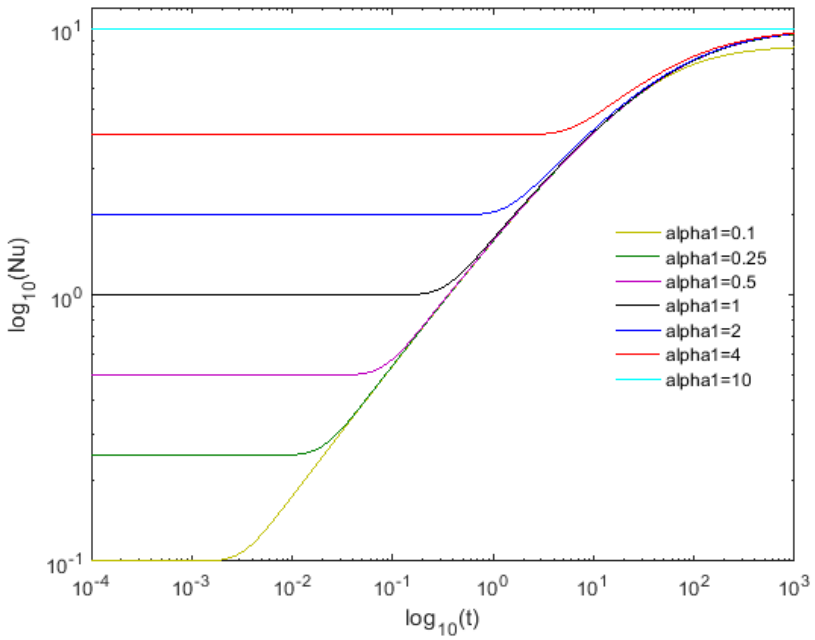

Figure 4.7: Evolution of Nu in the range, $0 < \log_{10}(t) < 1000$ for $k_1 = 0.1$ at corresponding $\alpha_1 = 0.1, 0.25, 0.5, 1, 2, 4, 10$ for two-layer case.

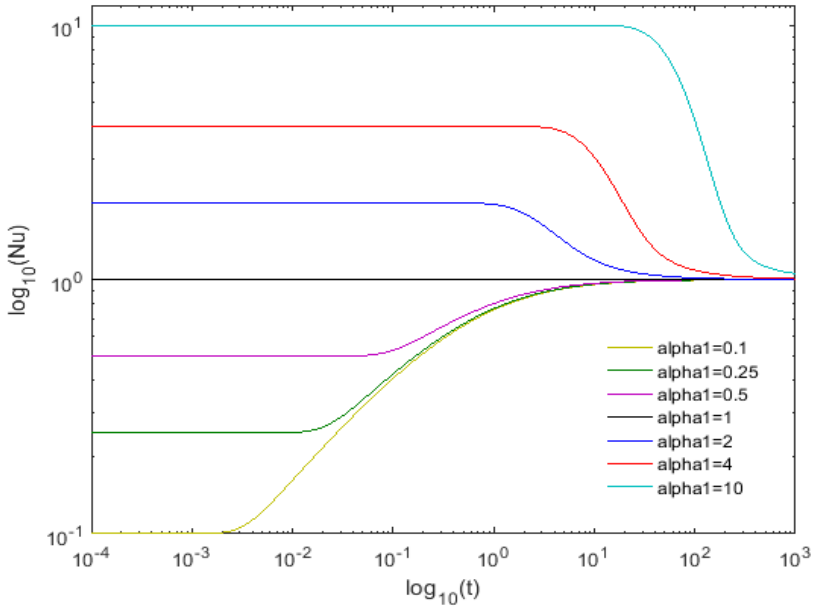

Figure 4.8: Evolution of Nu in the range, $0 < \log_{10}(t) < 100$ for k_1 = 1 at corresponding α_1 = 0.1, 0.25, 0.5, 1, 2, 4, 10 for two-layer case.

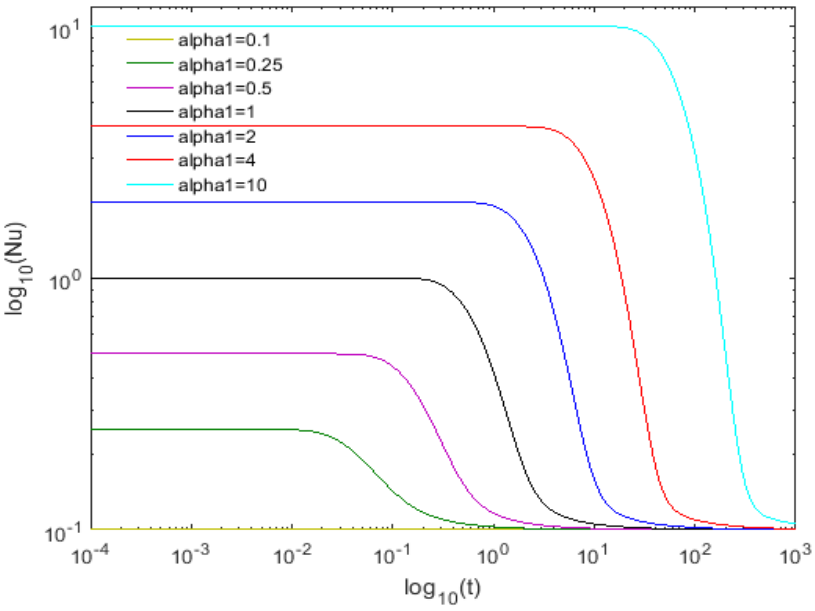

Figure 4.9: Evolution of Nu in the range, $0 < \log_{10}(t) < 1000$ for k_1 = 10 at corresponding α_1 = 0.1, 0.25, 0.5, 1, 2, 4, 10 for two-layer case.

4.7.3 The three-layer case.

For the three-layer case $\dfrac{\partial\theta_1}{\partial x}$ at x=0 is given as follows:

$$\frac{\partial\theta_1}{\partial x}=\left(-\frac{\alpha_1}{\sqrt{\pi t}}\right)\sum_{n=0}^{\infty}\sum_{i=0}^{n}\sum_{j=0}^{n-i}C^{*}_{i,j,n}\begin{bmatrix}\left(k_1\alpha_1-k_2\alpha_2\right)\left(k_2\alpha_2-k_3\alpha_3\right)\mathrm{e}^{-\left(\frac{\alpha_1(2n-2j+x)+\alpha_2(2n-2i+2)}{2\sqrt{t}}\right)^2}\\+\left(k_1\alpha_1+k_2\alpha_2\right)\left(k_2\alpha_2+k_3\alpha_3\right)\mathrm{e}^{-\left(\frac{\alpha_1(2n-2j+x)+\alpha_2(2n-2i)}{2\sqrt{t}}\right)^2}\\-\left(k_1\alpha_1+k_2\alpha_2\right)\left(k_2\alpha_2-k_3\alpha_3\right)\mathrm{e}^{-\left(\frac{\alpha_1(2n-2j+2-x)+\alpha_2(2n-2i+2)}{2\sqrt{t}}\right)^2}\\-\left(k_1\alpha_1-k_2\alpha_2\right)\left(k_2\alpha_2+k_3\alpha_3\right)\mathrm{e}^{-\left(\frac{\alpha_1(2n-2j+2-x)+\alpha_2(2n-2i)}{2\sqrt{t}}\right)^2}\end{bmatrix},$$

(4.51)

and hence Nu takes the form,

$$\mathrm{Nu}=-\sqrt{\pi t}\left.\frac{\partial\theta_1}{\partial x}\right|_{x=0}$$

$$=\alpha_1\sum_{n=0}^{\infty}\sum_{i=0}^{n}\sum_{j=0}^{n-i}C^{*}_{i,j,n}\begin{bmatrix}\left(k_1\alpha_1-k_2\alpha_2\right)\left(k_2\alpha_2-k_3\alpha_3\right)\mathrm{e}^{-\left(\frac{\alpha_1(2n-2j)+\alpha_2(2n-2i+2)}{2\sqrt{t}}\right)^2}\\+\left(k_1\alpha_1+k_2\alpha_2\right)\left(k_2\alpha_2+k_3\alpha_3\right)\mathrm{e}^{-\left(\frac{\alpha_1(2n-2j)+\alpha_2(2n-2i)}{2\sqrt{t}}\right)^2}\\-\left(k_1\alpha_1+k_2\alpha_2\right)\left(k_2\alpha_2-k_3\alpha_3\right)\mathrm{e}^{-\left(\frac{\alpha_1(2n-2j+2)+\alpha_2(2n-2i+2)}{2\sqrt{t}}\right)^2}\\-\left(k_1\alpha_1-k_2\alpha_2\right)\left(k_2\alpha_2+k_3\alpha_3\right)\mathrm{e}^{-\left(\frac{\alpha_1(2n-2j+2)+\alpha_2(2n-2i)}{2\sqrt{t}}\right)^2}\end{bmatrix}.$$

(4.52)

The three-layer counterparts to Figs. 4.7 to 4.9 are now shown in Figs. 4.10 to 4.12. The values of k_2 and α_2 take the same respective values as did k_1 and α_1 in Figs. 4.7 to 4.9, while the conductivities and diffusivities of layers 1 and 3 take unit values. Given that layers 1 and 3 form the reference layers, it may be shown fairly quickly

that Nu ~ 1 as t tends to zero. It is much more complicated to find the large-t behavior of Nu for three layers than for two, but a full analysis eventually yields:

$$\text{Nu} \sim \frac{k_3\alpha_3}{k_1} = 1 \text{ as } t \to \infty. \tag{4.53}$$

Thus the role of layer 2 is either to enhance or to decrease the rate of heat transfer over an intermediate interval of time, and this happens depends on the values of k_2 and α_2, or, more accurately, on their product.

When $k_2 = 1$, as shown in Fig. 4.11, we see that Nu is unchanged from 1 until approximately $t = 0.1$ after which point in time the developing thermal boundary layer enters layer 2 (which is also true for the other two cases shown in Figs. 4.10 and 4.12). When the diffusivity of layer 2 is larger than 1 (which corresponds to when $\alpha_2 < 1$), then the heat diffuses more rapidly, and this results in a smaller Nusselt number. Clearly the opposite effect arises when $\alpha_2 > 1$.

When $k_2 = 0.1$, the general effect is that Nu decreases for all but one of the chosen values of α_2, the exceptional case being $\alpha_2 = 10$. This unique case corresponds to the special case, $k_2\alpha_2 = 1$, which corresponds to the situation where the solution in layer 1 is independent of the value of the conductivity of layer 2; hence Nu = 1. Values of α_2 which are larger than 10 when $k_2 = 0.1$ causes Nu to rise above 1 initially, before returning. Thus the general principle is that Nu rises when $k_2\alpha_2 > 1$, decreases when $k_2\alpha_2 < 1$, and remains constant when $k_2\alpha_2 = 1$. This is also shown in Fig. 4.12, for which $k_2 = 10$.

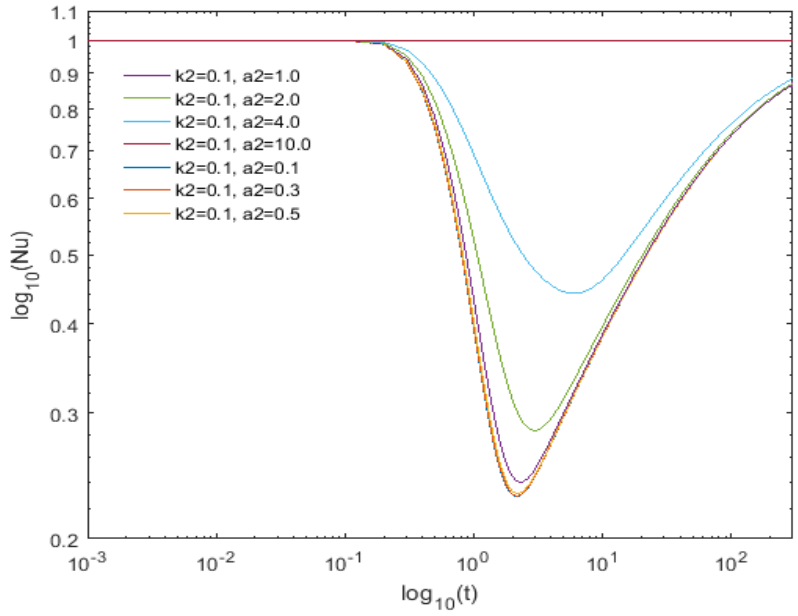

Figure 4.10: Evolution of Nu in the range, $0 < \log_{10}(t) < 1000$ for k_2 = 0.1 with α_2 = 0.1, 0.25, 0.5, 1, 2, 4, 10 for the three-layer case.

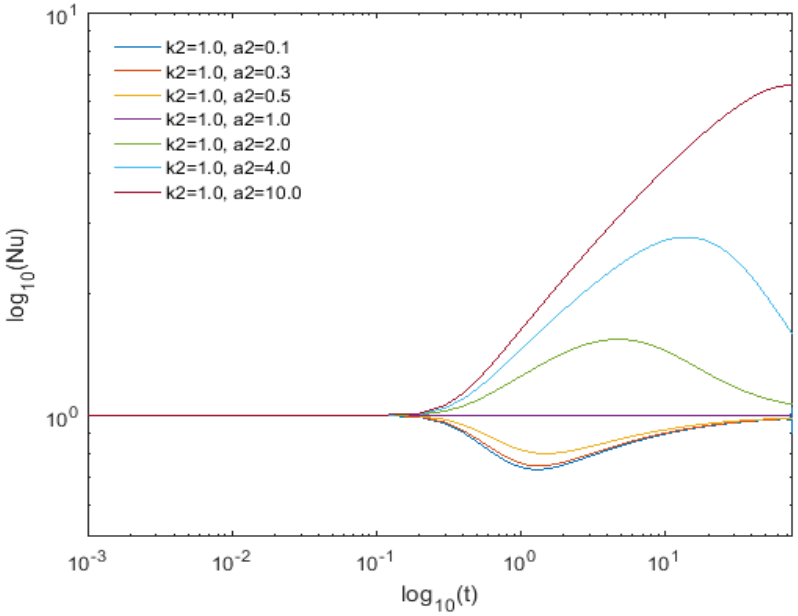

Figure 4.11: Evolution of Nu in the range, $0 < \log_{10}(t) < 1000$ for k_2 = 1 with α_2 = 0.1, 0.25, 0.5, 1, 2, 4, 10 the for three-layer case.

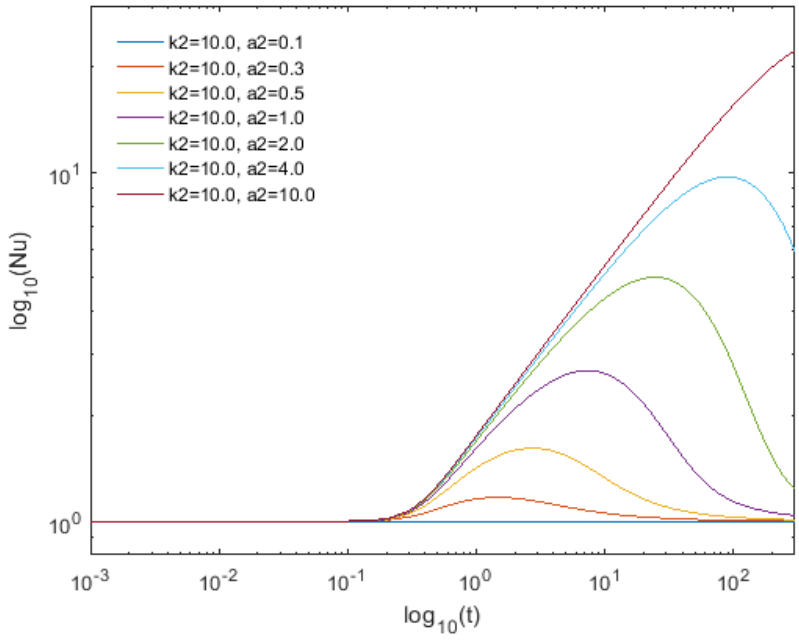

Figure 4.12: Evolution of Nu in the range, $0 < \log_{10}(t) < 1000$ for k_2 = 10 with α_2 = 0.1, 0.25, 0.5, 1, 2, 4, 10 for the three-layer case.

4.8 Conclusion

The analytical solution of the effect of layering on the unsteady conduction as well as of the consequences of having different values of the thermal diffusivity and thermal conductivity in multilayer systems has been determined. An analytical solution was found using a Laplace Transform technique, followed by a binomial or quadrinomial expansion and the inverse Laplace Transform to yield expressions consisting of summations of complementary error functions. These erfc functions may be interpreted as being akin to an image system of source terms. The solution for a two-layer system involves one summation, but it needs three summations for three layers. We haven't tackled more complicated systems, but it is clear that, for four sublayers, there be will be eight summations. Accordingly, we can predict the expressions for N layers solution to be $(N-1)^2-1$ or N^2-2N summations. Therefore, as the number of layers increases, this analytical technique rapidly becomes impractical.

In addition, the present analytical solutions show that multilayer systems can mimic a single layer system (i.e a uniform system) in terms of the measured rate of heat transfer whenever $k\alpha$ is the same in all the sublayers. This is true only from the point of view of the rate of heat transfer at $x = 0$, for the evolving profiles will differ from one another. Thus the detailed structure of the layered medium cannot be determined uniquely from the heat transfer variation with time at $x = 0$.

The detailed manner in which the Nusselt number varies in time (i.e. its speed of variation and whether it increases or not) is ultimately related to the properties of the layer which is not at ambient/reference conditions, but there is no variation in Nu when the value of $k\alpha$ is the same in every layer, although the detailed evolution of the temperature profiles depend on both the values of k and α in the layer which isn't the reference layer. The value of Nu has been determined for when $t << 1$ and when $t >> 1$. In the former case Nu is dependent only on α_1, but in the latter case it depends

on the value of α of the final layer and the ratio of the values of k for the last and the first layer.

Although it may be impractical to develop this type of analysis to more than three layers, there may be some scope to develop an analytical solution via a suitable algebraic manipulation package. But even then, the very large number of summations required may cause even this approach to be too lengthy to compute. On the other hand, we believe that the present approach may be extended to cases where the boundary at $x = 0$ is subject to an impulsive heating with a constant heat flux.

4.9 References

[1] Barry,S.I., Sweatman, W.L. (2009). Modelling heat transfer in steel coils. *ANZIAM J. (E)*, **50**, C668-C681.

[2] McGuinness, M, Sweatman, W.L, Baowan, D.Y., Barry,S.I (2009). Annealing steel coils. in: T. Marchant, M. Edwards, G.N. Mercer (Ed), MISG proceedings.

[3] Pontrelli, G, Monte, F.D. (2007). Mass diffusion through two-layer porous media: an application to the drug-eluting stent. *Int. J. Heat Mass Transfer*, **50**, 3658-3669.

[4] Monte, F.D. (2006). Multi-layer transient heat conduction using transition time scales. *Int. J. Thermal Sciences*, **45**, 882-892.

[5] Ash, R., Barrer, M., Petropoulos, J.H. (1963). Diffusion in heterogeneous media: properties of a laminated slab. *Brit. J. Appl. Phys*, **14**, 854-864.

[6] Lu, X., Tervola, P., Viljanen, M. (2006). Transient analytical solution to heat conduction in composite circular cylinder. *Int. J. Heat Mass Transfer*, **49**, 341-348.

[7] Kayhani, M.H., Norouzi, M., Delouei, A.A. (2012). A general analytical solution for heat conduction in cylindrical multilayer composite laminates. *Int. J. Thermal Sciences*, **52**, 73-83.

[8] Dalir, N., Nourazar, S.S. (2014). Analytical solution of the problem on the three-dimensional transient heat conduction in a multilayer cylinder. *J. Eng. Phys. Thermo*, **87**,89-97 .

[9] Monte, F.D. (2002). An analytic approach to the unsteady heat conduction processes in one-dimensional composite media. *Int. J. Heat Mass Transfer*, **45**, 1333-1343.

[10] Miller, J.R., Weaver, P.M. (2003). Temperature profiles in composite plates subject to time-dependent complex boundary conditions. *Composite structures*, **59**, 267-278.

[11] Hickson, R.I., Barry,S.I., Mercer, G.N. (2009). Exact and numerical solutions for effective diffusivity and time lag through multiple layers. *ANZIAM J. (E)*, **50**, C682-C695.

[12] Hickson, R.I., Barry,S.I., Mercer, G.N. (2009). Critical times in multilayer diffusion. Part 1: Exact solutions. *Int. J. Heat Mass Transfer*, **52**, 5776-5783.

[13] Hickson, R.I., Barry,S.I., Mercer, G.N. (2009). Critical times in multilayer diffusion. Part 2: Approximate solutions. *Int. J. Heat Mass Transfer*, **52**, 5784-5791.

[14] Diard, J.P., Glandut, N., Montella, C., Sanchez, J.Y. (2005). One layer, two layers, etc. An introduction to the EIS study of multilayer electrodes. Part 1: Theory. *J. Electroanalytical Chem*., **578**, 247-257.

[15] Azeez, M.F.A., Vakakis, A.F. (2000). Axisymmetric transient solutions of the heat diffusion problem in layered composite media. *Int. J. Heat Mass Transfer*, **43**, 3883-3895.

Chapter 5

A Weakly Nonlinear Analysis of the Onset of Darcy-Bénard Convection with Local Thermal Non-Equilibrium.

5.1 Abstract

In this work we extend the work of Banu and Rees [1] into the weakly nonlinear regime. Banu and Rees [1] gave a detailed and comprehensive study of the effect of Local Thermal Non-Equilibrium on the onset of Darcy-Benard convection. The aim of this chapter is to determine whether the convection pattern immediately post-onset is two dimensional (rolls) or three dimensional (square cells). This is achieved using a weakly nonlinear theory to analyse the cross-roll instability.

5.2 Nomenclature

A, B, C	amplitudes
c	specific heat
d	depth
g	gravity
H	inter-phase heat transfer coefficient
k	wavenumber

K	permeability
L	length scale
p	Pressure
t	Time
T	temperature
u, v	velocity in x-direction and y-direction
x, y	Cartesian coordinates
i	$\sqrt{-1}$

Greek letters

α	thermal diffusivity
β	thermal expansion coefficient
γ	porosity - modified conductivity ratio
δ	amplitude of disturbance
η	similarity variable
θ	temperature profile
Θ	temperature disturbance
κ	diffusivity
μ	dynamic viscosity
ρ	fluid density

τ	scaled time
ϕ	angle
Φ	angle disturbance
ψ	streamfunction
Ψ	streamfunction disturbance
Ω	porosity

Superscripts and subscripts

$\bar{}$	dimensional quantities
f	fluid
l	lower
s	solid
u	upper

5.3 Introduction

Darcy-Bénard problem is a fundamental work in the study of convection in a porous medium heated uniformly from the lower boundary which has been mentioned very often in the previous chapter in this thesis (refer Horton and Rogers [2] and Lapwood [3]). Straus [4] then initiated the extension of Darcy-Bénard problem into non-linear regime and found that there is no stable two dimensional solution occurs for $Ra \geq 380$ of a finite band of horizontal wavenumbers.

Later, Rees and Riley [5] used the weakly nonlinear analysis of Newell and Whitehead [6] to study the effect of small-amplitude boundary imperfections on weakly nonlinear Darcy-Bénard convection. They found that the destabilisation due to the thermal imperfection is enhanced to a lower Ra number and the cellular pattern that arises is observed to be rolls. If the wavelength of the imperfections is slightly detuned from the critical value, then it is also possible to have rolls with wavy axes. In fact, they also found that the cross-roll instability generally forms the most dangerous disturbance. This instability arises when the disturbances are in the form of rolls whose axes are at an angle to those of the original rolls. However, for this case cross-roll disturbances do not destabilise the roll pattern. According to Rees [7], the eventual pattern of the flow depends on the "coupling" coefficient which arises in the amplitude equations which are obtained via the weakly nonlinear theory which, if greater than 1 then rolls are the stable planform, but if less than 1 then square or rectangular cells are. One example of a configuration which yields convection with a square planform is the layered form of the Darcy-Bénard problem considered in Rees and Riley [8] They found regions in parameter space where this happens for both two and three layer systems.

All the above-mentioned authors were concerned exclusively with cases where local thermal equilibrium (LTE) applies – this is the assumption that the fluid and solid phases may be modelled using one temperature field. The opposite situation is Local thermal non-equilibrium (LTNE) where each of the solid and fluid

phase temperature fields are modelled separately. Combarnous [9] was among the earliest researchers who worked on fully two-dimensional nonlinear computations of Darcy-Benard with local thermal non-equilibrium (LTNE). The equations for unsteady heat transfer in a saturated porous medium when assuming a LTNE regime are given by Nield and Bejan [10]. A coupled pair of energy equations, the so called the two-field model, models the fluid and solid phases separately by considering the heat lost to and gained from the other phase. The coefficients of the source/sink terms, h, in this formulation have attracted much attention, and very many correlations have been found, one example of which is Quintard [11]. He presented numerical results for the effective properties of two macroscopic media which are modelled by a heat transfer coefficient, h, whose value relies on the many properties of the saturating fluid and the porous medium including the diffusivities and conductivities. A year later, Quintard [12] considered an additional factor; the effect of interfacial thermal barriers, to the previous work of the two-field model dealing with LTNE heat transfer in porous medium.

On adopting the same model for microscopic heat transfer, Rees and Pop [13] analysed the steady free convective stagnation-point flow in porous medium. They found the non-equilibrium effect strongly develops when H (the nondimensionalised form of the heat transfer coefficient, h) is small. An increase in H, decreases the thickness of the solid-phase temperature field. Further increases in H cause the flow to tend towards the local thermal equilibrium case where the temperature fields of solid and fluid phase are identical. Then, Rees and Pop [14] considered a free convection boundary layer using the two-field mode and they found the effect of LTNE is found to transform the behavior of the flow mainly within a small distance from the leading edge. The subsequent review work by Rees and Pop [15] provided a good compilation as reference in the studies of LTNE effect on free convection in porous medium.

In between the years, Banu and Rees [1] have modified the linearised stability analysis to investigate the onset criterion for convection of the two-field two dimensional non-equilibrium model. Generally, they found that the presence of thermal non-equilibrium affect the Ra and wavenumber. Comparison between asymptotic solution and numerical solutions of the inter-phase heat transfer coefficient, H suggested that the critical wavenumber of the LTNE is always greater than LTE case which is π for intermediate value of H. In fact, in some cases, the critical wavenumber for LTNE convection can be very much larger than the value of π for the LTE case.

Until now, there has been no weakly nonlinear analysis for the Darcy-Bénard problem with LTNE effects present, even though it has been 16 years since the publication of Banu and Rees [1]. Other researchers have considered the evolution of small amplitude disturbances to determine the criterion for the onset of convection with the two-field model for other configurations, but these analyses have been confined to linear theory. However, due to the limitations of linear stability analyses, whose usefulness lies only with determining if disturbances with small amplitudes grow or decay and if they do so if the exponential growth rate is real or complex, we choose to employ a weakly nonlinear analysis to determine whether the convection pattern immediately post-onset is two dimensional (rolls) or three dimensional (square cells). In fact, weakly nonlinear analysis is the best solution to investigate further how the solution curve for the disturbances bifurcates from zero disturbance solution. Apart from that, the addition of LTNE can yield some surprises. For example Banu and Rees [1] found a region of parameter space (large values of H and small values of γ) where the critical wavenumber becomes very large; . Therefore it is also worth checking the speculation that LTNE might possibly yield square cell patterns in that or some other region of parameter space.

5.4 Governing equations

The main interest of this study is to investigate the onset and subsequent development of Darcy-Bénard convection in porous medium when the solid and fluid phases are not in local thermal equilibrium. Thus we consider unsteady three-dimensional convection when the local thermal non-equilibrium (LTNE) two-field model is valid, and where the lower bounding surface is held at the constant temperature, T_1, while the upper surface is held at the lower temperature, T_u. The governing equations for Darcy-Bénard convection where a two-field model of microscopic heat transfer applies are given by Nield and Bejan [9]:

$$\frac{\partial \bar{u}}{\partial \bar{x}} + \frac{\partial \bar{v}}{\partial \bar{y}} + \frac{\partial \bar{w}}{\partial \bar{z}} = 0, \tag{5.1}$$

$$\bar{u} = -\frac{K}{\mu}\frac{\partial \bar{p}}{\partial \bar{x}}, \tag{5.2}$$

$$\bar{v} = -\frac{K}{\mu}\frac{\partial \bar{p}}{\partial \bar{y}}, \tag{5.3}$$

$$\bar{w} = -\frac{K}{\mu}\frac{\partial \bar{p}}{\partial \bar{y}} + \frac{\rho_f g \beta K}{\mu}\left(T_f - T_u\right), \tag{5.4}$$

$$\Omega(\rho c)_f \frac{\partial T_f}{\partial \bar{t}} + (\rho c)_f \left(\bar{u}\frac{\partial T_f}{\partial \bar{x}} + \bar{v}\frac{\partial T_f}{\partial \bar{y}} + \bar{w}\frac{\partial T_f}{\partial \bar{z}} \right) = \Omega k_f \left(\frac{\partial^2 T_f}{\partial \bar{x}^2} + \frac{\partial^2 T_f}{\partial \bar{y}^2} + \frac{\partial^2 T_f}{\partial \bar{z}^2} \right) + h\left(T_s - T_f\right), \tag{5.5}$$

$$(1-\Omega)(\rho c)_s \frac{\partial T_s}{\partial \bar{t}} = (1-\Omega) k_s \left(\frac{\partial^2 T_s}{\partial \bar{x}^2} + \frac{\partial^2 T_s}{\partial \bar{y}^2} + \frac{\partial^2 T_s}{\partial \bar{z}^2} \right) - h\left(T_s - T_f\right), \tag{5.6}$$

Here, $\bar{u}$, $\bar{v}$ are the fluid flux velocities in the horizontal directions, $\bar{x}$ and $\bar{y}$, respectively, while $\bar{w}$ is the fluid flux velocity in the vertical direction $\bar{z}$. In addition, $\bar{p}$ is pressure, T is temperature, $\bar{t}$ is time, f and s are subscripts denoting the fluid phase and the solid phase, respectively. Other properties of fluid and medium are as follows: ρ is the density, β is the coefficient of cubical expansion, K is the

permeability, μ is the fluid density, Ω is the porosity, c is the specific heat, k is the thermal conductivity and g is gravity. We assume that the phases have identical temperatures at the bounding surfaces and that the layer has depth, d.

Now the resulting three-dimensional flow given by solutions of equations (5.1) - (5.6) may be studied by introducing the following transformations:

$$(\bar{x},\bar{y},\bar{z}) = d(x,y,z),\ (\bar{u},\bar{v},\bar{w}) = \frac{\Omega k_f}{d(\rho c)_f}(u,v,w),\ \bar{p} = \frac{\mu k_f}{K(\rho c)_f}p,\ \bar{t} = \frac{(\rho c)_f}{k_f}d^2 t,$$

$$T_f = (T_1 - T_u)\theta + T_u,\ T_s = (T_1 - T_u)\phi + T_u. \tag{5.7}$$

By replacing equation (5.7) into equations (5.1) - (5.6) and eliminating the velocities term, we obtained the following non-dimensionalised governing equations:

$$\frac{\partial^2 p}{\partial x^2} + \frac{\partial^2 p}{\partial y^2} + \frac{\partial^2 p}{\partial z^2} - Ra\frac{\partial \theta}{\partial z} = 0, \tag{5.8}$$

$$\frac{\partial \theta}{\partial t} - \frac{\partial p}{\partial x}\left(\frac{\partial \theta}{\partial x}\right) - \frac{\partial p}{\partial y}\left(\frac{\partial \theta}{\partial y}\right) - \frac{\partial p}{\partial z}\left(\frac{\partial \theta}{\partial z}\right) + Ra\theta\frac{\partial \theta}{\partial z} = \frac{\partial^2 \theta}{\partial x^2} + \frac{\partial^2 \theta}{\partial y^2} + \frac{\partial^2 \theta}{\partial z^2} + H(\phi - \theta), \tag{5.9}$$

$$\alpha\frac{\partial \phi}{\partial t} = \frac{\partial^2 \phi}{\partial x^2} + \frac{\partial^2 \phi}{\partial y^2} + \frac{\partial^2 \phi}{\partial z^2} - \gamma H(\phi - \theta), \tag{5.10}$$

where ϕ and θ are the scaled temperatures of the solid and fluid phases, respectively while

$$\gamma = \frac{\Omega k_f}{(1-\Omega)k_s},\ H = \frac{d^2 h}{\Omega k_f},\ \kappa_f = \frac{k_f}{(\rho c)_f},\ \kappa_s = \frac{k_s}{(\rho c)_s} \text{ and } \alpha = \frac{\kappa_f}{\kappa_s}. \tag{5.11}$$

Equations (5.8) - (5.10) are subject to boundary conditions:

$$\theta = 1, \quad \phi = 1, \quad p_z = Ra \quad \text{at } z = 0,$$

$$\theta = 0, \quad \phi = 0, \quad p_z = 0 \quad \text{at } z = 1, \tag{5.12}$$

and the basic state the stability of which is being discussed is given by:

$$\theta = \phi = 1 - z \quad \text{and} \quad p = Ra\left(z - \tfrac{1}{2}z^2\right) + \text{constant}. \tag{5.13}$$

Next we perturb equations (5.8) - (5.10) about this basic solution by setting:

$$\theta = 1 - z + \Theta, \tag{5.14a}$$

$$\phi = 1 - z + \Phi, \tag{5.14b}$$

$$p = Ra\left(z - \tfrac{1}{2}z^2\right) + \text{constant} + P. \tag{5.14c}$$

Thus

$$\frac{\partial^2 P}{\partial x^2} + \frac{\partial^2 P}{\partial y^2} + \frac{\partial^2 P}{\partial z^2} = Ra\frac{\partial \Theta}{\partial z}, \tag{5.15}$$

$$\frac{\partial \Theta}{\partial t} - \frac{\partial P}{\partial x}\left(\frac{\partial \Theta}{\partial x}\right) - \frac{\partial P}{\partial y}\left(\frac{\partial \Theta}{\partial y}\right) - \frac{\partial P}{\partial z}\left(\frac{\partial \Theta}{\partial z}\right) + Ra\Theta\frac{\partial \Theta}{\partial z} = \frac{\partial^2 \Theta}{\partial x^2} + \frac{\partial^2 \Theta}{\partial y^2} + \frac{\partial^2 \Theta}{\partial z^2} + H\left(\Phi - \Theta\right), \tag{5.16}$$

$$\alpha\frac{\partial \Phi}{\partial t} = \frac{\partial^2 \Phi}{\partial x^2} + \frac{\partial^2 \Phi}{\partial y^2} + \frac{\partial^2 \Phi}{\partial z^2} - \gamma H\left(\Phi - \Theta\right), \tag{5.17}$$

which are subject to boundary conditions

$$\Theta = 0,\ \Phi = 0,\ \frac{\partial P}{\partial z} = 0 \quad \text{at } z = 0,$$

$$\Theta = 0,\ \Phi = 0,\ \frac{\partial P}{\partial z} = 0 \quad \text{at } z = 1, \tag{5.18}$$

5.5 Weakly non-linear theory

Weakly non-linear theory (WNLT) is an extension to linear stability theory which will allow an analysis of Darcy-Bénard convection when Ra is very close to Ra_c and where the amplitude of the disturbance is now small but finite, as opposed to infinitesimal for linearized theory. In this case the nonlinearity will eventually saturate and further postcritical growth of the disturbance ceases. Thus, performing the WNLT in such cases will provide the answer to the question of what will eventually occur to the exponentially growing disturbance which arises from linearized theory.

To explain, at its simplest the aim for weakly nonlinear theory is to derive a Landau equation of the type

$$A_t = R_2 A - cA^3, \tag{5.19}$$

where R_2 is a measure of the small deviation of the Rayleigh number from its critical value. If one neglects the nonlinear term, then A will grow exponentially when $R_2 > 0$, but will decay exponentially when $R_2 < 0$. In very many cases the constant, *c*, is positive, which means that growing solutions when *A* is small will saturate and eventually tend to $\sqrt{\frac{R_2}{c}}$. Thus the A = 0 solution is unstable when $R_2 > 0$. This situation represents a supercritical bifurcation. However, in the Wooding problem, *c* is negative, which means that the bifurcation is subcritical and solutions for $R_2 < 0$ eventually tend to $\sqrt{-\frac{R_2}{c}}$.

For the present problem and when considering the cross-roll instability, there will be two rolls and hence two amplitude equations, one for each roll. Equation (5.20) show the typical Landau equation for the roll amplitudes, B and C, which are found in a wide variety of stability problems.

$$B_\tau = R_2 B - cB\left[B^2 + d\,C^2\right], \tag{5.20a}$$

$$C_\tau = R_2 C - cC\left[C^2 + dB^2\right]. \tag{5.20b}$$

Of most interest is the value of *d*, for if its minimum (over the angle between the rolls) is greater than 1, then rolls are stable and square cells (*B* = C) are unstable, but if the minimum is less than 1, then rolls are unstable and square cells are stable.

A solution for *P*, Θ and Φ in equations (5.15) - (5.17) may be found in terms of power series expansion of ε,

$$\begin{pmatrix} P \\ \Theta \\ \Phi \end{pmatrix} = \varepsilon \begin{pmatrix} p_1 \\ \theta_1 \\ \phi_1 \end{pmatrix} + \varepsilon^2 \begin{pmatrix} p_2 \\ \theta_2 \\ \phi_2 \end{pmatrix} + \varepsilon^3 \begin{pmatrix} p_3 \\ \theta_3 \\ \phi_3 \end{pmatrix} + \cdots, \tag{5.21}$$

while the Rayleigh number, Ra takes the form

$$Ra = Ra_o + \varepsilon^2 Ra_2 + \cdots, \tag{5.22}$$

which defines ε, given that *Ra* is just slightly above Ra_o; see Newell and Whitehead [5]. Note that $Ra_o = Ra_c$. By substituting equation (5.22) and introducing rescaling of time, $\tau = \frac{1}{2}\epsilon^2 t$ into equations (5.15) - (5.17) yield the following disturbance equations:

$$P_{xx} + P_{yy} + P_{zz} = \left(Ra_o + \in^2 Ra_2\right)\Theta_z, \tag{5.23}$$

$$\begin{aligned} &\frac{1}{2}\in^2 \Theta_\tau - \left[P_x\Theta_x + P_y\Theta_y + P_z\Theta_z\right] + \left(Ra_o + \in^2 Ra_2\right)\Theta\Theta_z \\ &= \Theta_{xx} + \Theta_{yy} + \Theta_{zz} + \left(Ra_o + \in^2 Ra_2\right)\Theta - P_z + H\left(\Phi - \Theta\right), \end{aligned} \tag{5.24}$$

$$\frac{1}{2}\alpha \in^2 \Phi_\tau = \Phi_{xx} + \Phi_{yy} + \Phi_{zz} - \gamma H\left(\Phi - \Theta\right). \tag{5.25}$$

Applying equation (5.21) into equations (5.23) - (5.25) then we may transform the equations into a series of nonlinear expansions.

$$\begin{aligned}&\left[\in P_{1xx}+\in^2 P_{2xx}+\in^3 P_{3xx}+\cdots\right]+\left[\in P_{1yy}+\in^2 P_{2yy}+\in^3 P_{3yy}+\cdots\right]\\&+\left[\in P_{1zz}+\in^2 P_{2zz}+\in^3 P_{3zz}+\cdots\right]=\left(Ra_o+\in^2 Ra_2\right)\left[\in\Theta_{1z}+\in^2\Theta_{2z}+\in^3\Theta_{3z}+\cdots\right],\end{aligned}\tag{5.26}$$

$$\begin{aligned}&\frac{1}{2}\in^2\left[\in\Theta_{1\tau}+\in^2\Theta_{2\tau}+\in^3\Theta_{3\tau}+\cdots\right]\\&-\begin{bmatrix}\left(\in P_{1x}+\in^2 P_{2x}+\in^3 P_{3x}+\cdots\right)\left(\in\Theta_{1x}+\in^2\Theta_{2x}+\in^3\Theta_{3x}+\cdots\right)+\\\left(\in P_{1y}+\in^2 P_{2y}+\in^3 P_{3y}+\cdots\right)\left(\in\Theta_{1y}+\in^2\Theta_{2y}+\in^3\Theta_{3y}+\cdots\right)+\\\left(\in P_{1z}+\in^2 P_{2z}+\in^3 P_{3z}+\cdots\right)\left(\in\Theta_{1z}+\in^2\Theta_{2z}+\in^3\Theta_{3z}+\cdots\right)\end{bmatrix}\\&+\left(Ra_o+\in^2 Ra_2\right)\left(\in\Theta_1+\in^2\Theta_2+\in^3\Theta_3+\cdots\right)\left(\in\Theta_{1z}+\in^2\Theta_{2z}+\in^3\Theta_{3z}+\cdots\right)\\&=\left[\in\Theta_{1xx}+\in^2\Theta_{2xx}+\in^3\Theta_{3xx}+\cdots\right]+\left[\in\Theta_{1yy}+\in^2\Theta_{2yy}+\in^3\Theta_{3yy}+\cdots\right]\\&+\left[\in\Theta_{1zz}+\in^2\Theta_{2zz}+\in^3\Theta_{3zz}+\cdots\right]\\&+\left(Ra_o+\in^2 Ra_2\right)\left(\in\Theta_1+\in^2\Theta_2+\in^3\Theta_3+\cdots\right)-\left(\in P_{1z}+\in^2 P_{2z}+\in^3 P_{3z}+\cdots\right)\\&+H\left[\left(\in\Phi_1+\in^2\Phi_2+\in^3\Phi_3+\cdots\right)-\left(\in\Theta_1+\in^2\Theta_2+\in^3\Theta_3+\cdots\right)\right],\end{aligned}\tag{5.27}$$

$$\begin{aligned}&\frac{1}{2}\alpha\in^2\left[\in\Phi_{1\tau}+\in^2\Phi_{2\tau}+\in^3\Phi_{3\tau}+\cdots\right]=\left[\in\Phi_{1xx}+\in^2\Phi_{2xx}+\in^3\Phi_{3xx}+\cdots\right]\\&+\left[\in\Phi_{1yy}+\in^2\Phi_{2yy}+\in^3\Phi_{3yy}+\cdots\right]+\left[\in\Phi_{1zz}+\in^2\Phi_{2zz}+\in^3\Phi_{3zz}+\cdots\right]\\&-\gamma H\left[\left(\in\Phi_1+\in^2\Phi_2+\in^3\Phi_3+\cdots\right)-\left(\in\Theta_1+\in^2\Theta_2+\in^3\Theta_3+\cdots\right)\right].\end{aligned}\tag{5.28}$$

We now equate terms at the successive orders of expansion in powers of $\in$ in equations (5.26) - (5.28). We obtain the following system at $O(\in)$ in the expansion:

$$P_{1xx}+P_{1yy}+P_{1zz}=Ra_o\Theta_{1z},\tag{5.29i}$$

$$\Theta_{1xx}+\Theta_{1yy}+\Theta_{1zz}+Ra_o\Theta_1-P_{1z}+H\left(\Phi_1-\Theta_1\right)=0,\tag{5.29ii}$$

$$\Phi_{1xx}+\Phi_{1yy}+\Phi_{1zz}-\gamma H\left(\Phi_1-\Theta_1\right)=0.\tag{5.29iii}$$

Equations (5.29) reproduce the linearised theory of Banu and Rees [1] although these equations are in the pressure/temperature form, rather than the streamfunction/temperature used in [1]. At $O(\in^2)$:

$$P_{2xx} + P_{2yy} + P_{2zz} = Ra_o \Theta_{2z}, \tag{5.30i}$$

$$\begin{aligned} -\left[P_{1x}\Theta_{1x} + P_{1y}\Theta_{1y} + P_{1z}\Theta_{1z} \right] + Ra_o \Theta_1 \Theta_{1z} &= \Theta_{2xx} + \Theta_{2yy} + \Theta_{2zz} \\ &\quad + Ra_o \Theta_2 - P_{2z} + H\left(\Phi_2 - \Theta_2\right), \end{aligned} \tag{5.30ii}$$

$$\Phi_{2xx} + \Phi_{2yy} + \Phi_{2zz} - \gamma H\left(\Phi_2 - \Theta_2\right) = 0. \tag{5.30iii}$$

At $O\left(\in^3\right)$:

$$P_{3xx} + P_{3yy} + P_{3zz} = Ra_o \Theta_{3z} + Ra_2 \Theta_{1z}, \tag{5.31i}$$

$$\begin{aligned} &\frac{1}{2}\Theta_{1\tau} - \begin{bmatrix} P_{1x}\Theta_{2x} + P_{2x}\Theta_{1x} \\ + P_{1y}\Theta_{2y} + P_{2y}\Theta_{1y} \\ + P_{1z}\Theta_{2z} + P_{2z}\Theta_{1z} \end{bmatrix} + Ra_o\left(\Theta_1\Theta_{2z} + \Theta_2\Theta_{1z}\right) \\ &= \Theta_{3xx} + \Theta_{3yy} + \Theta_{3zz} + \left[Ra_o\Theta_3 + Ra_2\Theta_1\right] - P_{3z} + H\left(\Phi_3 - \Theta_3\right), \end{aligned} \tag{5.31ii}$$

$$\frac{1}{2}\alpha\Theta_{1\tau} = \Phi_{3xx} + \Phi_{3yy} + \Phi_{3zz} - \gamma H\left(\Phi_3 - \Theta_3\right). \tag{5.31iii}$$

We remain interested in the stability at the bottom of the natural curve, but equations (5.29) need to be solved to determine this point as a function of *H* and γ. Therefore we may use the following as an eigensolution of the homogeneous system (5.29i) - (5.29iii).

$$P_1 = A_1\left[Ce^{ikx} + \overline{C}e^{-ikx}\right]\cos\pi z,$$

(5.32i)

$$\Theta_1 = A_2\left[Ce^{ikx} + \overline{C}e^{-ikx}\right]\sin\pi z, \tag{5.32ii}$$

$$\Phi_1 = A_3\left[Ce^{ikx} + \overline{C}e^{-ikx}\right]\sin\pi z. \tag{5.32iii}$$

Here we assume that $A = A(\tau)$ only and this corresponds to a single roll solution with axes in the *y*-direction. However, we are interested in the stability of one roll with respect to disturbances in the form of another roll aligned at a relative angle of ϕ and therefore we will introduce two roll solutions to replace equations (5.32).

$$P_1 = A_1\left[Ce^{ikx} + \overline{C}e^{-ikx}\right]\cos\pi z + A_1\left[Be^{ik(x\cos\phi - y\sin\phi)} + \overline{B}e^{-ik(x\cos\phi - y\sin\phi)}\right]\cos\pi z\,, \qquad (5.33\text{i})$$

$$\Theta_1 = A_2\left[Ce^{ikx} + \overline{C}e^{-ikx}\right]\sin\pi z + A_2\left[Be^{ik(x\cos\phi - y\sin\phi)} + \overline{B}e^{-ik(x\cos\phi - y\sin\phi)}\right]\sin\pi z\,, \qquad (5.33\text{ii})$$

$$\Phi_1 = A_3\left[Ce^{ikx} + \overline{C}e^{-ikx}\right]\sin\pi z + A_3\left[Be^{ik(x\cos\phi - y\sin\phi)} + \overline{B}e^{-ik(x\cos\phi - y\sin\phi)}\right]\sin\pi z\,. \qquad (5.33\text{iii})$$

Note that these *C* and *B* components represent precisely the same form of solution as one another, except for the fact that they are aligned at different angles to the horizontal coordinate directions.

The linear stability theory of Banu and Rees [1] is reproduced by substituting equations (5.33i) - (5.33iii) into equations (5.29i) - (5.29iii); this yields the following three equations for A_1, A_2 and A_3:

$$-A_1\left(k^2 + \pi^2\right) = Ra_o\pi A_2\,, \qquad (5.34\text{i})$$

$$\left(-k^2 - \pi^2 + Ra_o - H\right)A_2 + \pi A_1 + HA_3 = 0\,, \qquad (5.34\text{ii})$$

$$\left(-k^2 - \pi^2 - \gamma H\right)A_3 + \gamma HA_2 = 0\,. \qquad (5.34\text{iii})$$

These equations (5.34i) - (5.34iii) may be transformed into matrix/vector form, $M\underline{A} = 0$:

$$\begin{pmatrix} k^2+\pi^2 & Ra_o\pi & 0 \\ -\pi & k^2+\pi^2-Ra_o+H & -H \\ 0 & -\gamma H & k^2+\pi^2+H \end{pmatrix}\begin{pmatrix} A_1 \\ A_2 \\ A_3 \end{pmatrix} = \begin{pmatrix} 0 \\ 0 \\ 0 \end{pmatrix}. \qquad (5.35)$$

This eigenvalue problem for Ra_0 may be solved by first setting determinant of matrix M equal to zero, $\det|M| = 0$. In this way we get the following expression for Ra:

$$\left(k^2 + \pi^2\right)\begin{vmatrix} k^2+\pi^2-Ra_o+H & -H \\ -\gamma H & k^2+\pi^2+H \end{vmatrix} - Ra_o\pi\begin{vmatrix} -\pi & -H \\ 0 & k^2+\pi^2+H \end{vmatrix} = 0\,,$$

and hence,

$$Ra_o = \frac{\left(k^2+\pi^2\right)^2}{k^2}\left[\frac{k^2+\pi^2+H\left(1+\gamma\right)}{k^2+\pi^2+\gamma H}\right]. \tag{5.36}$$

It proves convenient to take A_2 to be equal to one which reproduces the value used by Rees [7] for the LTE case, and this aids with the checking of our later algebra. Therefore we have $A_2 = \dfrac{-\left(k^2+\pi^2\right)}{Ra_o k}$ which then gives $A_1 = \dfrac{\pi}{k}$, and finally equation (5.34iii) yields $A_3 = \left[\dfrac{-\gamma H\left(k^2+\pi^2\right)}{Ra_o k\left(k^2+\pi^2+\gamma H\right)}\right]$. Neutral curves corresponding to equation (5.36) may be found in Banu and Rees [1]. In all cases the curves are unimodal with a single well-defined minimum, and the onset of convection is stationary.

Now for the solving for the $O\left(\in^2\right)$ terms, we substitute A_1, A_2, A_3, Ra_0, and equations (5.33i) - (5.33iii) into equations (5.30i) - (5.30iii). This yields

$$P_{2xx} + P_{2yy} + P_{2zz} - Ra_o\Theta_{2z} = 0, \tag{5.37i}$$

$$\begin{bmatrix}\Theta_{2xx}+\Theta_{2yy}+\Theta_{2zz}\\ +Ra_o\Theta_2 - P_{2z}\\ +H\left(\Phi_2-\Theta_2\right)\end{bmatrix} = \frac{\pi\left(k^2+\pi^2\right)}{Ra}\begin{bmatrix} 2\left(B\overline{B}+C\overline{C}\right)\\ +\left(1-\cos\phi\right)\begin{pmatrix} CBe^{ik\left(x\left(1+\cos\phi\right)-y\sin\phi\right)}\\ +\overline{C}\,\overline{B}e^{-ik\left(x\left(1+\cos\phi\right)-y\sin\phi\right)}\end{pmatrix}\\ +\left(1+\cos\phi\right)\begin{pmatrix} C\overline{B}e^{ik\left(x\left(1-\cos\phi\right)+y\sin\phi\right)}\\ +\overline{C}Be^{-ik\left(x\left(1-\cos\phi\right)+y\sin\phi\right)}\end{pmatrix}\end{bmatrix}\sin 2\pi z, \tag{5.37ii}$$

$$\Phi_{2xx} + \Phi_{2yy} + \Phi_{2zz} - \gamma H\left(\Phi_2 - \Theta_2\right) = 0. \tag{5.37iii}$$

As the order increases, the mathematical analysis becomes very complex and extremely lengthy both to do and to write. Given that it will be relatively easy to encode a sequence of nested expressions on a computer, and thus to keep the present writing neat and tidy, we have chosen to simplify the presentation of the equations by first defining the coefficients E_B and E_C to be the complex exponentials multiplying B and C, respectively in Equations (5.33) and overbars denote complex conjugation; see appendix (i) for the full analysis and definition of the simplifications done in this work.

In order to find the solution of equations (5.37i) - (5.37iii), we first note that the Complementary Function may be set to zero for one may assume that all the wavenumber-k contributions arise at $O(\in)$ – this is quite standard in weakly nonlinear theory. Second, the forcing terms corresponding to horizontal wavenumbers which are not equal to k and therefore non-resonant and may be solved. Thus the determination of the Particular Integrals are just a matter of performing lengthy algebra. Although it could be argued that one may have resonance (i.e. a wavenumber of k) when the rolls are at an angle of 60^o the vertical component of the forcing terms are sin $2\pi z$ and therefore this case is also non-resonant. Therefore we may find the particular integral (PI) for each of the inhomogeneous terms in equation (5.37) in turn by using the following three substitutions:

$$\begin{pmatrix} p_2 \\ \Theta_2 \\ \Phi_2 \end{pmatrix} = \begin{pmatrix} m_1 \cos 2\pi z \\ m_2 \sin 2\pi z \\ m_3 \sin 2\pi z \end{pmatrix} \left(B\overline{B} + C\overline{C} \right), \tag{5.38i}$$

$$\begin{pmatrix} p_2 \\ \Theta_2 \\ \Phi_2 \end{pmatrix} = \begin{pmatrix} m_4 \cos 2\pi z \\ m_5 \sin 2\pi z \\ m_6 \sin 2\pi z \end{pmatrix} \left(CBE_c E_B + \overline{C}\,\overline{B}\,\overline{E_c}\,\overline{E_B} \right) \tag{5.38ii}$$

$$\begin{pmatrix} p_2 \\ \Theta_2 \\ \Phi_2 \end{pmatrix} = \begin{pmatrix} m_7 \cos 2\pi z \\ m_8 \sin 2\pi z \\ m_9 \sin 2\pi z \end{pmatrix} \left(C\overline{B}E_C \overline{E_B} + \overline{C}B\overline{E_C}E_B \right) \tag{5.38iii}$$

This eventually yields,

$$m_1 = \frac{\left(4\pi^2 + \gamma H\right)\left(k^2 + \pi^2\right)}{\left(16\pi^4 + 4\pi^2 H\left(1+\gamma\right)\right)},$$

$$m_2 = -\frac{\left(4\pi^2 + \gamma H\right)\left(k^2 + \pi^2\right)}{2\pi Ra_o\left(4\pi^2 + H\left(1+\gamma\right)\right)},$$

$$m_3 = -\frac{2\pi\gamma H\left(k^2 + \pi^2\right)}{Ra_o\left(16\pi^4 + 4\pi^2 H\left(1+\gamma\right)\right)},$$

$$m_4 = \frac{-2\pi^2\left(k^2 + \pi^2\right)\left(1-\cos\phi\right)\left(\xi_1 + \gamma H\right)}{\gamma H\left(-\xi_1^2 + \xi_1 Ra_o - 4\pi^2 Ra_o\right) - H\xi_1^2 - \xi_1^3 + \xi_1^2 Ra_o - 4\pi^2 Ra_o\xi_1},$$

$$m_5 = \frac{\pi\left(k^2 + \pi^2\right)\left(1-\cos\phi\right)\xi_1\left(\xi_1 + \gamma H\right)}{Ra_o\left[\gamma H\left(-\xi_1^2 + \xi_1 Ra_o - 4\pi^2 Ra_o\right) - H\xi_1^2 - \xi_1^3 + \xi_1^2 Ra_o - 4\pi^2 Ra_o\xi_1\right]},$$

$$m_6 = \frac{\pi\left(k^2 + \pi^2\right)\left(1-\cos\phi\right)\xi_1\gamma H}{Ra_o\left[\gamma H\left(-\xi_1^2 + \xi_1 Ra_o - 4\pi^2 Ra_o\right) - H\xi_1^2 - \xi_1^3 + \xi_1^2 Ra_o - 4\pi^2 Ra_o\xi_1\right]},$$

$$m_7 = \frac{-2\pi^2\left(k^2 + \pi^2\right)\left(1+\cos\phi\right)\left(\xi_2 + \gamma H\right)}{\gamma H\left(-\xi_2^2 + \xi_2 Ra_o - 4\pi^2 Ra_o\right) - H\xi_2^2 - \xi_2^3 + \xi_2^2 Ra_o - 4\pi^2 Ra_o\xi_2},$$

$$m_8 = \frac{\pi\left(k^2 + \pi^2\right)\left(1+\cos\phi\right)\xi_2\left(\xi_2 + \gamma H\right)}{Ra_o\left[\gamma H\left(-\xi_2^2 + \xi_2 Ra_o - 4\pi^2 Ra_o\right) - H\xi_2^2 - \xi_2^3 + \xi_2^2 Ra_o - 4\pi^2 Ra_o\xi_2\right]},$$

$$m_9 = \frac{\pi\left(k^2 + \pi^2\right)\left(1+\cos\phi\right)\xi_2\gamma H}{Ra_o\left[\gamma H\left(-\xi_2^2 + \xi_2 Ra_o - 4\pi^2 Ra_o\right) - H\xi_2^2 - \xi_2^3 + \xi_2^2 Ra_o - 4\pi^2 Ra_o\xi_2\right]},$$

where,

$$\xi_1 = k^2\left(1+\cos\phi\right)^2 + k^2\sin^2\phi + 4\pi^2,$$

$$\xi_2 = k^2\left(1-\cos\phi\right)^2 + k^2\sin^2\phi + 4\pi^2.$$

Finally, it is necessary to solve for the $O\left(\in^3\right)$ systems. We rearrange equations (5.38) and let:

$$P_2 = \begin{bmatrix} m_1\left(B\overline{B}+C\overline{C}\right)+ \\ m_4\left(CBE_cE_B+\overline{C}\,\overline{B}\,\overline{E_c}\,\overline{E_B}\right)+ \\ m_7\left(C\overline{B}E_C\overline{E_B}+\overline{C}B\overline{E_C}E_B\right) \end{bmatrix}\cos 2\pi z, \tag{5.39i}$$

$$\Theta_2 = \begin{bmatrix} m_2\left(B\overline{B}+C\overline{C}\right)+ \\ m_5\left(CBE_cE_B+\overline{C}\,\overline{B}\,\overline{E_c}\,\overline{E_B}\right)+ \\ m_8\left(C\overline{B}E_C\overline{E_B}+\overline{C}B\overline{E_C}E_B\right) \end{bmatrix}\sin 2\pi z, \tag{5.39ii}$$

$$\Phi_2 = \begin{bmatrix} m_3\left(B\overline{B}+C\overline{C}\right)+ \\ m_6\left(CBE_cE_B+\overline{C}\,\overline{B}\,\overline{E_c}\,\overline{E_B}\right)+ \\ m_9\left(C\overline{B}E_C\overline{E_B}+\overline{C}B\overline{E_C}E_B\right) \end{bmatrix}\sin 2\pi z, \tag{5.39iii}$$

which m_1, m_2, m_3, m_4, m_5, m_6, m_7, m_8, m_9, ξ_1 and ξ_2, are defined as above. Next, replace the derivatives of equations (5.39i) - (5.39iii) into equations of $O\left(\in^3\right)$; (5.31i) - (5.31iii). These substitutions yield the following equations:

$$\nabla^2 P_3 - Ra_o \Theta_{3z} = \frac{-\pi\left(k^2+\pi^2\right) Ra_2 \cos\pi z}{Ra_o k}\left[CE_C + \overline{C}\,\overline{E_C} + BE_B + \overline{B}\,\overline{E_B}\right], \tag{5.40i}$$

$$\nabla^2 \Phi_3 - \gamma H\left(\Phi_3 - \Theta_3\right) = \frac{\alpha}{2}\left[\frac{-\gamma H\left(k^2+\pi^2\right)}{Ra_o k\left(k^2+\pi^2+\gamma H\right)}\right]\sin\pi z\begin{bmatrix} C_\tau E_C + \overline{C_\tau}\,\overline{E_C} + \\ B_\tau E_B + \overline{B_\tau}\,\overline{E_B} \end{bmatrix}, \tag{5.40ii}$$

$$\nabla^2 \Theta_3 + Ra_o \Theta_3 - P_{3z} + H\left(\Phi_3 - \Theta_3\right) \tag{5.40iii}$$

$$= \frac{-\left(k^2+\pi^2\right)}{2Ra_o k}\begin{bmatrix} C_\tau E_C + \\ \overline{C_\tau}\,\overline{E_C} + \\ B_\tau E_B + \\ \overline{B_\tau}\,\overline{E_B} \end{bmatrix}\sin\pi z + \frac{\left(k^2+\pi^2\right)}{Ra_o k} Ra_2 \sin\pi z \begin{pmatrix} CE_C + \\ \overline{C}\,\overline{E_C} + \\ BE_B + \\ \overline{B}\,\overline{E_B} \end{pmatrix} + \pi k \cos\pi z \sin 2\pi z \begin{bmatrix} \left(1+\cos\phi\right) m_5 \left[\begin{pmatrix} C^2 BE_C^2 E_B - \\ C\overline{C}\,\overline{B}\,\overline{E_B} - \\ C\overline{C}BE_B + \\ \overline{C}^2\,\overline{B}\,\overline{E}_C^2\,\overline{E_B} \end{pmatrix} + \cos\phi \begin{pmatrix} CB^2 E_C E_B^2 - \\ \overline{C}B\overline{B}\,\overline{E_C} - \\ CB\overline{B}E_C + \\ \overline{C}\,\overline{B}^2\,\overline{E_C}\,\overline{E}_B^2 \end{pmatrix}\right] \\ +\left(1-\cos\phi\right) m_8 \left[\begin{pmatrix} C^2 \overline{B}E_C^2\,\overline{E_B} - \\ C\overline{C}BE_B - \\ C\overline{C}\,\overline{B}\,\overline{E_B} + \\ \overline{C}^2 B\overline{E}_C^2 E_B \end{pmatrix} + \cos\phi \begin{pmatrix} CB\overline{B}E_C - \\ \overline{C}B^2\,\overline{E_C}E_B^2 - \\ C\overline{B}^2 E_C \overline{E}_B^2 + \\ \overline{C}B\overline{B}\,\overline{E_C} \end{pmatrix}\right] \end{bmatrix}$$

$$+\pi k\cos\pi z\sin 2\pi z\sin^2\phi\left[m_5\begin{pmatrix}C^2BE_C^2E_B+\\ \overline{C}\,\overline{B}^2\,\overline{E_C}\,\overline{E}_B^2-\\ CB\overline{B}E_C-\\ \overline{C}\,\overline{B}B\overline{E_C}\end{pmatrix}+m_8\begin{pmatrix}C\overline{B}^2E_C\overline{E}_B^2+\\ \overline{C}B^2\overline{E_C}E_B^2-\\ CB\overline{B}E_C-\\ \overline{C}\,\overline{B}B\overline{E_C}\end{pmatrix}\right]-\frac{k\left(k^2+\pi^2\right)}{Ra_o}\sin\pi z\cos 2\pi z\sin^2\phi\left[m_4\begin{pmatrix}C^2BE_C^2E_B+\\ \overline{C}\,\overline{B}^2\,\overline{E_C}\,\overline{E}_B^2-\\ CB\overline{B}E_C-\\ \overline{C}\,\overline{B}B\overline{E_C}\end{pmatrix}+m_7\begin{pmatrix}C\overline{B}^2E_C\overline{E}_B^2+\\ \overline{C}B^2\overline{E_C}E_B^2-\\ CB\overline{B}E_C-\\ \overline{C}\,\overline{B}B\overline{E_C}\end{pmatrix}\right]$$

$$-\frac{k\left(k^2+\pi^2\right)}{Ra_o}\sin\pi z\cos 2\pi z\left[\left(1+\cos\phi\right)m_4\left[\begin{pmatrix}C^2BE_C^2E_B-\\ C\overline{C}B\overline{E_B}-\\ C\overline{C}BE_B+\\ \overline{C}^2B\overline{E}_C^2\overline{E_B}\end{pmatrix}+\cos\phi\begin{pmatrix}CB^2E_CE_B^2-\\ \overline{C}B\overline{B}\overline{E_C}-\\ CB\overline{B}E_C+\\ \overline{C}\,\overline{B}^2\overline{E_C}\overline{E}_B^2\end{pmatrix}\right]+\left(1-\cos\phi\right)m_7\left[\begin{pmatrix}C^2\overline{B}E_C^2\overline{E_B}-\\ C\overline{C}BE_B-\\ C\overline{C}B\overline{E_B}+\\ \overline{C}^2B\overline{E}_C^2E_B\end{pmatrix}+\cos\phi\begin{pmatrix}CB\overline{B}E_C-\\ \overline{C}B^2\overline{E_C}E_B^2-\\ C\overline{B}^2E_C\overline{E}_B^2+\\ \overline{C}B\overline{B}\overline{E_C}\end{pmatrix}\right]\right]$$

$$+\left[\begin{pmatrix}\frac{2\pi^3}{k}-\frac{-2\pi\left(k^2+\pi^2\right)}{k}\end{pmatrix}\sin\pi z\cos 2\pi z\right.\\ \left.+\left[-\frac{\pi\left(k^2+\pi^2\right)}{k}\cos\pi z\sin 2\pi z\right]\right.\left[m_2\begin{bmatrix}\left(C^2\overline{C}+CB\overline{B}\right)E_C\\ +\left(C\overline{C^2}+\overline{C}B\overline{B}\right)\overline{E_C}\\ +\left(C\overline{C}B+B^2\overline{B}\right)E_B\\ +\left(\overline{C}C\overline{B}+B\overline{B^2}\right)\overline{E_B}\end{bmatrix}+m_5\begin{pmatrix}C^2BE_C^2E_B+C\overline{C}\,\overline{B}\overline{E_B}\\ +C\overline{C}BE_B+\overline{C}^2B\overline{E}_C^2\overline{E_B}\\ +CB^2E_CE_B^2+\overline{C}B\overline{B}\overline{E_C}\\ +CB\overline{B}E_C+\overline{C}\,\overline{B}^2\overline{E_C}\overline{E}_B^2\end{pmatrix}+m_8\begin{pmatrix}C^2\overline{B}E_C^2\overline{E_B}+C\overline{C}BE_B\\ +C\overline{C}\,\overline{B}\overline{E_B}+\overline{C}^2B\overline{E}_C^2E_B\\ +CB\overline{B}E_C+\overline{C}B^2\overline{E_C}E_B^2\\ +C\overline{B}^2E_C\overline{E}_B^2+\overline{C}B\overline{B}\overline{E_C}\end{pmatrix}\right]$$

$$-\frac{2\pi^2\left(k^2+\pi^2\right)}{Ra_ok}\cos\pi z\sin 2\pi z\left[m_1\begin{bmatrix}\left(C^2\overline{C}+CB\overline{B}\right)E_C\\ +\left(C\overline{C^2}+\overline{C}B\overline{B}\right)\overline{E_C}\\ +\left(C\overline{C}B+B^2\overline{B}\right)E_B\\ +\left(\overline{C}C\overline{B}+B\overline{B^2}\right)\overline{E_B}\end{bmatrix}+m_4\begin{pmatrix}C^2BE_C^2E_B+C\overline{C}\,\overline{B}\overline{E_B}\\ +C\overline{C}BE_B+\overline{C}^2B\overline{E}_C^2\overline{E_B}\\ +CB^2E_CE_B^2+\overline{C}B\overline{B}\overline{E_C}\\ +CB\overline{B}E_C+\overline{C}\,\overline{B}^2\overline{E_C}\overline{E}_B^2\end{pmatrix}+m_7\begin{pmatrix}C^2\overline{B}E_C^2\overline{E_B}+C\overline{C}BE_B\\ +C\overline{C}\,\overline{B}\overline{E_B}+\overline{C}^2B\overline{E}_C^2E_B\\ +CB\overline{B}E_C+\overline{C}B^2\overline{E_C}E_B^2\\ +C\overline{B}^2E_C\overline{E}_B^2+\overline{C}B\overline{B}\overline{E_C}\end{pmatrix}\right]$$

However, out of the very lengthy terms in equations (5.40i) - (5.40iii), we need to consider only the E_C (exponential of C) term. This is because the nonlinear terms in equations (5.40) contain many components which are nonresonant and therefore solutions corresponding to those may be obtained if one had the need, the will and the time. However, our aim here is to find the condition which guarantees a solution for the system and which, therefore, renders nonresonant all of the inhomogeneities which might appear to be resonant (i.e. those with the critical horizontal wavenumber and which are proportional to sin πz). Such a solvability condition is given by equation (5.43) later. After ignoring the nonresonant terms, equations (5.40i - 5.40iii) now become:

$$\nabla^2 P_3 - Ra_o \Theta_{3z} = \frac{-\pi\left(k^2+\pi^2\right) Ra_2 \cos \pi z}{Ra_o k}\left[CE_C\right], \tag{5.41i}$$

$$\nabla^2 \Phi_3 - \gamma H\left(\Phi_3 - \Theta_3\right) = \frac{\alpha}{2}\left[\frac{-\gamma H\left(k^2+\pi^2\right)}{Ra_o k\left(k^2+\pi^2+\gamma H\right)}\right] \sin \pi z\left[C_\tau E_C\right], \tag{5.41ii}$$

$$\begin{aligned} &\nabla^2 \Theta_3 + Ra_o \Theta_3 - P_{3z} + H\left(\Phi_3 - \Theta_3\right) \\ &= \frac{-\left(k^2+\pi^2\right)}{2Ra_o k}\left(C_\tau E_C\right) \sin \pi z + \frac{\left(k^2+\pi^2\right)}{Ra_o k} Ra_2 \sin \pi z\left(CE_C\right) \end{aligned} \tag{5.41iii}$$

$$\begin{aligned} &+\pi k \cos \pi z \sin 2\pi z\left[\left(1+\cos\phi\right) m_5 \cos\phi\left(-CB\overline{B}E_C\right) + \left(1-\cos\phi\right) m_8 \cos\phi\left(CB\overline{B}E_C\right)\right] \\ &-\frac{k\left(k^2+\pi^2\right)}{Ra_o} \sin \pi z \cos 2\pi z \begin{bmatrix} \left(1+\cos\phi\right) m_4 \cos\phi\left(-CB\overline{B}E_C\right) \\ +\left(1-\cos\phi\right) m_7 \cos\phi\left(CB\overline{B}E_C\right) \end{bmatrix} \\ &+\pi k \cos \pi z \sin 2\pi z \sin^2\phi\left[m_5\left(-CB\overline{B}E_C\right) + m_8\left(-CB\overline{B}E_C\right)\right] \\ &-\frac{k\left(k^2+\pi^2\right)}{Ra_o} \sin \pi z \cos 2\pi z \sin^2\phi\left[m_4\left(-CB\overline{B}E_C\right) + m_7\left(-CB\overline{B}E_C\right)\right] \\ &-\begin{bmatrix} 2\pi k \sin \pi z \cos 2\pi z \\ +\frac{\pi\left(k^2+\pi^2\right)}{k} \cos \pi z \sin 2\pi z \end{bmatrix}\left[m_2\left(C^2\overline{C} + CB\overline{B}\right)E_C + m_5\left(CB\overline{B}E_C\right) + m_8\left(CB\overline{B}E_C\right)\right] \end{aligned}$$

$$-\frac{2\pi^2\left(k^2+\pi^2\right)}{Ra_o k}\cos\pi z\sin 2\pi z\begin{bmatrix} m_1\left(C^2\overline{C}+CB\overline{B}\right)E_C+ \\ m_4\left(CB\overline{B}E_C\right)+m_7\left(CB\overline{B}E_C\right)\end{bmatrix}.$$

We proceed by rewriting equations (5.41i) - (5.41iii) in the following form:

$$\nabla^2 P_3 - Ra_o\Theta_{3z} = \Re_1, \tag{5.42i}$$

$$\nabla^2\Theta_3 + Ra_o\Theta_3 - P_{3z} + H\left(\Phi_3-\Theta_3\right) = \Re_2, \tag{5.42ii}$$

$$\nabla^2\Phi_3 - \gamma H\left(\Phi_3-\Theta_3\right) = \Re_3, \tag{5.42iii}$$

for notational convenience, where the right hand sides terms are confined to being the coefficients of E_C in Eqs. (5.41), and by then forming the following integral from 0 to $2\pi/k$ in the *x*–direction, because this represents one horizontal wavelength, and from 0 to 1 in the *y* and *z* directions.

$$I=\int_0^{2\pi/k}\int_0^1\int_0^1\begin{bmatrix}\left(\nabla^2 P_3 - Ra_o\Theta_{3z}\right)P_1-\begin{pmatrix}\nabla^2\Theta_3+Ra_o\Theta_3- \\ P_{3z}+H\left(\Phi_3-\Theta_3\right)\end{pmatrix}Ra_o\theta_1- \\ \left(\nabla^2\Phi_3-\gamma H\left(\Phi_3-\Theta_3\right)\right)Ra_o\phi_1\end{bmatrix}dzdydx. \tag{5.43}$$

$$I=\int_0^{2\pi/k}\int_0^1\begin{bmatrix}\left(\nabla^2 P_1 - Ra_o\theta_{1z}\right)P_3-\begin{pmatrix}\nabla^2\theta_1+Ra_o\theta_1-P_{1z} \\ +H\left(\phi_1-\theta_1\right)\end{pmatrix}Ra_o\theta_3 \\ -\left(\nabla^2\phi_1-\gamma H\left(\phi_1-\theta_1\right)\right)\dfrac{Ra_o\phi_3}{\gamma}\end{bmatrix}dzdx, \tag{5.44}$$

where we have taken into account the fact that $P_n=\Theta_n=\Phi_n=0$ on $z=0$ and $z=1$ for all values of *n*. That this integral is zero follows from the fact that the terms in the large round brackets are zero by definition; see equations (5.29) at $O(\in)$. Therefore the substitution of equations (5.42i) - (5.42iii) into (5.43) yields the solvability condition:

$$I = \iiint \left[\Re_1 P_1 - \Re_2 Ra_o \theta_1 - \frac{\Re_3 Ra_o \phi_1}{\gamma} \right] dzdydx = 0 \,. \tag{5.45}$$

where

$$\Re_1 = \frac{-Ra_2 \pi \left(k^2 + \pi^2\right)}{Ra_o k} \cos \pi z C E_c \,, \tag{5.46}$$

$$\begin{aligned}
\Re_2 = {} & \frac{-\left(k^2 + \pi^2\right)}{2Ra_o k} C_\tau E_c \sin \pi z + \frac{Ra_2 \left(k^2 + \pi^2\right)}{Ra_o k} C E_c \sin \pi z \\
& - \begin{bmatrix} \pi k \cos \phi \left(m_5 - m_8\right) + \pi k \left(m_5 + m_8\right) \\ + \dfrac{\pi \left(k^2 + \pi^2\right)}{k} \left(m_2 + m_5 + m_8\right) \\ + \dfrac{2\pi^2 \left(k^2 + \pi^2\right)}{Ra_o k} \left(m_1 + m_4 + m_7\right) \end{bmatrix} C B \overline{B} E_c \cos \pi z \sin 2\pi z \\
& + \begin{bmatrix} \dfrac{k \left(k^2 + \pi^2\right)}{Ra_o} \left(m_4 + m_7\right) \\ + \dfrac{k \left(k^2 + \pi^2\right)}{Ra_o} \cos \phi \left(m_4 - m_7\right) \\ -2\pi k \left(m_2 + m_5 + m_8\right) \end{bmatrix} C B \overline{B} E_c \sin \pi z \cos 2\pi z \\
& -2\pi k \left(m_2\right) C^2 \overline{C} E_c \sin \pi z \cos 2\pi z \\
& - \left[\frac{\pi \left(k^2 + \pi^2\right)}{k} \left(m_2\right) + \frac{2\pi^2 \left(k^2 + \pi^2\right)}{Ra_o k} \left(m_1\right) \right] C^2 \overline{C} E_c \cos \pi z \sin 2\pi z,
\end{aligned} \tag{5.47}$$

$$\Re_3 = -\frac{\alpha}{2} \left[\frac{\gamma H \left(k^2 + \pi^2\right)}{Ra_o k \left(k^2 + \pi^2 + \gamma H\right)} \right] C_\tau e^{ikx} \sin \pi z \,, \tag{5.48}$$

The solvability condition in equation (5.45) becomes:

$$I=\int_0^{2\pi/k}\int_0^1\int_0^1\left[\begin{array}{l}\left(\dfrac{-Ra_2\pi\left(k^2+\pi^2\right)}{Ra_o k}\cos\pi z C\right)P_1- \\ \left(\begin{array}{l}\dfrac{-\left(k^2+\pi^2\right)}{2Ra_o k}C_\tau\sin\pi z+ \\ \dfrac{Ra_2\left(k^2+\pi^2\right)}{Ra_o k}C\sin\pi z \\ -\left[\begin{array}{l}\pi k\cos\phi\left(m_5-m_8\right)+ \\ \pi k\left(m_5+m_8\right)+ \\ \dfrac{\pi\left(k^2+\pi^2\right)}{k}\left(m_2+m_5+m_8\right)+ \\ \dfrac{2\pi^2\left(k^2+\pi^2\right)}{Ra_o k}\left(m_1+m_4+m_7\right)\end{array}\right]CB\overline{B}\cos\pi z\sin 2\pi z \\ +\left[\begin{array}{l}\dfrac{k\left(k^2+\pi^2\right)}{Ra_o}\left(m_4+m_7\right)+ \\ \dfrac{k\left(k^2+\pi^2\right)}{Ra_o}\cos\phi\left(m_4-m_7\right) \\ -2\pi k\left(m_2+m_5+m_8\right)\end{array}\right]CB\overline{B}\sin\pi z\cos 2\pi z \\ -2\pi k\left(m_2\right)C^2\overline{C}\sin\pi z\cos 2\pi z \\ -\left[\begin{array}{l}\dfrac{\pi\left(k^2+\pi^2\right)}{k}\left(m_2\right)+ \\ \dfrac{2\pi^2\left(k^2+\pi^2\right)}{Ra_o k}\left(m_1\right)\end{array}\right]C^2\overline{C}\cos\pi z\sin 2\pi z\end{array}\right) \\ \left(-\dfrac{\alpha}{2}\left[\dfrac{\gamma H\left(k^2+\pi^2\right)}{Ra_o k\left(k^2+\pi^2+\gamma H\right)}\right]C_\tau e^{ikx}\sin\pi z\right)\dfrac{Ra_o\phi_1}{\gamma}\end{array}\right]Ra_o\theta_1-\left.\right]dzdydx=0$$

. (5.49)

The result of evaluating this integral is the following solvability condition:

$$-\left[\frac{\pi\left(k^2+\pi^2\right)^2}{2Ra_o k^3}+\frac{\alpha\pi\gamma H^2\left(k^2+\pi^2\right)^2}{2Ra_o k^3\left(k^2+\pi^2+\gamma H\right)^2}\right]C_\tau+$$

$$\left[\frac{\pi\left(k^2+\pi^2\right)^2}{Ra_o k^3}-\frac{\pi^3\left(k^2+\pi^2\right)}{Ra_o k^3}\right]Ra_2 C-$$

$$\left(\frac{\pi^3\left(k^2+\pi^2\right)^2}{Ra_o k^3}m_1-\frac{\pi^2\left(k^4-\pi^4\right)}{2k^3}m_2\right)C^2\overline{C}$$

$$-\frac{\pi\left(k^2+\pi^2\right)}{2k}\left[\begin{array}{l}\pi\cos\phi\left(m_5-m_8\right)+\\ \frac{\pi\left(2k^2+\pi^2\right)}{k^2}\left(m_5+m_8\right)+\\ \frac{\pi\left(k^2+\pi^2\right)}{k^2}\left(m_2\right)+\\ \frac{2\pi^2\left(k^2+\pi^2\right)}{Ra_o k^2}\left(m_1\right)+\\ \frac{2\pi^2\left(k^2+\pi^2\right)}{Ra_o k^2}\left(m_4+m_7\right)\\ +\frac{\left(k^2+\pi^2\right)}{Ra_o}\left(m_4+m_7\right)-\\ 2\pi m_2-2\pi\left(m_5+m_8\right)+\\ \frac{\left(k^2+\pi^2\right)}{Ra_o}\cos\phi\left(m_4-m_7\right)\end{array}\right]CB\overline{B}=0 \quad . \qquad (5.50)$$

We let:

$$c_1=\left[\frac{\pi\left(k^2+\pi^2\right)^2}{2Ra_o k^3}+\frac{\alpha\pi\gamma H^2\left(k^2+\pi^2\right)^2}{2Ra_o k^3\left(k^2+\pi^2+\gamma H\right)^2}\right]$$

$$c_2=\left[\frac{\pi\left(k^2+\pi^2\right)^2}{Ra_o k^3}-\frac{\pi^3\left(k^2+\pi^2\right)}{Ra_o k^3}\right]$$

$$c_3 = \left(\frac{\pi^3 \left(k^2+\pi^2\right)^2}{Ra_o k^3} m_1 - \frac{\pi^2 \left(k^4-\pi^4\right)}{2k^3} m_2 \right)$$

$$c_4 = \frac{\pi\left(k^2+\pi^2\right)}{2k} \left[\begin{array}{l} \pi\cos\phi\left(m_5-m_8\right) + \dfrac{\pi\left(2k^2+\pi^2\right)}{k^2}\left(m_5+m_8\right) + \\ \dfrac{\pi\left(k^2+\pi^2\right)}{k^2}\left(m_2\right) + \dfrac{2\pi^2\left(k^2+\pi^2\right)}{Ra_o k^2}\left(m_1\right) + \\ \dfrac{2\pi^2\left(k^2+\pi^2\right)}{Ra_o k^2}\left(m_4+m_7\right) + \dfrac{\left(k^2+\pi^2\right)}{Ra_o}\left(m_4+m_7\right) \\ -2\pi m_2 - 2\pi\left(m_5+m_8\right) + \dfrac{\left(k^2+\pi^2\right)}{Ra_o}\cos\phi\left(m_4-m_7\right) \end{array} \right],$$

Thus solvability condition for C-roll is

$$c_1 C_\tau = c_2 Ra_2 C - c_3 C^2 \overline{C} - c_4 CB\overline{B}\,, \tag{5.51a}$$

and for B-roll naturally follows as

$$c_1 B_\tau = c_2 Ra_2 B - c_3 B^2 \overline{B} - c_4 BC\overline{C}\,. \tag{5.51b}$$

because of the rotational symmetry of the plane.

5.6 Analysis of the limit $H \to 0$ and $H \to \infty$

From Banu and Rees [1], we have $Ra = 4\pi^2$ and $k = \pi$ as the linear stability condition when *H* is small. On the contrary, when *H* is large, $Ra = 4\pi^2\left(\frac{\gamma}{1+\gamma}\right)$ while $k = \pi$ remains. These conditions allow the full solution of P_1, Θ_1 and Φ_1 to be:

$$P_1 = -\frac{1}{\pi}\left[Ce^{ikx} + \overline{C}e^{-ikx}\right]\cos\pi z - \frac{1}{\pi}\left[Be^{ik(x\cos\phi - y\sin\phi)} + \overline{B}e^{-ik(x\cos\phi - y\sin\phi)}\right]\cos\pi z\,,$$

$$\Theta_1 = \frac{1}{2\pi^2}\left[Ce^{ikx} + \overline{C}e^{-ikx}\right]\sin\pi z + \frac{1}{2\pi^2}\left[Be^{ik(x\cos\phi - y\sin\phi)} + \overline{B}e^{-ik(x\cos\phi - y\sin\phi)}\right]\sin\pi z\,,$$

$$\Phi_1 = 0,\,.$$

when *H* is small.

$$P_1 = -\frac{1}{\pi}\left[Ce^{ikx} + \overline{C}e^{-ikx}\right]\cos\pi z - \frac{1}{\pi}\left[Be^{ik(x\cos\phi - y\sin\phi)} + \overline{B}e^{-ik(x\cos\phi - y\sin\phi)}\right]\cos\pi z\,,$$

$$\Theta_1 = \frac{1}{2\pi^2}\left[Ce^{ikx} + \overline{C}e^{-ikx}\right]\sin\pi z + \frac{1}{2\pi^2}\left[Be^{ik(x\cos\phi - y\sin\phi)} + \overline{B}e^{-ik(x\cos\phi - y\sin\phi)}\right]\sin\pi z\,,$$

$$\Phi_1 = \frac{1}{2\pi^2}\left[Ce^{ikx} + \overline{C}e^{-ikx}\right]\sin\pi z + \frac{1}{2\pi^2}\left[Be^{ik(x\cos\phi - y\sin\phi)} + \overline{B}e^{-ik(x\cos\phi - y\sin\phi)}\right]\sin\pi z\,,$$

when *H* is large. While P_2, Θ_2 and Φ_2 are taking the following equations when *H* is small:

$$P_2 = \left[\begin{array}{l}\frac{1}{2}\left(B\overline{B} + C\overline{C}\right) + \frac{1-\cos\phi}{\cos^2\phi + 4\cos\phi + 7}\left(CBE_cE_B + \overline{C}\,\overline{B}\,\overline{E_c}\,\overline{E_B}\right) + \\ \frac{1+\cos\phi}{\cos^2\phi - 4\cos\phi + 7}\left(C\overline{B}E_C\overline{E_B} + \overline{C}B\overline{E_C}E_B\right)\end{array}\right]\cos 2\pi z,$$

$$\Theta_2 = \left[\begin{array}{l} -\frac{1}{4\pi}\left(B\overline{B}+C\overline{C}\right)+\frac{1}{4\pi}\frac{\left(\cos^2\phi+2\cos\phi-3\right)}{\left(\cos^2\phi+4\cos\phi+7\right)}\left(CBE_cE_B+\overline{C}\,\overline{B}\,\overline{E_c}\,\overline{E_B}\right)+ \\ \frac{1}{4\pi}\frac{\left(\cos^2\phi-2\cos\phi-3\right)}{\left(\cos^2\phi-4\cos\phi+7\right)}\left(C\overline{B}E_C\overline{E_B}+\overline{C}B\overline{E_C}E_B\right) \end{array} \right] \sin 2\pi z,$$

$$\Phi_2 = 0,$$

and H is large

$$P_2 = \left[\begin{array}{l} \frac{1}{2}\left(\frac{\gamma}{1+\gamma}\right)\left(B\overline{B}+C\overline{C}\right)+ \\ \frac{1-\cos\phi}{\cos^2\phi+4\cos\phi+7}\left(\frac{\gamma}{1+\gamma}\right)\left(CBE_cE_B+\overline{C}\,\overline{B}\,\overline{E_c}\,\overline{E_B}\right)+ \\ \frac{1+\cos\phi}{\cos^2\phi-4\cos\phi+7}\left(\frac{\gamma}{1+\gamma}\right)\left(C\overline{B}E_C\overline{E_B}+\overline{C}B\overline{E_C}E_B\right) \end{array} \right] \cos 2\pi z,$$

$$\Theta_2 = \left[\begin{array}{l} -\frac{1}{4\pi}\left(\frac{\gamma}{1+\gamma}\right)^2\left(B\overline{B}+C\overline{C}\right)+ \\ \frac{1}{4\pi}\left(\frac{\gamma}{1+\gamma}\right)^2\frac{\left(\cos^2\phi+2\cos\phi-3\right)}{\left(\cos^2\phi+4\cos\phi+7\right)}\left(CBE_cE_B+\overline{C}\,\overline{B}\,\overline{E_c}\,\overline{E_B}\right)+ \\ \frac{1}{4\pi}\left(\frac{\gamma}{1+\gamma}\right)^2\frac{\left(\cos^2\phi-2\cos\phi-3\right)}{\left(\cos^2\phi-4\cos\phi+7\right)}\left(C\overline{B}E_C\overline{E_B}+\overline{C}B\overline{E_C}E_B\right) \end{array} \right] \sin 2\pi z,$$

$$\Phi_2 = \left[\begin{array}{l} -\frac{1}{4\pi}\left(\frac{\gamma}{1+\gamma}\right)^2\left(B\overline{B}+C\overline{C}\right)+ \\ \frac{1}{4\pi}\left(\frac{\gamma}{1+\gamma}\right)^2\frac{\left(\cos^2\phi+2\cos\phi-3\right)}{\left(\cos^2\phi+4\cos\phi+7\right)}\left(CBE_cE_B+\overline{C}\,\overline{B}\,\overline{E_c}\,\overline{E_B}\right)+ \\ \frac{1}{4\pi}\left(\frac{\gamma}{1+\gamma}\right)^2\frac{\left(\cos^2\phi-2\cos\phi-3\right)}{\left(\cos^2\phi-4\cos\phi+7\right)}\left(C\overline{B}E_C\overline{E_B}+\overline{C}B\overline{E_C}E_B\right) \end{array} \right] \sin 2\pi z.$$

Apart from that, the coefficients of the solvability condition for C-roll and B-roll are as follows when H is small:

$$c_1 = \frac{1}{2},\ c_2 = \frac{1}{2},\ c_3 = \frac{\pi^2}{2},\ \text{and}\ c_4 = \frac{\pi^2}{2}\left(\frac{-2\cos^4\phi + 28\cos^2\phi + 70}{\cos^4\phi - 2\cos^2\phi + 49}\right), \tag{5.52}$$

where the stability characteristics of the convective flow depend greatly on the angle, ϕ of coefficient, c_4/c_3.

Meanwhile when H is large, the coefficients of the solvability condition for both rolls are:

$$c_1 = \frac{1}{2}\left(\frac{1+\gamma}{\gamma}\right),\ c_2 = \frac{1}{2}\left(\frac{1+\gamma}{\gamma}\right),\ c_3 = \frac{\pi^2}{2}\left(\frac{1+\gamma}{\gamma}\right),$$

$$\text{and}\ c_4 = \frac{\pi^2}{2}\left(\frac{-2\cos^4\phi + 28\cos^2\phi + 70}{\cos^4\phi - 2\cos^2\phi + 49}\right)\left(\frac{1+\gamma}{\gamma}\right)^2. \tag{5.53}$$

Comparing the given form of equation (5.20) and the analysis obtained in this paper as in equations (5.51a- 5.51a), the important value which will determine the form of the cell either rolls or square is depend on the ratio c_4/c_3.

In fact, it is easily shown that c_4/c_3 is equal to 2 when $\phi = 0$ and takes its minimum of 10/7 when $\phi = 90$ degrees which mean the minimum is above 1, and therefore rolls are stable and square cells are unstable.

5.7 Numerical results and discussion

Analysis given in 5.6 shows that Ra_c is independent of γ and takes the value close to $4\pi^2$ at small values of H. This can be proven graphically from the variation of Ra_c with $\log_{10} H$ for specific values of γ presented in Figure 5.1 which is taken

from Banu and Rees [1]. The explanation of the independence of Ra_c towards γ is that there is almost zero heat transfer occurring between the phases and thus the onset criterion is independent of the solid phase properties. In addition, Ra is defined in terms of the fluid properties. This independence also arises when H is large in Figure 5.2. Here the quantity being plotted is the Darcy-Rayleigh number based on the porous medium properties, and the large – H limit is the LTNE limit. Banu and Rees [1] noted that these two versions of the Darcy-Rayleigh number are necessary in order to describe the onset of convection in such extreme cases. As seen in Figure 5.1 Ra_c is inappropriate to use when H is large, and in Figure 5.2 $Ra_c\gamma/(1+\gamma)$ is inappropriate when H is small.

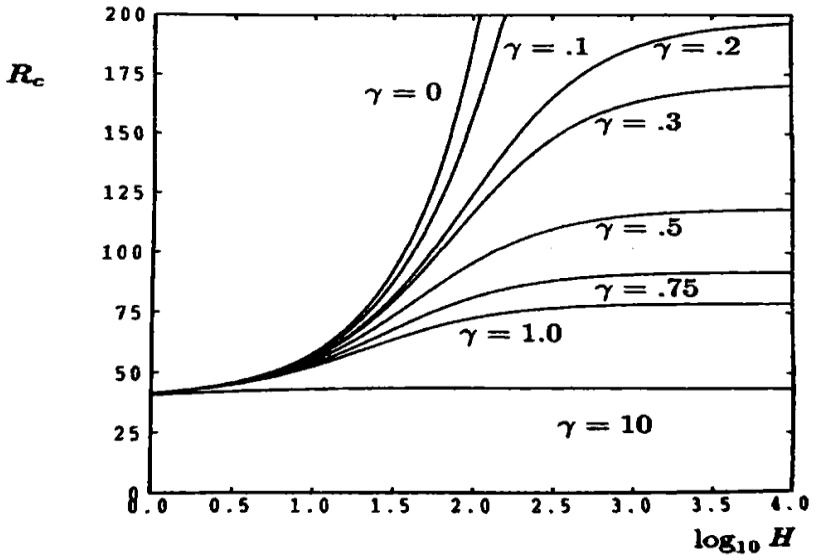

Figure 5.1: Variation of Ra_c with $\log_{10} H$ for specific values of γ (Banu and Rees, 2002)

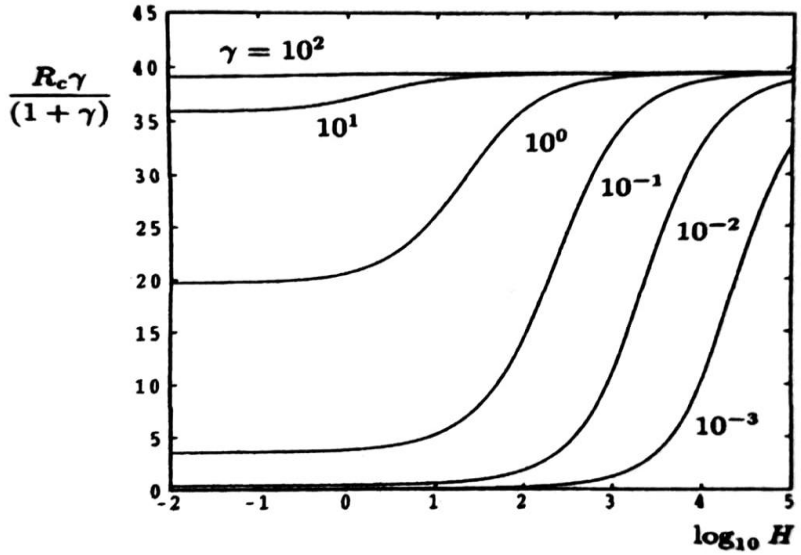

Figure 5.2: Variation of $Ra_c\gamma/(1+\gamma)$ with $\log_{10} H$ for specific values of γ (Banu and Rees, 2002)

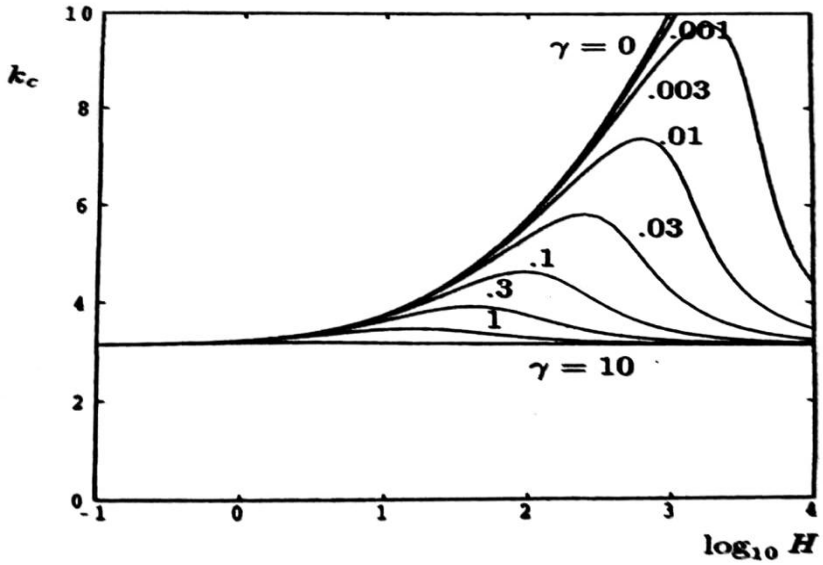

Figure 5.3: Variation of the critical wavenumber, k_c with $\log_{10} H$ for specific values of γ (Banu and Rees, 2002)

The variation of the critical wavenumber, k_c with $\log_{10} H$ for specific values of γ is displayed in Figure 5.3. It shows that for both limit of H ($H \to 0$ and $H \to \infty$), k_c takes the limit of π. The physical reason of the situation when $H \to 0$ is that there is no effect of solid phase on the dynamics of the fluid phase, which is a single phase, whereas as $H \to \infty$, the solid and fluid phase have approximately equal temperature such that both may be treated as single phase and therefore $k_c \to \pi$. In between the extreme H values shown in Figure 5.3, it is noticed that $k_c > \pi$ in all cases.

The variation of the coupling coefficient, c_4/c_3, with $\log_{10} H$ for chosen values of $\log_{10} \gamma$ is displayed in Figure 5.4. As has already been mentioned, the coefficient c_4/c_3 plays an important role in the identity of the most unstable mode near to the onset of convection. In all of our testing, we found that c_4/c_3 achieves its minimum when the two rolls are at right angles, which corresponds to square cells. Figure 5.4 shows that, when $H \to 0$, c_4/c_3 tends toward 10/7 and that the same value is also obtained as $H \to \infty$ which mean that the rolls are stable, but this was to be expected because both limits reproduce the classical LTE case. Just as the critical wavenumber always lies above π so the value of c_4/c_3 always lies above 10/7, and therefore we conclude that rolls are always stable when LTNE is present.

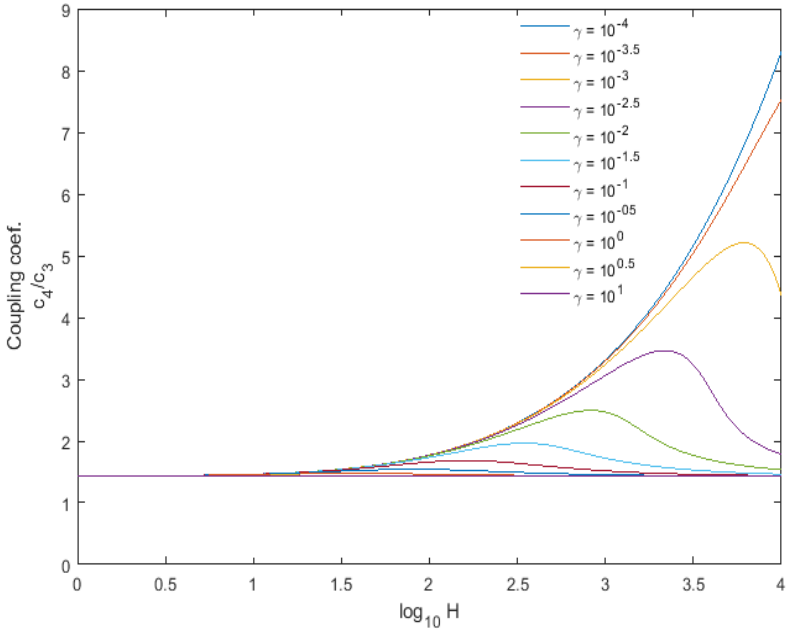

Figure 5.4: Variation of the coupling coefficient c_4/c_3 with $\log_{10} H$ for specific values of γ.

5.8 Conclusion

A study has been undertaken of the effect of LTNE on weakly nonlinear Darcy-Bénard convection in order to determine whether 2D rolls always form the stable post-onset pattern of convection or whether square cells can arise in any region of parameter space. The conclusion is that rolls remain stable, and that changes in H and γ do not affect this conclusion. Moreover, the coupling coefficient is generally larger than the LTE value of 10/7.

5.9 References

[1] Banu, N., Rees, D.A.S. (2002). Onset of Darcy-Bénard convection using a thermal non-equilibrium model. *Int. J. Heat Mass Transfer*, **45**, 2221-2228.

[2] Horton, C.W., Rogers, F.T. (1945). Convection currents in a porous medium. *J. Appl. Phys*., **16,** 367–370.

[3] Lapwood, E.R. (1948). Convection of a fluid in a porous medium. Math. Proc. Camb. Phil. Soc., **44**, 508–521.

[4] Straus, J.M. (1974). Large amplitude convection in porous media. *J. Fluid Mech*., **64,** 51–63.

[5] Rees, D.A.S., Riley, D.S. (1989). The effects of boundary imperfections on convection in a saturated porous layer: near-resonant wavelength excitation. *J. Fluid Mech.*, **199,** 133–154.

[6] Newell, A.C., Whitehead, J.C. (1969). Finite bandwidth, finite amplitude convection. *J. Fluid Mech*., **38,** 279–303.

[7] Rees, D.A.S. (2001). Stability analysis of Darcy-Bénard convection. Neptune Notes, Romania.

[8] Rees, D.A.S., Riley, D.S. (1990). The three-dimensional stability of finite-amplitude convection in a layered porous medium heated from below. *J. Fluid Mech.*, **211,** 437–461.

[9] Combarnous, M., Bories, S. (1973). Modelisation de la convection naturelle au sein d'une couche poreuse horizontale a l'aide d'un coefficient de transfert solide-fluide. *Int. J. Heat Mass Transfer*, **17**, 505-515.

[10] Nield, D. A. & Bejan, A. (2013). Convection in Porous Media. New York: Springer.

[11] Quintard, M., Kaviany, M., Whitaker, S. (1997). Two-medium treatment of heat transfer in porous media: numerical results for effective properties. *Advances in Water Resources*, **20**, 11-94.

[12] Quintard, M. (1998). Modelling local non-equilibrium heat transfer in porous media. *Proceedings of 11th IHTC, Kyongju, Korea*, **1**, 279-285.

[13] Rees, D.A.S., Pop, I. (1999). Free convective stagnation-point flow in a porous medium thermal non-equilibrium model. *Int. Comm. Heat Mass Transfer*, **26**, 945-954.

[14] Rees, D.A.S., Pop, I. (2000). Vertical free convective boundary-layer flow in a porous medium using a thermal nonequilibrium model. *Journal of porous media*, **3**, 31-41.

[15] Rees, D.A.S., Pop, I. (2005). Local thermal non-equilibrium in porous medium convection. Transport Phenomena in Porous Media III eds. D.B.Ingham and I.Pop. (Pergamon) 147–173.

5.10 Appendixes

5.10.1 Stability analysis of Equation (5.20)

Recall equation (5.20):

$$B_\tau = R_2 B - cB\left[B^2 + d\,C^2\right], \tag{A5.1a}$$

$$C_\tau = R_2 C - cC\left[C^2 + dB^2\right]. \tag{A5.1b}$$

and the solutions for roll are:

$$B = \frac{R_2^{\frac{1}{2}}}{\sqrt{c}} \text{ and } C = 0, \tag{A5.2}$$

$$\text{Let } B = \frac{R_2^{\frac{1}{2}}}{\sqrt{c}} + \delta B \text{ and } C = \delta C \tag{A5.3}$$

Substitute (A5.3) into (A5.1a) yield:

$$\delta B_\tau = R_2\left(\frac{R_2^{\frac{1}{2}}}{\sqrt{c}} + \delta B\right) - c\left(\frac{R_2^{\frac{1}{2}}}{\sqrt{c}} + \delta B\right)\left[\left(\frac{R_2^{\frac{1}{2}}}{\sqrt{c}} + \delta B\right)^2 + d\left(\delta C\right)^2\right],$$

$$= \frac{R_2^{\frac{3}{2}}}{\sqrt{c}} + R_2\delta B - \frac{R_2^{\frac{3}{2}}}{\sqrt{c}} - 2R_2\delta B - R_2\delta B - \frac{cR_2^{\frac{1}{2}}}{\sqrt{c}}\delta B^2 + \frac{cdR_2^{\frac{1}{2}}}{\sqrt{c}}\delta C^2$$

$$- \frac{2cR_2^{\frac{1}{2}}}{\sqrt{c}}\delta B^2 - c\delta B^3 - cd\,\delta B^2\delta C,$$

Neglecting higher order terms yield:

$$\delta B_\tau = -2R_2\delta B,$$

δB_τ decay exponentially, therefore δB_t is stable. So disturbances in B is decay.

Substituting (A5.3) into (A5.1b) yields:

$$\delta \mathrm{C}_{\tau} = \mathrm{R}_2 \delta C \text{ - } c\delta C \left[\left(\delta \mathrm{C}\right)^2 + d\left(\frac{R_2^{\frac{1}{2}}}{\sqrt{c}} + \delta \mathrm{B} \right)^2 \right],$$

$$= \mathrm{R}_2 \delta \mathrm{C} - c\delta \mathrm{C}^3 - dR_2 \delta \mathrm{C} - 2dR_2^{\frac{1}{2}} \delta \mathrm{B} \delta \mathrm{C} - cd\delta \mathrm{B}^2 \delta \mathrm{C}$$

Neglecting higher order terms yields:

$$\delta \mathrm{C}_{\tau} = \left(1 - d\right) \mathrm{R}_2 \delta \mathrm{C},$$

so C decays whenever $d > 1$ but grows when $d < 1$. Therefore it can be concluded that rolls are stable whenever $d > 1$ but are unstable otherwise.

while solution for square are:

$$\mathrm{B} = \frac{R_2^{\frac{1}{2}}}{\sqrt{c\left(1+d\right)}} \text{ and } \mathrm{B} = \mathrm{C}. \tag{A5.4}$$

The stability of square cells may be analysed by setting

$$\mathrm{B} = \frac{R_2^{\frac{1}{2}}}{\sqrt{c\left(1+d\right)}} + \delta \mathrm{B} \text{ and } \mathrm{C} = \frac{R_2^{\frac{1}{2}}}{\sqrt{c\left(1+d\right)}} + \delta \mathrm{C} \tag{A5.5}$$

into (A5.1a) and this yields:

$$\delta \mathrm{B}_{\tau} = \mathrm{R}_2 \left(\frac{R_2^{\frac{1}{2}}}{\sqrt{c\left(1+d\right)}} + \delta \mathrm{B} \right) \text{ - } c \left(\frac{R_2^{\frac{1}{2}}}{\sqrt{c\left(1+d\right)}} + \delta \mathrm{B} \right) \left[\left(\frac{R_2^{\frac{1}{2}}}{\sqrt{c\left(1+d\right)}} + \delta \mathrm{B} \right)^2 + d \left(\frac{R_2^{\frac{1}{2}}}{\sqrt{c\left(1+d\right)}} + \delta \mathrm{C} \right)^2 \right],$$

$$= \frac{R_2^{\frac{3}{2}}}{\sqrt{c\left(1+d\right)}} + \mathrm{R}_2 \delta \mathrm{B} - c \left(\frac{R_2^{\frac{1}{2}}}{\sqrt{c\left(1+d\right)}} + \delta \mathrm{B} \right) \left[\frac{R_2}{c\left(1+d\right)} + \frac{2R_2^{\frac{1}{2}}}{\sqrt{c\left(1+d\right)}} \delta \mathrm{B} + \delta \mathrm{B}^2 + d \left(\frac{R_2}{c\left(1+d\right)} + \frac{2R_2^{\frac{1}{2}}}{\sqrt{c\left(1+d\right)}} \delta \mathrm{C} + \delta \mathrm{C}^2 \right) \right],$$

Neglecting higher order terms yields:

$$= \frac{R_2^{\frac{3}{2}}}{\sqrt{c(1+d)}} + \mathrm{R}_2\delta\mathrm{B} - c\left[(1+d)\frac{R_2^{\frac{3}{2}}}{c(1+d)\sqrt{c(1+d)}} + \frac{2\mathrm{R}_2}{c(1+d)}(\delta\mathrm{B}+d\delta\mathrm{C}) + \frac{(1+d)\mathrm{R}_2}{c(1+d)}\delta\mathrm{B}\right]$$

$$\delta\mathrm{B}_\tau = -\left(\frac{2\mathrm{R}_2}{1+d}\right)(\delta\mathrm{B}+d\delta\mathrm{C}). \tag{A5.6}$$

Substitute (A5.5) into (A5.1b) yields:

$$\delta\mathrm{C}_\tau = \mathrm{R}_2\left(\frac{R_2^{\frac{1}{2}}}{\sqrt{c(1+d)}} + \delta\mathrm{C}\right) - c\left(\frac{R_2^{\frac{1}{2}}}{\sqrt{c(1+d)}} + \delta\mathrm{C}\right)\left[\left(\frac{R_2^{\frac{1}{2}}}{\sqrt{c(1+d)}} + \delta\mathrm{C}\right)^2 + d\left(\frac{R_2^{\frac{1}{2}}}{\sqrt{c(1+d)}} + \delta\mathrm{B}\right)^2\right],$$

$$= \frac{R_2^{\frac{3}{2}}}{\sqrt{c(1+d)}} + \mathrm{R}_2\delta\mathrm{C} - c\left(\frac{R_2^{\frac{1}{2}}}{\sqrt{c(1+d)}} + \delta\mathrm{C}\right)\left[\frac{R_2}{c(1+d)} + \frac{2R_2^{\frac{1}{2}}}{\sqrt{c(1+d)}}\delta\mathrm{C} + \delta\mathrm{C}^2 + d\left(\frac{R_2}{c(1+d)} + \frac{2R_2^{\frac{1}{2}}}{\sqrt{c(1+d)}}\delta\mathrm{B} + \delta\mathrm{B}^2\right)\right],$$

Neglecting higher order terms yields:

$$= \frac{R_2^{\frac{3}{2}}}{\sqrt{c(1+d)}} + \mathrm{R}_2\delta\mathrm{C} - c\left[(1+d)\frac{R_2^{\frac{3}{2}}}{c(1+d)\sqrt{c(1+d)}} + \frac{2\mathrm{R}_2}{c(1+d)}(d\delta\mathrm{B}+\delta\mathrm{C}) + \frac{(1+d)\mathrm{R}_2}{c(1+d)}\delta\mathrm{C}\right]$$

$$\delta\mathrm{C}_\tau = -\left(\frac{2\mathrm{R}_2}{1+d}\right)(d\delta\mathrm{B}+\delta\mathrm{C}). \tag{A5.7}$$

Let $\begin{pmatrix}\delta\mathrm{B}\\ \delta\mathrm{C}\end{pmatrix} = e^{\lambda\tau}\begin{pmatrix}m\\ n\end{pmatrix}$. (A5.8)

Substitute (A5.8) into equation (A5.6) and (A5.7), yield:

$$\lambda m e^{\lambda\tau} = -\frac{2R_2}{1+d}e^{\lambda\tau}(m+nd),$$

$$\lambda n e^{\lambda\tau} = -\frac{2R_2}{1+d}e^{\lambda\tau}(dm+n),$$

$$m\left(\lambda+\frac{2R_2}{1+d}\right)+\left(\frac{2dR_2}{1+d}\right)n=0,$$
$$m\left(\frac{2dR_2}{1+d}\right)+\left(\lambda+\frac{2R_2}{1+d}\right)n=0,$$

$$\begin{bmatrix}\lambda+\frac{2R_2}{1+d} & \frac{2dR_2}{1+d}\\ \frac{2dR_2}{1+d} & \lambda+\frac{2R_2}{1+d}\end{bmatrix}\begin{bmatrix}m\\ n\end{bmatrix}=\begin{bmatrix}0\\ 0\end{bmatrix}. \qquad \text{(A5.9)}$$

Find the determinant of the matrix yields:

$$\begin{vmatrix}\lambda+\frac{2R_2}{1+d} & \frac{2dR_2}{1+d}\\ \frac{2dR_2}{1+d} & \lambda+\frac{2R_2}{1+d}\end{vmatrix}=0$$

$$\lambda^2+\lambda\left(\frac{4R_2}{1+d}\right)+\left(\frac{4R_2^2}{(1+d)^2}\left(1-d^2\right)\right)=0$$
$$\left(\lambda+\frac{2R_2}{1+d}(1+d)\right)\left(\lambda+\frac{2R_2}{1+d}(1-d)\right)=0$$
$\lambda_1=-2R_2$ and $\lambda_2=-\frac{2R_2}{1+d}(1-d)$ are the eigenvalues.

The first eigenvalue correspond to the following eigenvector, but disturbances of this form decay. Substitution of the eigenvalue, $\lambda_1=-2R_2$ into equation (A5.9) gives:

$$\begin{bmatrix}-\frac{2dR_2}{1+d} & \frac{2dR_2}{1+d}\\ \frac{2dR_2}{1+d} & -\frac{2dR_2}{1+d}\end{bmatrix}\begin{bmatrix}m\\ n\end{bmatrix}=\begin{bmatrix}0\\ 0\end{bmatrix}.$$

and this yield the following reduced matrix: $\left[\begin{array}{cc|c} 1 & -1 & 0 \\ 0 & 0 & 0 \end{array}\right]$ which equivalent to $m-n=0$. Let $n=P$, thus $m=P$. Therefore, the corresponding eigenvector for $\lambda_1=-2R_2$ is

$$\begin{pmatrix} m \\ n \end{pmatrix} = P\begin{pmatrix} 1 \\ 1 \end{pmatrix}.$$

Finally, substitute eigenvalue, $\lambda_2=-\frac{2R_2}{1+d}(1-d)$ into equtaion (A5.9) gives:

$$\begin{bmatrix} \frac{2dR_2}{1+d} & \frac{2dR_2}{1+d} \\ \frac{2dR_2}{1+d} & \frac{2dR_2}{1+d} \end{bmatrix}\begin{bmatrix} m \\ n \end{bmatrix} = \begin{bmatrix} 0 \\ 0 \end{bmatrix}.$$

$$\left[\begin{array}{cc|c} \frac{2dR_2}{1+d} & \frac{2dR_2}{1+d} & 0 \\ \frac{2dR_2}{1+d} & \frac{2dR_2}{1+d} & 0 \end{array}\right] \xrightarrow{\frac{1+d}{2dR_2}(row1)} \left[\begin{array}{cc|c} 1 & 1 & 0 \\ \frac{2dR_2}{1+d} & -\frac{2dR_2}{1+d} & 0 \end{array}\right] \xrightarrow{(row2)-\frac{2dR_2}{1+d}(row1)} \left[\begin{array}{cc|c} 1 & 1 & 0 \\ 0 & 0 & 0 \end{array}\right].$$

and the reduced matrix is $\left[\begin{array}{cc|c} 1 & 1 & 0 \\ 0 & 0 & 0 \end{array}\right]$ which equivalent to $m+n=0$. Let $m=Q$, thus $n=-Q$. Therefore, the corresponding eigenvector for $\lambda_2=-\frac{2R_2}{1+d}(1-d)$ is

$$\begin{pmatrix} m \\ n \end{pmatrix} = Q\begin{pmatrix} 1 \\ -1 \end{pmatrix}.$$

Therefore the eigenvectors for $\lambda_1=-2R_2$ and $\lambda_2=-\frac{2R_2}{1+d}(1-d)$ is:

$$\begin{pmatrix} \delta \mathrm{B} \\ \delta \mathrm{C} \end{pmatrix} = Pe^{\lambda_1 \tau}\begin{pmatrix} 1 \\ 1 \end{pmatrix} + Qe^{\lambda_2 \tau}\begin{pmatrix} 1 \\ -1 \end{pmatrix}, \qquad \text{(A5.10)}$$

From equation (A5.10), it is obvious that general disturbances, δB and δC , will decay are stable when d < 1 but one of the eigenmodes becomes unstable whenever d > 1.

We conclude that rolls form the stable solution whenever d > 1, but square form the stable solution otherwise.

5.10.2 Table of exponential abbreviations

	$E_C = e^{ikx}$	$\overline{E_C} = e^{-ikx}$	$E_B = e^{ik(x\cos\phi - y\sin\phi)}$	$\overline{E_B} = e^{-ik(x\cos\phi - y\sin\phi)}$
E_C	$E_C E_C = E_C^2 = e^{2ikx}$	$\overline{E_C} E_C = 0$	$E_B E_C = e^{ik\left[(1+\cos\phi)x - y\sin\phi\right]}$	$\overline{E_B} E_C = e^{ik\left[(1-\cos\phi)x + y\sin\phi\right]}$
$\overline{E_C}$	$E_C \overline{E_C} = 0$	$\overline{E_C}\,\overline{E_C} = \overline{E}_C^2 = e^{-2ikx}$	$E_B \overline{E_C} = e^{-ik\left[(1-\cos\phi)x + y\sin\phi\right]}$	$\overline{E_B}\,\overline{E_C} = e^{-ik\left[(1+\cos\phi)x - y\sin\phi\right]}$
E_B	$E_B E_C = e^{ik\left[(1+\cos\phi)x - y\sin\phi\right]}$	$E_B \overline{E_C} = e^{-ik\left[(1-\cos\phi)x + y\sin\phi\right]}$	$E_B E_B = E_B^2 = e^{2ik[x\cos\phi - y\sin\phi]}$	$\overline{E_B} E_B = 0$
$\overline{E_B}$	$\overline{E_B} E_C = e^{ik\left[(1-\cos\phi)x + y\sin\phi\right]}$	$\overline{E_B}\,\overline{E_C} = e^{-ik\left[(1+\cos\phi)x - y\sin\phi\right]}$	$\overline{E_B} E_B = 0$	$\overline{E_B}\,\overline{E_B} = \overline{E}_B^2 e^{-2ik\left[(1+\cos\phi)x - y\sin\phi\right]}$

	$E_B E_C$	$\overline{E_B}\,\overline{E_C}$	$\overline{E_B} E_C$	$E_B \overline{E_C}$
E_C	$E_C^2 E_B = e^{ik\left[(2+\cos\phi)x - y\sin\phi\right]}$	$E_C \overline{E_C}\,\overline{E_B} = \overline{E_B} = e^{-ik[x\cos\phi - y\sin\phi]}$	$E_C^2 \overline{E}_B = e^{ik\left[(2-\cos\phi)x + y\sin\phi\right]}$	$\overline{E_C} E_C E_B = E_B = e^{ik[x\cos\phi - y\sin\phi]}$
$\overline{E_C}$	$\overline{E_C} E_C E_B = E_B = e^{ik[x\cos\phi - y\sin\phi]}$	$\overline{E}_C^2 \overline{E}_B = e^{-ik\left[(2+\cos\phi)x + y\sin\phi\right]}$	$E_C \overline{E_C}\,\overline{E_B} = \overline{E_B} = e^{-ik[x\cos\phi - y\sin\phi]}$	$\overline{E}_C^2 E_B = e^{-ik\left[(2-\cos\phi)x + y\sin\phi\right]}$
E_B	$E_C E_B^2 = e^{ik\left[(1+2\cos\phi)x - 2y\sin\phi\right]}$	$E_B \overline{E_B}\,\overline{E_C} = \overline{E_C} = e^{-ikx}$	$\overline{E_B} E_B E_C = E_C = e^{ikx}$	$\overline{E_C} E_B^2 = e^{-ik\left[(1-2\cos\phi)x + 2y\sin\phi\right]}$
$\overline{E_B}$	$\overline{E_B} E_B E_C = e^{ikx}$	$\overline{E_C}\,\overline{E_B^2} = e^{-ik\left[(1+2\cos\phi)x - 2y\sin\phi\right]}$	$\overline{E_B^2} E_C = e^{ik\left[(1-2\cos\phi)x + 2y\sin\phi\right]}$	$E_B \overline{E_B}\,\overline{E_C} = \overline{E_C} = e^{-ikx}$